NAVAL POSTGRADUATE SCHOOL

MONTEREY, CALIFORNIA

THESIS

CLIMATE AND WEATHER ANALYSIS OF AFGHANISTAN THUNDERSTORMS

by

Chad E. Geis

September 2011

Thesis Advisor:	Tom Murphree
Co-Advisor:	Paul Frederickson

Approved for public release; distribution is unlimited

THIS PAGE INTENTIONALLY LEFT BLANK

REPORT DOCUMENTATION PAGE		Form Approved OMB No. 0704-0188

Public reporting burden for this collection of information is estimated to average 1 hour per response, including the time for reviewing instruction, searching existing data sources, gathering and maintaining the data needed, and completing and reviewing the collection of information. Send comments regarding this burden estimate or any other aspect of this collection of information, including suggestions for reducing this burden, to Washington headquarters Services, Directorate for Information Operations and Reports, 1215 Jefferson Davis Highway, Suite 1204, Arlington, VA 22202-4302, and to the Office of Management and Budget, Paperwork Reduction Project (0704-0188) Washington DC 20503.

1. AGENCY USE ONLY *(Leave blank)*	2. REPORT DATE September 2011	3. REPORT TYPE AND DATES COVERED Master's Thesis

4. TITLE AND SUBTITLE Climate and Weather Analysis of Afghanistan Thunderstorms	5. FUNDING NUMBERS
6. AUTHOR(S) Chad E. Geis	
7. PERFORMING ORGANIZATION NAME(S) AND ADDRESS(ES) Naval Postgraduate School Monterey, CA 93943-5000	8. PERFORMING ORGANIZATION REPORT NUMBER
9. SPONSORING /MONITORING AGENCY NAME(S) AND ADDRESS(ES) N/A	10. SPONSORING/MONITORING AGENCY REPORT NUMBER

11. SUPPLEMENTARY NOTES The views expressed in this thesis are those of the author and do not reflect the official policy or position of the Department of Defense or the U.S. Government. IRB Protocol number _____N/A_____.

12a. DISTRIBUTION / AVAILABILITY STATEMENT Approved for public release; distribution is unlimited	12b. DISTRIBUTION CODE

13. ABSTRACT (maximum 200 words)

Thunderstorms are a significant factor in the planning and execution of Department of Defense (DoD) operations in Afghanistan, especially in the spring and summer. Skillful forecasting of Afghanistan thunderstorms has proven difficult, even at relatively short lead times of 24 hours or less. This has led to adverse effects on a wide range of DoD missions. One potential reason for the forecasting difficulties is a lack of understanding of the conditions that lead to static instability and thunderstorms in the elevated desert mountain environment that characterizes much of Afghanistan. Much of the thunderstorm forecasting for Afghanistan is based on forecasting methods developed for the contiguous U.S. (CONUS)—for example, the use of CONUS-based static stability indices as indicators of the potential for thunderstorm development. We have investigated methods for improving thunderstorm forecasting in and near Kabul, Afghanistan, by: (1) analyzing interannual to hourly variations in thunderstorm activity; and (2) analyzing the large-scale conditions that are favorable and unfavorable for thunderstorms. We used in situ surface and radiosonde data to characterize the local conditions associated with thunderstorm variations. Our focus was on March–May, the period with the most thunderstorm activity in Kabul. We also used global reanalysis data to analyze the large-scale conditions that are favorable and unfavorable for thunderstorm development. We developed and tested two new static stability indices for use in Kabul. We also developed a large-scale circulation index to describe the regional factors that contribute to thunderstorm variations. Finally, we identified outgoing longwave radiation anomalies that occurred in specific tropical ocean basins as potential precursors for predicting thunderstorm and nonthunderstorm events at lead times of 5–15 days.

14. SUBJECT TERMS Kabul, Afghanistan, Forecasting, Elevated Desert Mountain Environment, Thunderstorms, Static Stability, Indices, Climate, Climate Variations, Climate Analysis, Medium Range Forecasting, Long Range Forecasting, Mission Planning	15. NUMBER OF PAGES 169
	16. PRICE CODE

17. SECURITY CLASSIFICATION OF REPORT	18. SECURITY CLASSIFICATION OF THIS PAGE	19. SECURITY CLASSIFICATION OF ABSTRACT	20. LIMITATION OF ABSTRACT
Unclassified	Unclassified	Unclassified	UU

NSN 7540-01-280-5500

Standard Form 298 (Rev. 8-98)
Prescribed by ANSI Std. Z39.18

THIS PAGE INTENTIONALLY LEFT BLANK

Approved for public release; distribution is unlimited

CLIMATE AND WEATHER ANALYSIS OF AFGHANISTAN THUNDERSTORMS

Chad E. Geis
Lieutenant Junior Grade, United States Navy
B.S., Fitchburg State College, 2000

Submitted in partial fulfillment of the
requirements for the degree of

MASTER OF SCIENCE IN METEOROLOGY AND PHYSICAL OCEANOGRAPHY

from the

NAVAL POSTGRADUATE SCHOOL
September 2011

Author: Chad E. Geis

Approved by: Tom Murphree
Thesis Advisor

Paul Frederickson
Co-Advisor

Wendell Nuss
Chair, Department of Meteorology

THIS PAGE INTENTIONALLY LEFT BLANK

ABSTRACT

Thunderstorms are a significant factor in the planning and execution of Department of Defense (DoD) operations in Afghanistan, especially in the spring and summer. Skillful forecasting of Afghanistan thunderstorms has proven difficult, even at relatively short lead times of 24 hours or less. This has led to adverse effects on a wide range of DoD missions. One potential reason for the forecasting difficulties is a lack of understanding of the conditions that lead to static instability and thunderstorms in the elevated desert mountain environment that characterizes much of Afghanistan. Much of the thunderstorm forecasting for Afghanistan is based on forecasting methods developed for the contiguous U.S. (CONUS)—for example, the use of CONUS-based static stability indices as indicators of the potential for thunderstorm development. We have investigated methods for improving thunderstorm forecasting in and near Kabul, Afghanistan, by: (1) analyzing interannual to hourly variations in thunderstorm activity; and (2) analyzing the large-scale conditions that are favorable and unfavorable for thunderstorms. We used in situ surface and radiosonde data to characterize the local conditions associated with thunderstorm variations. Our focus was on March–May, the period with the most thunderstorm activity in Kabul. We also used global reanalysis data to analyze the large-scale conditions that are favorable and unfavorable for thunderstorm development. We developed and tested two new static stability indices for use in Kabul. We also developed a large-scale circulation index to describe the regional factors that contribute to thunderstorm variations. Finally, we identified outgoing longwave radiation anomalies that occurred in specific tropical ocean basins as potential precursors for predicting thunderstorm and nonthunderstorm events at lead times of 5–15 days.

THIS PAGE INTENTIONALLY LEFT BLANK

TABLE OF CONTENTS

I. INTRODUCTION 1
A. BACKGROUND 1
1. Motivation 1
B. GEOGRAPHY OF THE STUDY REGION 3
1. Geography of Southwest Asia 3
2. Geography of Afghanistan 6
3. Geography of Kabul, Afghanistan 8
C. LONG-TERM MEAN MARCH–MAY CLIMATOLOGY OF KABUL 10
1. Winter Climatology 10
2. Spring Climatology 11
D. THUNDERSTORM FORECASTING BY 28TH 0WS FOR KABUL 15
E. NATIONAL WEATHER SERVICE METHODS FOR THUNDERSTORM FORECASTING IN HIGH ELEVATION REGIONS 17
1. The High Level Total Totals 17
2. Other NWS Elevated Thunderstorm Forecast Methods 20
F. OTHER REGION SPECIFIC INSTABILITY INDEX STUDIES 21
G. RESEARCH MOTIVATION AND SCOPE 22
1. Specific Problems that Limit Skill in Forecasting Thunderstorms in Kabul 22
a. Failure of CONUS-Based Static Stability/Instability Indices 22
b. Inadequate Observational Data Used for Research and as Inputs to Instability Analyses and Forecast Models 23
c. Lack of Documented Empirical Studies 23
2. Scientific Motivations 24
3. Operational Motivations 24
4. Research Questions and Hypotheses 24
5. Thesis Outline 25

II. DATA AND METHODS 27
A. DATA SETS 27
1. 14th Weather Squadron Kabul Surface Observations 27
a. Description of Data Set 27
b. Strengths 27
c. Limitations 28
2. 14th Weather Squadron Kabul Radiosonde Observations 28
a. Description of Data Set 28
b. Strengths 29

c. Limitations 29
3. 14th Weather Squadron Kabul Static Data on Stability Indices and Thermodynamic Levels 30
a. Description of Data Set 30
b. Strengths 30
c. Limitations 30
4. University of Wyoming Kabul Radiosonde Observations 31
a. Description of Data Set 31
b. Strengths 32
c. Limitations 32
5. NCEP/NCAR Reanalysis 1 32
a. Description of Data Set 32
b. Strengths 33
c. Limitations 33
6. Comments on Data Availability 33
a. Data Sets Not Used and Why 33
b. Data We Wished Existed but Does Not 34
B. ANALYSIS METHODS 34
1. Selection of Kabul TSTM and NTSTM Surface Observation Data Sets and Time Periods Used 34
2. Selection of Kabul TSTM and NTSTM Radiosonde Observation Data Sets and Time Periods Used 35
3. Selection of Kabul TSTM and NTSTM Static Stability Indices and Thermodynamic Levels Data Sets and Time Periods Used 36
4. Variables Used for TSTM and NTSTM Conditional Composite Anomalies, Correlations, and Teleconnections 36
a. 200 hPa Geopotential Height 37
b. 850 hPa Geopotential Height 37
c. 850 hPa Air Temperature 37
d. 850 hPa Specific Humidity 38
e. Precipitable Water 38
f. Precipitation Rate 38
g. Outgoing Longwave Radiation 38
h. 500 hPa Omega 38
i. Sea Surface Temperature 38
j. Lifted Index 39
5. TSTM and NTSTM Analysis Methods 39
a. Necessary Ingredients for Thunderstorm Development 39
b. Skew T – Log P Analyses 40
c. Static Stability/Instability Indices 43
d. TSTM and NTSTM Anomaly Regime Indices 43

III. RESULTS 45
A. THUNDERSTORM AND PRECIPITATION TIME SERIES ANALYSIS 45
1. Seasonal Cycle of Thunderstorm and Precipitation Activity (Monthly and Bi-weekly) 45
2. Hourly Variations in Thunderstorm Activity 49
3. Intraseasonal and Interannual Variations in Thunderstorm Activity 55
B. LONG-TERM MEAN (LTM) REGIONAL CLIMATE 60
1. LTM MAM SST, T850, Z850, Z200, SH850, OLR, and PR 60
C. CLIMATE VARIATION ANALYSIS 66
1. TSTM Conditional Composite Anomaly Results 66
a. Z850 Anomalies 67
b. T850 Anomalies 71
c. SH850 Anomalies 72
d. PW Anomalies 73
e. OLR Anomalies 74
f. Z200 Anomalies 75
g. ω500 Anomalies 76
h. PR Anomalies 77
i. LI Anomalies 78
j. SST Anomalies 79
2. NTSTM Conditional Composite Anomaly Results 80
a. Z850 Anomalies 81
b. T850 Anomalies 84
c. SH850 Anomalies 85
d. PW Anomalies 86
e. OLR Anomalies 87
f. Z200 Anomalies 88
g. ω500 Anomalies 89
h. PR Anomalies 90
i. LI Anomalies 91
j. SST Anomalies 92
3. Comparison of Select TSTM and NTSTM Conditional Composite Anomaly Results 93
a. Z850 TSTM and NTSTM Anomalies 93
b. PW TSTM and NTSTM Anomalies 96
c. TSTM and NTSTM Large-Scale Schematics 98
D. SKEW T – LOG P RESULTS 101
1. TSTM Sounding Analyses 101
a. CAPE, CIN, and LI 102
b. Winds 105
c. Moisture 105
d. High Level Total Totals (HLTT) 106
2. NTSTM Sounding Analyses 106

a. CAPE, CIN, and LI 106
b. Winds 110
c. Moisture 110
d. High Level Total Totals (HLTT) 111
E. NEWLY DEVELOPED KABUL STATIC STABILITY AND INSTABILITY INDICES 111
1. Kabul High Level Total Totals (KHLTT) 112
2. Kabul Thunderstorm Index (KTI) 115
F. TSTM AND NTSTM REGIME INDICES RESULTS 119
G. OLRA PRECURSORS AND POTENTIAL PREDICTORS FOR MEDIUM AND LONG RANGE FORECASTING 124
1. TSTM OLRAs for Minus 15 to 5 Days 125
2. NTSTM OLRAs for Minus 15 to 5 Days 127

IV. SUMMARY, CONCLUSIONS, AND RECOMMENDATIONS 129
A. KEY RESULTS AND CONCLUSIONS 129
B MOTIVATION AND APPLICABILITY TO DOD OPERATIONS 130
C. RECOMMENDATIONS FOR FURTHER RESEARCH 130

LIST OF REFERENCES 133

INITIAL DISTRIBUTION LIST 137

LIST OF FIGURES

Figure 1. The USCENTCOM AOR. Image from ALTERMEDIA.INFO [Accessed online at: http://fr.altermedia.info/general/le-commandement-central-americain-a-un-nouveau-patron_17540.html, March 2011]..... 2

Figure 2. Geography of southwest Asia (SWA). Note the high elevations and complex topography of Afghanistan and the surrounding regions. Also, note the potential sources of moisture for Afghanistan, including the Mediterranean Sea, Black Sea, Caspian Sea, Aral Sea, Red Sea, Gulf of Aden, Arabian Gulf, Arabian Sea, Gulf of Oman, northern Indian Ocean, Bay of Bengal, and western tropical Pacific (not shown). Image adapted from 28 OWS (2011). 4

Figure 3. Geography of Afghanistan and surrounding countries. Note the complex topography that dominates Iran, Afghanistan, Pakistan, Tajikistan, Kyrgyzstan, and western China. Image adapted from 28 OWS (2011). 5

Figure 4. Detailed topography of Afghanistan. Note that Kabul lies on a valley floor surrounded by high mountains. Also note how the orientation of the mountains surrounding Kabul can (1) steer lower tropospheric winds so that they travel along approximately north-south and west-east paths and (2) force orographic lifting very near Kabul. This steering and lifting can contribute to TSTM development over and near Kabul. Image from Tradepoint Afghanistan LTD [Accessed online at: http: //www.tpeu.nl/media/img/big_map_afghanistan.jpg., March 2011]..... 7

Figure 5. Topographic map of Kabul and the surrounding area. Key locations are described in blue text. Winds approaching Kabul along the valley axes are shown schematically by red arrows. Note that Kabul lies on a valley floor that is approximately 5,877 feet above sea level and is flanked on the west, north, and east by mountain ranges and hills, which can cause orographic lifting for winds approaching from the south and/or east. Also note how winds from the north-northeast can be funneled into Kabul. Image adapted from 28 OWS Kabul FRN (2010). 9

Figure 6. Long-term mean (LTM) number of Afghanistan precipitation days during March (top left), April (top right), and May (bottom) based on surface weather observations. A precipitation day is defined as a day with a precipitation water equivalent that is greater than the trace threshold of 0.005 inches. Note the increase in precipitation days from March–April, and a decrease from April–May. Data at individual observation locations are interpolated to provide continuous spatial coverage. Images from 14 WS AFG CR (1991)... 12

Figure 7. Long-term mean (LTM) number of Afghanistan TSTM days during March (top left), April (top right), and May (bottom) based on surface weather observations. A TSTM day is defined as a day with at least one recorded TSTM. Note the large increase in TSTM days from March–April and the large spatial extent of TSTM activity in April. Data at individual observation locations are interpolated to provide continuous spatial coverage. Images from 14 WS AFG CR (1991). 14
Figure 8. The relationships between the high level total totals (HLTT) instability index and precipitation (top left), TSTMs (top right), and severe TSTMs (SVR) and tornado activity (TOR) (bottom) for Reno, NV region, from Milne (2004). Note that higher values of HLTT tend to correspond to higher precipitation, TSTMs, and severe weather. For details, see Milne (2004). 19
Figure 9. Observed Kabul TSTM days for each month of the year (top) and each half-month block of the year (bottom). Based on Kabul TSTM observations during the study period of 04 Mar 2002–31 Jul 2010. A TSTM day is defined as a day that has at least one observed TSTM. Note that March, April, and May (MAM, red box) account for 60% of the TSTM days during the study period. Note the gradual increase in TSTM day frequency beginning during early March and peaking in the middle of April, which is then followed by a gradual decrease as spring transitions to summer during late May. 46
Figure 10. Observed Kabul monthly precip and TSTM hours. Based on Kabul precip and TSTM observations during the study period of 04 Mar 2002–31 Jul 2010. A precip hour is defined as an hour with a precipitation water equivalent greater than the trace threshold value of 0.005 inches. A TSTM hour is defined as an hour with at least one TSTM. Note: (1) the largest number of both precip hours and TSTM hours in March-April-May (MAM); and (2) the indications of an overall positive correlation on a monthly basis between precip hours and TSTM hours. 47
Figure 11. Observed Kabul half-monthly precipitation hours and TSTM hours during March-April-May (MAM). Based on Kabul precipitation and TSTM observations during the study period of 04 Mar 2002–31 Jul 2010. A precipitation hour is defined as an hour with a precipitation water equivalent greater than the trace threshold value of 0.005 inches. A TSTM hour is defined as an hour that has at least one TSTM. Note that there is a general correspondence between precipitation hours and TSTM hours, but that the peak in precipitation hours occurs in the second half of March and first half of April, about two to four weeks prior to the peak in TSTM hours in the second half of April. 48

Figure 12. Time of day when Kabul TSTMs occur for: (top) all months of the year and (bottom) March-April-May (MAM). Based on Kabul TSTM observations during the study period of 04 Mar 2002–31 Jul 2010. Note that, when averaged over all months, the peak time of day for TSTM activity is approximately 1400 UTC/1830 Kabul local time (KLT). But, when averaged over only MAM, the peak time of day for TSTM activity is approximately 1200 UTC/1630 KLT. 50
Figure 13. Time of day when Kabul TSTMs occur for: (top) March; (bottom left) 01–16 March; and (bottom right) 17–31 March. Based on Kabul TSTM observations during the study period of 04 Mar 2002–31 Jul 2010. Note that the March peak in TSTM activity is at approximately 0900–1400 UTC/1330–1830 KLT. 52
Figure 14. Time of day when Kabul TSTMs occur for: (top) April; (bottom left) 01–15 April; and (bottom right) 16–30 April. Based on Kabul TSTM observations during the study period of 04 Mar 2002–31 Jul 2010. Note that the April peak in TSTM activity is at approximately 0700–1600 UTC/1130–2030 KLT..... 53
Figure 15. Time of day when Kabul TSTMs occur for: (top) May; (bottom left) 01–16 May; and (bottom right) 17–31 May. Based on Kabul TSTM observations during the study period of 04 Mar 2002–31 Jul 2010. Note that the May peak in TSTM activity is at approximately 0800–1500 UTC/1230–1930 KLT..... 54
Figure 16. Observed Kabul TSTM days in March, April, and May (MAM) during 2002–2010. Based on Kabul TSTM observations during the study period of 04 Mar 2002–31 Jul 2010. A TSTM day is defined as a day that has at least one TSTM. Note the large intraseasonal and interannual variability in March–May TSTM activity, and the absence of TSTM days during May 2006 and March 2010. 56
Figure 17. Observed Kabul TSTM days in March (top left), April (top right), and May (bottom) during 2002–2010. Based on Kabul TSTM observations during the study period of 04 Mar 2002–31 Jul 2010. A TSTM day is defined as a day that has at least one TSTM. Note the large percentage interannual variability in March– May TSTM activity, and the absence of TSTM days during May 2006 and March 2010. The curves in each panel represent a smooth fit to the individual monthly values (Figure 16). The straight black lines represent nine-year linear trends. Note that: (1) March shows a decreasing linear trend and evidence of an interannual variation with a four-year period; (2) April shows an increasing linear trend and evidence of an interannual variation with a five-year period; and (3) May shows an increasing linear trend and evidence of an interannual variation with a four- year period..... 58
Figure 18. Observed Kabul TSTM hours in March (top left), April (top right), and May (bottom) during 2002–2010. Based on Kabul TSTM observations during the study period of 04 Mar 2002–31 Jul 2010.

A TSTM hour is defined as an hour that has at least one TSTM. Note the large interannual variability in March–May hourly TSTM activity, and the absence of TSTM hours during May 2006 and March 2010. The red lines in each panel represent a moving average based on the previous two-year average value of TSTM hours observed. The straight black lines represent nine-year linear trends. Note that each month shows evidence of interannual variations with periods of about 4–5 years, and that March shows a decreasing linear trend. Comparison of Figures 13–18 provides evidence of a positive correlation between the number of TSTM days and the number of TSTM hours for March and April (MA) and a negative correlation between the number of TSTM days and the number of TSTM hours for May. Thus, when MA has a large (small) number of TSTM days they also tend to have a large (small) number of TSTM hours. When May has a large (small) number of TSTM days, it tends to have a smaller (larger) number of TSTM hours. 59

Figure 19. Long-term mean (LTM) sea surface temperature (SST; $^{\circ}$C) for March-April-May (MAM). Note the warm tropical and subtropical waters to the south and east of AFG and the cooler waters in the Mediterranean, Caspian, Black, and Aral Seas to the north and west of AFG. LTM base period: 1968–1996. 61

Figure 20. Long-term mean (LTM) 850 hPa (Z850) air temperature (T850; $^{\circ}$C) for March-April-May (MAM). Note the warm (cool) air to the south (north) of Afghanistan and the large temperature gradients to the north of Afghanistan. LTM base period: 1968–1996. 61

Figure 21. Long-term mean (LTM) 850 hPa specific humidity (SH850, kg/kg) for March-April-May (MAM). The contour interval is 0.0004 kg/kg. Note the generally high SH850 in the tropics and southeast Asia extending into northern Pakistan and northeast Afghanistan, and the generally low SH850 over SWA and most of India. LTM base period: 1968–1996. 62

Figure 22. Long-term mean (LTM) 850 hPa geopotential height (Z850, gpm) for March-April-May (MAM). Note the ridging centered near the Arabian Peninsula and western China, with a trough extending southeastward from Iran, across AFG, Pakistan, and north India. LTM base period: 1968–1996. 63

Figure 23. Long-term mean (LTM) 200 hPa geopotential height (Z200, gpm) for March-April-May (MAM). Note that AFG lies to the east of a broad trough centered over southern Europe and to the west of broad ridge centered over western China. LTM base period: 1968–1996. 64

Figure 24. Long-term mean (LTM) outgoing longwave radiation (OLR, W/m^2) for March-April-May (MAM). Note: (1) the generally high OLR over the NIO, indicating low levels of non-convective activity; and (2) the

generally low OLR over western-central China, northern AFG, and west of the Caspian Sea, indicating cold surface and lower tropospheric temperatures and/or low levels of deep convective activity. LTM base period: 1968–1996. 65
Figure 25. Long-term mean (LTM) precipitation rate (PR, mm/day) for March-April-May (MAM). Note: (1) the low PR over northern Africa, SWA, and most of India; and (2) the relatively high PR over much of the tropics, Southeast Asia, and northern Afghanistan and Pakistan. LTM base period: 1968–1996. 66
Figure 26. TSTM conditional composite anomalies of 850 hPa geopotential height (Z850; gpm) for: (a) Mar, (b) Apr, and (c) May. Based on Kabul TSTM observations during 04 Mar 2002–31 Jul 2010. Note the similar patterns for the three months, especially the anomalous four-part pattern with a: (1) L centered near central Asia; (2) L centered near southeastern Saudi Arabia; (3) H centered near and east of the Caspian Sea; and (4) H centered near Tibet. This pattern is favorable for anomalous warm-moist air advection (WMAA) from the southeast and cold-dry air advection (CDAA) from the northwest into AFG. This leads to anomalous LLCON over AFG—for example, anomalous WMAA from the Arabian Sea and Bay of Bengal, and CDAA from central Eurasia east of the Caspian Sea. 68
Figure 27. TSTM conditional composite anomalies of 850 hPa geopotential height (Z850; gpm) for MAM. Based on Kabul TSTM observations during 04 Mar 2002–31 Jul 2010. Note: (1) the anomalous L centered over the Strait of Hormuz and the anomalous H centered over Tibet that together support anomalous WMAA into AFG; and (2) the anomalous H centered over the Caspian Sea and the anomalous L centered over central Asia that together support anomalous CDAA toward AFG. The net effect is anomalous LLCON over AFG of CDA from the north and WMA from the south. These anomaly patterns help identify the regional climate regimes and physical mechanisms that are favorable for TSTM activity over AFG. 69
Figure 28. TSTM conditional composite anomalies of 850 hPa geopotential height (Z850; gpm) for MAM. Based on Kabul TSTM observations during 04 Mar 2002–31 Jul 2010. Black arrows represent corresponding Z850 anomalous winds. Note the indications of anomalous advection of: (1) mT air from the Arabian Sea, Bay of Bengal, and South China Sea; (2) cP air from central Russia; and (3) LLCON of mT air and cP air over AFG. 70
Figure 29. TSTM conditional composite anomalies of 850 hPa air temperature (T850; °C) for MAM. Based on Kabul TSTM observations during 04 Mar 2002–31 Jul 2010. Black arrows represent corresponding Z850 anomalous winds (see Figure 28). Note the indications of: (1)

cool anomalies to the northwest of AFG associated with the anomalous northwestward flow from Russia; and (2) warm anomalies to the southeast of AFG associated with the anomalous southward flow from the Arabian Sea and Bay of Bengal..... 71
Figure 30. TSTM conditional composite anomalies of 850 hPa specific humidity (SH850; kg/kg) for MAM. Based on Kabul TSTM observations during 04 Mar 2002–31 Jul 2010. The contour interval is 0.0001 kg/kg. Black arrows represent corresponding Z850 anomalous winds (Figure 28). Note that the positive SH850 anomalies over the GoA, NIO, northern India, BoB, MC, and AFG are consistent with the WMAA from the south toward AFG indicated by the corresponding Z850 and T850 anomalies (Figures 28–29). 72
Figure 31. TSTM conditional composite anomalies of precipitable water (PW; kg/m^2) for MAM. Based on Kabul TSTM observations during 04 Mar 2002–31 Jul 2010. Black arrows represent corresponding Z850 anomalous winds (Figure 28). The PW anomalies are very similar to the SH850 anomalies (Figure 30). For example, both the SH850 and PW anomalies indicate that there is anomalous positive moisture advection into AFG from the NIO, northern India, and BoB..... 73
Figure 32. TSTM conditional composite anomalies of outgoing longwave radiation (OLR; W/m^2) for MAM. Based on Kabul TSTM observations during 04 Mar 2002–31 Jul 2010. Note the maximum negative OLR anomalies, consistent with anomalous deep convection, over northern AFG and the southern Stans region. Also, note the widespread negative OLR anomalies over the western tropical Pacific Ocean, BoB, and NIO. These tropical OLR anomalies indicate that AFG TSTM activity may be linked to remote tropical convective anomalies (e.g., those associated with climate variations, such as the Madden-Julian Oscillation, Indian Ocean Zonal Mode, and El Nino – La Nina)..... 75
Figure 33. TSTM conditional composite anomalies of 200 hPa geopotential height (Z200; gpm) for MAM. Based on Kabul TSTM observations during 04 Mar 2002–31 Jul 2010. The anomalous upper level trough-ridge pattern over south-central Asia and centered near AFG indicates anomalous upper level divergence, upward vertical motion, and positive vorticity advection—all favorable for TSTM development over AFG..... 76
Figure 34. TSTM conditional composite anomalies of 500 hPa omega (ω500; Pa/s) (top) and OLR (W/m^2) anomalies (bottom) for MAM. Based on Kabul TSTM observations during 04 Mar 2002–31 Jul 2010. The ω500 contour interval is 0.004 Pa/s. Note that the results in these two panels are consistent with each other and with prior TSTM composite figures in indicating anomalous LLCON of warm

moist air, UVM, and deep convection over AFG and PAK during TSTM periods (Figures 28–33). 77
Figure 35. TSTM conditional composite anomalies of 500 hPa omega (ω500; Pa/s) (top) and precipitation rate (PR; mm/day) anomalies (bottom) for MAM. Based on Kabul TSTM observations during 04 Mar 2002–31 Jul 2010. The ω500 contour interval is 0.004 Pa/s. The anomalous UVM and positive PR anomalies over AFG are consistent with the corresponding circulation and implied advection anomalies (Figures 28–34) and with enhanced TSTM activity near AFG. 78
Figure 36. TSTM conditional composite anomalies for MAM of: (top) 500 hPa omega (ω500; Pa/s) and (bottom) LI (^{o}C). Based on Kabul TSTM observations during 04 Mar 2002–31 Jul 2010. The ω500 contour interval is 0.004 Pa/s. Note the general correspondence between UVM (DVM) and negative (positive) values of LI, indicating instability (stability), especially near AFG and PAK (SWA and Tibet). 79
Figure 37. TSTM conditional composite anomalies of Z850 (gpm) (top) and Sea Surface Temperature Anomalies (SSTAs) ($^{\circ}$C) (bottom) for MAM. Based on Kabul TSTM observations during 04 Mar 2002–31 Jul 2010. Black arrows represent corresponding Z850 anomalous winds (Figure 28). Note that winds converging toward AFG from the south may be anomalously warm and moist due to positive SSTAs in the NIO, AS, BoB, and SCS. Anomalously warm moist air converging with cool dry air from the north over AFG would lead to enhanced instability. 80
Figure 38. NTSTM conditional composite anomalies of 850 hPa geopotential height (Z850; gpm) for: (a) Mar, (b) Apr, and (c) May. Based on Kabul NTSTM observations during 04 Mar 2002–31 Jul 2010. Note the similar patterns for the three months, especially the anomalous Hs across central Asia extending into SWA, leading to anomalous CDAA from the northeast into AFG and anomalous blocking of WMAA into AFG from the south. 82
Figure 39. NTSTM conditional composite anomalies of 850 hPa geopotential height (Z850; gpm) for MAM. Based on Kabul NTSTM observations during 04 Mar 2002–31 Jul 2010. Note the anomalous H centered over central Asia and extending to Iraq indicating anomalous CDAA into AFG from the northeast and anomalous blocking of WMAA into AFG from the south. These anomaly patterns help identify the climate regimes and physical mechanisms that are favorable for NTSTM activity near Kabul. 83
Figure 40. NTSTM conditional composite anomalies of 850 hPa geopotential height (Z850; gpm) for MAM. Based on Kabul NTSTM observations during 04 Mar 2002–31 Jul 2010. Black arrows represent corresponding Z850 anomalous winds. Note the

indications over and near AFG of anomalous: (1) advection of cP air from central and northern Asia toward AFG: and (2) blocking by the anomalous H over south-central Asia of ETCs and advection of mT from the tropics into AFG. 84
Figure 41. NTSTM conditional composite anomalies of 850 hPa air temperature (T850; °C) for MAM. Based on Kabul NTSTM observations during 04 Mar 2002–31 Jul 2010. Black arrows represent corresponding Z850 anomalous winds (Figure 40). Note that the T850 anomalies over much of Asia are broadly consistent with the anomalous advection and/or vertical motion implied by the corresponding LTM T850 and anomalous Z850 (Figures 20 and 40). 85
Figure 42. NTSTM conditional composite anomalies of 850 hPa specific humidity (SH850; kg/kg) for MAM. Based on Kabul NTSTM observations during 04 Mar 2002–31 Jul 2010. The contour interval is 0.0001 kg/kg. Black arrows represent corresponding Z850 anomalous winds (Figure 40). Note the band of negative SH850 anomalies extending from SWA across AFG and central China, consistent with the corresponding anomalous 850 hPa heights and winds. 86
Figure 43. NTSTM conditional composite anomalies of precipitable water (PW; kg/m^2) for MAM. Based on Kabul NTSTM observations during 04 Mar 2002–31 Jul 2010. Black arrows represent corresponding Z850 anomalous winds (Figure 40). The PW anomalies are similar to the SH850 anomalies (Figure 42) and provide additional evidence of anomalously negative moisture advection into AFG and nearby areas. 87
Figure 44. NTSTM conditional composite anomalies of outgoing longwave radiation (OLR; W/m^2) for MAM. Based on Kabul NTSTM observations during 04 Mar 2002–31 Jul 2010. Note the positive OLR anomaly area centered near AFG-PAK and indicating anomalously weak convection. Also, note the widespread negative OLR anomalies over much of the NIO, western tropical Pacific Ocean, and South Pacific Convergence Zone (SPCZ). These tropical OLR anomalies indicate that AFG NTSTM activity may be linked to remote tropical convective anomalies (e.g., those associated with climate variations, such as the Madden-Julian Oscillation, Indian Ocean Zonal Mode, and El Nino–La Nina). 88
Figure 45. NTSTM conditional composite anomalies of 200 hPa geopotential height (Z200; gpm) for MAM. Based on Kabul NTSTM observations during 04 Mar 2002–31 Jul 2010. The anomalous upper level trough-ridge-trough pattern over western Russia, SWA, and western China indicates anomalously unfavorable conditions over AFG-PAK for deep convection and TSTM development. 89

Figure 46. NTSTM conditional composite anomalies of 500 hPa omega (ω500; Pa/s) (top) and OLR (W/m^2) anomalies (bottom) for MAM. Based on Kabul NTSTM observations during 04 Mar 2002–31 Jul 2010. The ω500 contour interval is 0.004 Pa/s. Note that the results in these two panels are consistent with each other and with prior NTSTM conditional composite figures in indicating anomalous blocking of warm moist air, DVM, and weak or absent convection over AFG and PAK during NTSTM periods (Figures 40–45). 90
Figure 47. NTSTM conditional composite anomalies of 500 hPa omega (ω500; Pa/s) (top) and precipitation rate (PR; mm/day) anomalies (bottom) for MAM. Based on Kabul NTSTM observations during 04 Mar 2002–31 Jul 2010. The ω500 contour interval is 0.004 Pa/s. The anomalous DVM and negative PR anomalies over and near AFG and PAK are consistent with enhanced NTSTM activity near Kabul... 91
Figure 48. NTSTM conditional composite anomalies for MAM of: (top) 500 hPa omega (ω500; Pa/s) and (bottom) LI. Based on Kabul NTSTM observations during 04 Mar 2002–31 Jul 2010. The ω500 contour interval is 0.004 Pa/s. Note the DVM and positive values of LI, indicating stability over AFG and PAK. 92
Figure 49. NTSTM conditional composite anomalies of Z850 (gpm) (top) and SSTAs (°C) (bottom) for MAM. Based on Kabul NTSTM observations during 04 Mar 2002–31 Jul 2010. Black arrows represent corresponding Z850 anomalous winds. Note the positive SSTAs in the NIO and the indications of anomalous blocking of flow from the tropics toward AFG (see Figure 40). Compare with corresponding TSTM anomalies (Figure 37). 93
Figure 50. TSTM (left) and NTSTM (right) conditional composite anomalies of 850 hPa geopotential height (Z850; gpm) for MAM. Based on Kabul TSTM and NTSTM observations during 04 Mar 2002–31 Jul 2010. Black arrows represent corresponding Z850 anomalous winds. Note the indications over and near AFG of anomalous: (1) LLCON of CDAA from the north and WMAA from the south over AFG in the TSTM composite (Figures 28–37); (2) CDAA from the NE and a blocking of ETCs and WMAA from the south over AFG in the NTSTM composite (Figures 40-49). 95
Figure 51. TSTM (left) and NTSTM (right) conditional composite anomalies of precipitable water (PW; kg/m^2) for MAM. Based on Kabul TSTM and NTSTM observations during 04 Mar 2002–31 Jul 2010. Black arrows represent corresponding Z850 anomalous winds. Note the indications over and near AFG of anomalous: (1) MAA from the south and DAA from the north (Figures 28–37) in the TSTM regime; (2) DAA from the northeast and a blocking of MAA from the south into AFG (Figures 40–49) in the NTSTM regime. 97
Figure 52. Schematic depiction of the large-scale low level geopotential heights (Z850) and wind anomalies for TSTM periods in Kabul,

Afghanistan during spring (March–May). Based on TSTM conditional composite anomalies of Z850 shown in Figure 28. Note the anomalous convergence over AFG of: (1) WMAA from the NIO, AS, BoB, and SCS; and (2) CDA from the north. These circulation anomalies are consistent with: (1) anomalous enhancements of moisture, lift, and instability; and (2) favorable conditions for TSTM development over AFG..... 99

Figure 53. Schematic depiction of the large-scale low level geopotential heights (Z850) and wind anomalies for NTSTM periods in Kabul, Afghanistan during spring (March–May). Based on NTSTM conditional composite anomalies of Z850 shown in Figure 40. Note that the anomalously high heights over SWA and central Asia lead to anomalous CDAA into AFG, and blocking over AFG of ETCs and warm moist air from the south. These circulation anomalies are consistent with unfavorable conditions for TSTM development over AFG. 100

Figure 54. Skew T – log p analysis of average MAM TSTM sounding. Thermodynamic parameters are determined by using the SFC heating of the air parcel method. Based on Kabul TSTM radiosonde observations from the 14 WS during 24 Feb 2003–30 Jun 2010 and the UWY radiosonde observations from 24 Feb 2003–24 Aug 2010. Note the: (1) large CAPE (red + area) and smaller CIN (blue–area); (2) SW-erly wind direction at 700 hPa and higher consistent with WMAA; (3) dew point depression of 5^{o}C or < from 650–500 hPa indicating LL moisture; (4) lower LCL and CCL compared to the NTSTM sounding (Figure 56) indicating more CAPE in TSTM conditions; (5) lower T_c compared to NTSTM T_c (Figure 56); (6) conditionally unstable air associated with LL moisture; (7) HLTT and LI values that are consistent with instability. 103

Figure 55. Skew T–log p analysis of average MAM TSTM sounding. Thermodynamic parameters are determined by using the SFC lifting of the air parcel method. Based on Kabul TSTM radiosonde observations from the 14 WS during 24 Feb 2003–30 Jun 2010 and the UWY radiosonde observations from 24 Feb 2003–24 Aug 2010. Note the: (1) small CAPE (red + area) and relatively small CIN (blue - area); (2) SW-erly wind direction from 700 hPa and up consistent with WMAA; (3) dew point depression of 5^{o}C or < from 650–500 hPa indicating LL moisture; (4) lower LCL and a LFC compared to the NTSTM LCL and lack of LFC (Figure 57) indicating more CAPE in TSTM conditions; (5) lower T_c compared to NTSTM T_c (Figure 57); (6) conditionally unstable air made associated with LL moisture; (7) HLTT and LI values that are consistent with instability. 104

Figure 56. Skew T–log p analysis of average MAM NTSTM sounding. Thermodynamic parameters are determined by using the SFC heating of the air parcel method. Based on Kabul NTSTM

radiosonde observations from the 14 WS during 24 Feb 2003–30 Jun 2010 and the UWY radiosonde observations from 24 Feb 2003–24 Aug 2010. Note the: (1) small CAPE and large CIN; (2) NW-erly winds at and above 700 hPa; (3) SFC dew point depression of 29°C; (4) higher LCL and CCL compared to the TSTM LCL and CCL (Figure 54) consistent with small CAPE; (5) higher T_c compared to TSTM T_c (Figure 54); (6) unrealized conditionally unstable air due to lack of LL moisture; (7) HLTT and LI values consistent with stable conditions. 108

Figure 57. Skew T–log p analysis of average MAM NTSTM sounding. Thermodynamic parameters are determined by using the SFC lifting of the air parcel method. Based on Kabul NTSTM radiosonde observations from the 14 WS during 24 Feb 2003–30 Jun 2010 and the UWY radiosonde observations from 24 Feb 2003–24 Aug 2010. Note the: (1) lack of CAPE and large CIN; (2) NW-erly winds at and above 700 hPa; (3) SFC dew point depression of 29°C; (4) higher LCL compared to the TSTM LCL (Figure 55) consistent with low CAPE; (5) higher T_c compared to TSTM T_c (Figure 55); (6) unrealized conditionally unstable air due to lack of LL moisture; (7) HLTT and LI values consistent with stable conditions. 109

Figure 58. The number of soundings by HLTT value and by TSTM (red) and NTSTM (blue) conditions. Based on Kabul TSTM and NTSTM radiosonde observations from the 14 WS during 24 Feb 2003–30 Jun 2010 and the UWY radiosonde observations from 24 Feb 2003–24 Aug 2010. Notice the large overlap in the distributions in the 26–34°C HLTT range and the similar HLTT values for the TSTM and NTSTM peaks. 112

Figure 59. MAM TSTM (solid) and NTSTM (dashed) soundings. Based on Kabul TSTM and NTSTM radiosonde observations from the 14 WS during 24 Feb 2003–30 Jun 2010 and the UWY radiosonde observations from 24 Feb 2003–24 Aug 2010. Note that the largest TSTM-NTSTM differences occur at about 800 hPa for both temperature and dew point. 113

Figure 60. The number of soundings by KHLTT value and by TSTM (red) and NTSTM (blue) conditions. Based on Kabul TSTM and NTSTM radiosonde observations from the 14 WS from 24 Feb 2003 to 30 Jun 2010 and the UWY radiosonde observations from 24 Feb 2003–24 Aug 2010. Notice how the peaks in TSTM and NTSTM occurrence are more widely spaced than those for the HLTT distributions (Figure 58). 114

Figure 61. Distributions for TSTM and NTSTM KTI values. Based on Kabul TSTM and NTSTM radiosonde observations from the 14 WS during 24 Feb 2003–30 Jun 2010 and the UWY radiosonde observations from 24 Feb 2003–24 Aug 2010. Notice how the TSTM and NTSTM peak occurrences and overall distributions are farther

spread apart than the KHLTT distributions. This indicates that the KTI predicts stability and instability more accurately than the KHLTT. 116
Figure 62. Probability of detection (PoD, red line) and false alarm rate (FAR, blue line) for 90 TSTM and 90 NTSTM KTI values. Based on Kabul TSTM and NTSTM radiosonde observations from the 14 WS during 24 Feb 2003–30 Jun 2010 and the UWY radiosonde observations from 24 Feb 2003–24 Aug 2010. Note that KTI threshold values of 20-24°C provide the best PoD to FAR ratios, with a KTI of 24°C yielding a PoD of 90% and a FAR of 16%. 118
Figure 63. The five regions (outlined by five black boxes) from which the Z850 anomalies were used to calculate the TSTM climate regime index. The color shading and contours show the TSTM conditional composite Z850 anomalies for MAM (Figure 28). The five boxes were selected to represent the centers of the circulation anomalies that are favorable for TSTM activity over AFG. 120
Figure 64. The four regions (outlined by four black boxes) from which the Z850 anomalies were used to calculate the NTSTM climate regime index. The color shading and contours show the NTSTM conditional composite Z850 anomalies for MAM (Figure 40). The four boxes were selected to represent the centers of the circulation anomalies that are favorable for NTSTM activity over AFG. 123
Figure 65. TSTM conditional composite anomalies of outgoing longwave radiation (OLR; W/m^2) during MAM for 15 days before TSTM event (top left), 10 days before TSTM event (top right), and 5 days before TSTM event (bottom). Based on Kabul TSTM observations during 04 Mar 2002–31 Jul 2010. Note the general decrease in implied convection over the NIO, BoB, SCS, and SPCZ as the lead-time decreases. 126
Figure 66. NTSTM conditional composite anomalies of outgoing longwave radiation (OLR; W/m^2) during MAM for 15 days before NTSTM event (top left), 10 days before NTSTM event (top right), and 5 days before NTSTM event (bottom). Based on Kabul NTSTM observations during 04 Mar 2002–31 Jul 2010. Note the general increase in implied convection over the NIO, BoB, SCS, western tropical Pacific, and SPCZ as the lead-time decreases. 128

LIST OF TABLES

Table 1. HLTT threshold values (^{o}C) and corresponding TSTM forecasts (From Milne 2004). 18
Table 2. TSTM and NTSTM conditional composite anomaly variables, abbreviations, and units. 37
Table 3. CONUS based CAPE threshold values and corresponding atmospheric stability or instability. CAPE values adapted from Wallace and Hobbs (2006). 41
Table 4. CONUS based LI threshold values and corresponding atmospheric stability or instability. LI values adapted from Weather Prediction Education and Resources [Accessed online at: http://www.theweatherprediction.com, March 2011]. 43
Table 5. MAM weighted average instability index values for TSTM periods. Weighted average index values calculated from individual index values provided by the 14 WS. The process used to identify TSTM periods is described in Chapter II, Section B.3. 105
Table 6. MAM weighted average instability index values for NTSTM periods. Weighted average index values calculated from individual index values provided by the 14 WS. The process used to identify NTSTM periods is described in Chapter II, Section B.3. 110
Table 7. Latitudes and longitudes for the five TSTM index boxes. 121
Table 8. Latitudes and longitudes for the four NTSTM index boxes. 124

THIS PAGE INTENTIONALLY LEFT BLANK

LIST OF ACRONYMS AND ABBREVIATIONS

14 WS	14th Weather Squadron
28 OWS	28th Operational Weather Squadron
AFCCC	Air Force Combat Climatology Center
AFG	Afghanistan
AG	Arabian Gulf
AM	April-May
AOR	Area of Responsibility
AS	Arabian Sea
BoB	Bay of Bengal
BRN	Bulk Richardson Number
°C	Degrees Celsius
CAPE	Convective Available Potential Energy
CCL	Convective Condensation Level
CDA	Cold Dry Air
CDAA	Cold Dry Air Advection
CIN	Convective Inhibition
Climo	Climatology
cm	Centimeter(s)
CONUS	Continental United States
cP	Continental Polar
CR	Climatology Report
CT	Cross Totals
DAA	Dry Air Advection
DALR	Dry Adiabatic Lapse Rate
DJFM	December-January-February-March
DoD	Department of Defense
DVM	Downward Vertical Motion
E	East
EL	Equilibrium Level
ELR	Environmental Lapse Rate
ENLN	El Nino – La Nina
ENSO	El Nino-Southern Oscillation
ESE	East-Southeast
ESRL	Earth System Research Laboratory
ETC	Extratropical Cyclone
FAR	False Alarm Rate
FOB	Forward Operating Base
FRN	Forecaster Reference Notebook
GFS	Global Forecast System
GoA	Gulf of Aden
GOES	Geostationary Operational Environmental Satellite
GoM	Glossary of Meteorology

GoO	Gulf of Oman
gpm	Geopotential Meter(s)
H	High Pressure Cell (Anticyclone)
HLTT	High Level Total Totals
hPa	Hectopascal(s)
in	Inches
IO	Indian Ocean
IOZM	Indian Ocean Zonal Mode
J/kg	Joules per Kilogram
K	Kelvin
KHLTT	Kabul High Level Total Totals
KI	K Index
KLT	Kabul Local Time
km	Kilometer(s)
km^2	Kilometer(s) Squared
KO	KO Index
KTI	Kabul Thunderstorm Index
kts	Knots
L	Low Pressure Cell (Cyclone)
LCL	Lifted Condensation Level
LFC	Level of Free Convection
LI	Lifted Index
LL	Low Level
LLCON	Low Level Convergence
LLDIV	Low Level Divergence
LRF	Long Range Forecast
LTM	Long-Term Mean(s)
m	Meter(s)
m^2	Meter(s) Squared
m/s	Meter(s) per Second
MA	March-April
MAA	Moist Air Advection
MALR	Moist Adiabatic Lapse Rate
MAM	March-April-May
MC	Maritime Continent
ME	Middle East
METAR	Meteorological Terminal Air Report
METOC	Meteorology and Oceanography
MJO	Madden-Julian Oscillation
MLCAPE	Mean Layer Convective Available Potential Energy
mm	Millimeter(s)
MRF	Medium Range Forecast
mT	Maritime Tropical
MUCAPE	Most Unstable Convective Available Potential Energy
N	North

NCAR	National Center for Atmospheric Research
NCEP	National Centers for Environmental Predication
NE	Northeast
NE-ern	Northeastern
NIO	Northern Indian Ocean
NNE	North-Northeast
NNW	North-Northwest
NOAA	National Oceanographic and Atmospheric Administration
NPS	Naval Postgraduate School
NRI	Non-thunderstorm Regime Index
NTSTM	Non-Thunderstorm
NVA	Negative Vorticity Advection
NW	Northwest
NW-erly	Northwesterly
NW-ern	Northwestern
NWP	Numerical Weather Prediction
NWS	National Weather Service
OCDS	Operational Climatic Data Summary
OEF-A	Operation Enduring Freedom-Afghanistan
OLR	Outgoing Longwave Radiation
OLRA	Outgoing Longwave Radiation Anomaly(ies)
Pa	Pascal
PAK	Pakistan
PoD	Probability of Detection
PR	Precipitation Rate
precip	Precipitation
PVA	Positive Vorticity Advection
PW	Precipitable Water
R1	NCEP Reanalysis Data Set One
RS	Red Sea
RoT	Rule(s) of Thumb
s	Second(s)
SA	Southern Asia
SCS	South China Sea
SE	Southeast
SE-erly	Southeasterly
SE-ern	Southeastern
SFC	Surface
SH850	Specific Humidity at 850 Hectopascals
SI	International System of Units
SoH	Strait of Hormuz
SPCZ	South Pacific Convergence Zone
SST	Sea Surface Temperature
SSTA	Sea Surface Temperature Anomaly(ies)
SSW	South-Southwest

SSW-erly	South-Southwesterly
STJ	Subtropical Jet
SVR	Severe Thunderstorms
SW	Southwest
SWA	Southwest Asia
SWEAT	Severe Weather Threat Index
SW-ern	Southwestern
T	Temperature
T850	Temperature at 850 Hectopascals
TAF	Terminal Aerodrome Forecast
T_c	Convective Temperature
TOR	Tornadoes
TRI	Thunderstorm Regime Index
TSTM	Thunderstorm
TT	Total Totals
UCAR	University Corporation for Atmospheric Research
UL	Upper Level
USAF	United States Air Force
USCENTCOM	United States Central Command
UTC	Coordinated Universal Time
UVM	Upward Vertical Motion
UWY	University of Wyoming
VT	Vertical Totals
ω	Omega
ω500	Omega at 500 Hectopascals
WMA	Warm Moist Air
WMAA	Warm Moist Air Advection
WMO	World Meteorological Organization
WWAs	Warnings Watches and Advisories
Z	Geopotential Height
Z200	200 Hectopascal Geopotential Height
Z850	850 Hectopascal Geopotential Height

ACKNOWLEDGMENTS

I owe a tremendous debt of gratitude to my advisors, Dr. Tom Murphree and Mr. Paul Frederickson. Dr. Murphree's brilliance in the fields of meteorology and climatology, along with his enlightening teaching abilities, provided unwavering support, which enabled the successful accomplishments of this thesis. Mr. Paul Frederickson's genius in Matlab programming allowed us the ability to analyze important data, which led to some of the most exciting breakthroughs in this thesis.

I would like to thank the 28th Operational Weather Squadron (28 OWS) for proposing this thesis topic and participating in the many telephone conferences and e-mails, which greatly helped us in achieving productive results for the operational forecaster. The 14th Weather Squadron (14 WS) and University of Wyoming (UWY) played a pivotal role in our success by providing invaluable thesis data. The National Weather Service (NWS) forecast offices in California, Wyoming, Utah, Idaho, Colorado, New Mexico, Arizona, and Nevada all provided us with helpful insights that led to our progress. Dr. Thomas Warner of the University Corporation for Atmospheric Research (UCAR) in Boulder, CO also provided suggestions that led to a better approach to our research topic. The National Oceanographic and Atmospheric Administration (NOAA) Earth Systems Research Laboratory (ESRL) websites were invaluable in providing access to and visualizations of the long-term means and composite anomalies shown in Chapter III, Sections B-C, F-G.

Finally, and dearest to my heart, I must thank my amazing and very sage parents, Carl and Margaret Geis, and my ingenious brother, Corey Geis, for their love and boundless support during all my years. To my angelic wife, Jamie, you have given me the precious moments of love, laughter, and sanity, which has kept me grounded during this long graduate school process. Thank you all for your love and support over the years.

THIS PAGE INTENTIONALLY LEFT BLANK

I. INTRODUCTION

A. BACKGROUND

1. Motivation

In response to the attacks on the U.S. on 11 September 2001, President George W. Bush committed U.S. troops to combat operations in Afghanistan (AFG) on 07 October 2001. During the last decade of the 20th century, and into the 21st century, the U.S. has been involved in its longest-lasting war, the war in Afghanistan, otherwise known as Operation Enduring Freedom-Afghanistan (OEF-A) (Nagorski 2010). During this campaign, the military's meteorology and oceanography (METOC) community has struggled with the unfamiliar environment of the Middle East (ME). Even with today's technology, weather forecasting for this area, part of the U.S. Central Command area of responsibility (USCENTCOM AOR, see Figure 1), has proven to be a challenge.

The 28th Operational Weather Squadron (28 OWS), located on Shaw Air Force Base in South Carolina, is responsible for producing and disseminating METOC analyses, forecasts, and briefings to support mission planning for all U.S. military forces operating in the USCENTCOM AOR. The 28 OWS provides base and post forecasts, briefings for transient aircrews, as well as all weather watches, warnings, and advisories (WWAs) for their geographical units (28 OWS 2011).

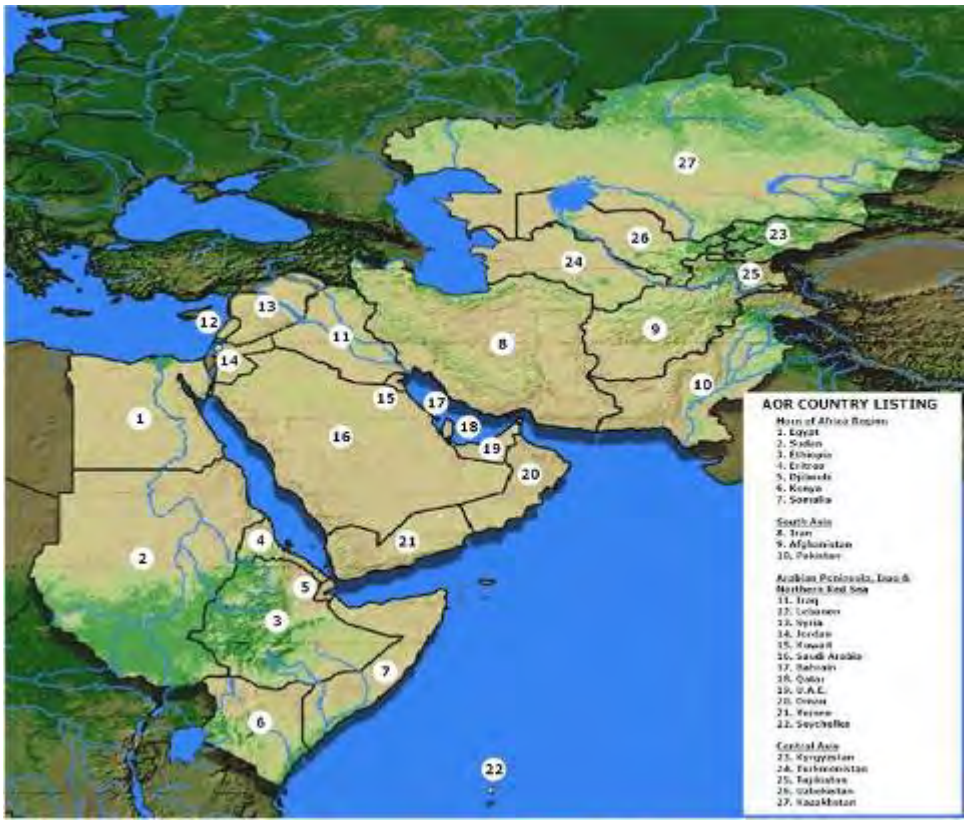

Figure 1. The USCENTCOM AOR. Image from ALTERMEDIA.INFO [Accessed online at: http://fr.altermedia.info/general/le-commandement-central-americain-a-un-nouveau-patron_17540.html, March 2011].

A representative from the 28 OWS came to the Naval Postgraduate School (NPS) in 2009 with proposals for several thesis research topics. One of these topics was the development, testing, and validation of a static stability/thunderstorm index for AFG. The 28 OWS's forecasters were having trouble with forecasting thunderstorms in AFG, and were issuing weather WWAs with high false-alarm rates (Capt. S. Smith 2010, personal communication). The 28 OWS's present capabilities limit them to using static stability indices, such as the lifted index (LI) and total totals (TT), that were developed for environmental conditions within the contiguous U.S. (CONUS) and do not account for the high desert mountain environment of AFG. The 28 OWS requested research to help develop a static stability index that accounts for the complex elevated desert environment of AFG (Capt. S. Smith and Mr. N. Triplett 2010, personal

communication). In 2010, we chose to address this research need, starting with a review of the data sets that were available for AFG. We decided that a research project focused on analyzing thunderstorm activity in and near Kabul was feasible. Unfortunately, the radiosonde and surface (SFC) observational data sets for other parts of AFG did not have the temporal extent and continuity needed for the requested research.

B. GEOGRAPHY OF THE STUDY REGION

1. Geography of Southwest Asia

The geography of southwest Asia (SWA, see Figure 2) influences the processes that support and inhibit the thunderstorm (TSTM) and nonthunderstorm (NTSTM) activity in AFG. In particular, the bodies of water surrounding SWA, as well as the Bay of Bengal (BoB) and western tropical Pacific, are potential moisture sources for synoptic-scale low pressure cell (L) systems that affect AFG, which are responsible for a majority of AFG precipitation (precip) (Vorhees 2006). The land topography of SWA also strongly influences the transport of moisture into AFG as part of the lower tropospheric circulation (Vorhees 2006; Hanson 2007; Moss 2007; Lemke 2010). In particular, the Zagros and Alborz Mountains in Iran, the Hindu Kush Mountains in AFG, the Pamir Mountains in Tajikistan, and the Himalayan Mountains in southwestern China and northern India (Figures 2–3) exert a major influence on the transport of moisture in SWA (Moss 2007). More detailed descriptions of the geography of SWA and how it influences the climate system can be found in reports by the 14th Weather Squadron (14 WS 2011) and the 28 OWS (2011).

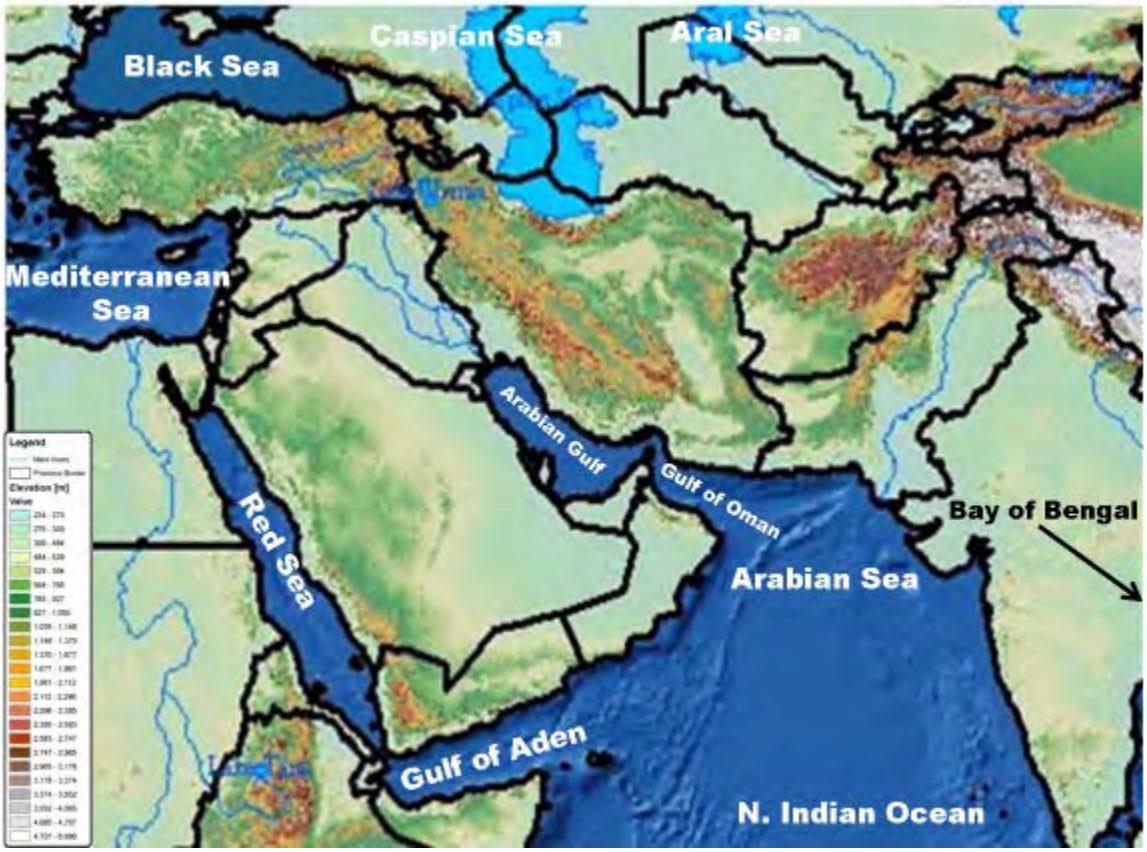

Figure 2. Geography of southwest Asia (SWA). Note the high elevations and complex topography of Afghanistan and the surrounding regions. Also, note the potential sources of moisture for Afghanistan, including the Mediterranean Sea, Black Sea, Caspian Sea, Aral Sea, Red Sea, Gulf of Aden, Arabian Gulf, Arabian Sea, Gulf of Oman, northern Indian Ocean, Bay of Bengal, and western tropical Pacific (not shown). Image adapted from 28 OWS (2011).

Figure 3. Geography of Afghanistan and surrounding countries. Note the complex topography that dominates Iran, Afghanistan, Pakistan, Tajikistan, Kyrgyzstan, and western China. Image adapted from 28 OWS (2011).

Depending on the direction of the synoptic flow, the mountain ranges shown in Figure 3 can either enhance or block the transport of low-level (LL) moisture (14 WS 2011). The southwest (SW) to northeast (NE) orientation of the Hindu Kush Mountains can guide moisture advection from the warm, moist tropical waters of the Red Sea (RS), Gulf of Aden (GoA), northern Indian Ocean (NIO), Arabian Sea (AS), Arabian Gulf (AG), and Gulf of Oman (GoO) into AFG when a south-southwesterly (SSW-erly) synoptic flow occurs (Hanson 2007; 14 WS 2011). When the synoptic flow is from the east-southeast (ESE), moisture advection into AFG comes from the warm moist tropical waters of the BoB (14 WS 2011). The Mediterranean Sea, Black Sea, Caspian Sea, and Aral Sea can

also contribute moisture to AFG, especially in winter when westerly LL flow into AFG and Extratropical cyclones (ETCs) are more common (14 WS 2011).

2. Geography of Afghanistan

AFG is a semiarid to arid, landlocked country bordered by Iran to the west, Turkmenistan, Uzbekistan, and Tajikistan to the north, China to the east, and Pakistan (PAK) to the east and south (CIA 2011; see Figure 3). AFG is approximately 652,000 square kilometers (km^2) in area, which is roughly the size of Texas (CIA 2011). The nearest large body of water is the AS, about 500 kilometers (km) to the south. AFG's topography varies throughout its borders and has an upslope pitch from SW to NE formed by the Hindu Kush Mountains that divide the comparatively fertile Northern provinces from the rest of the country (Afghan Facts 2011; see Figure 4).

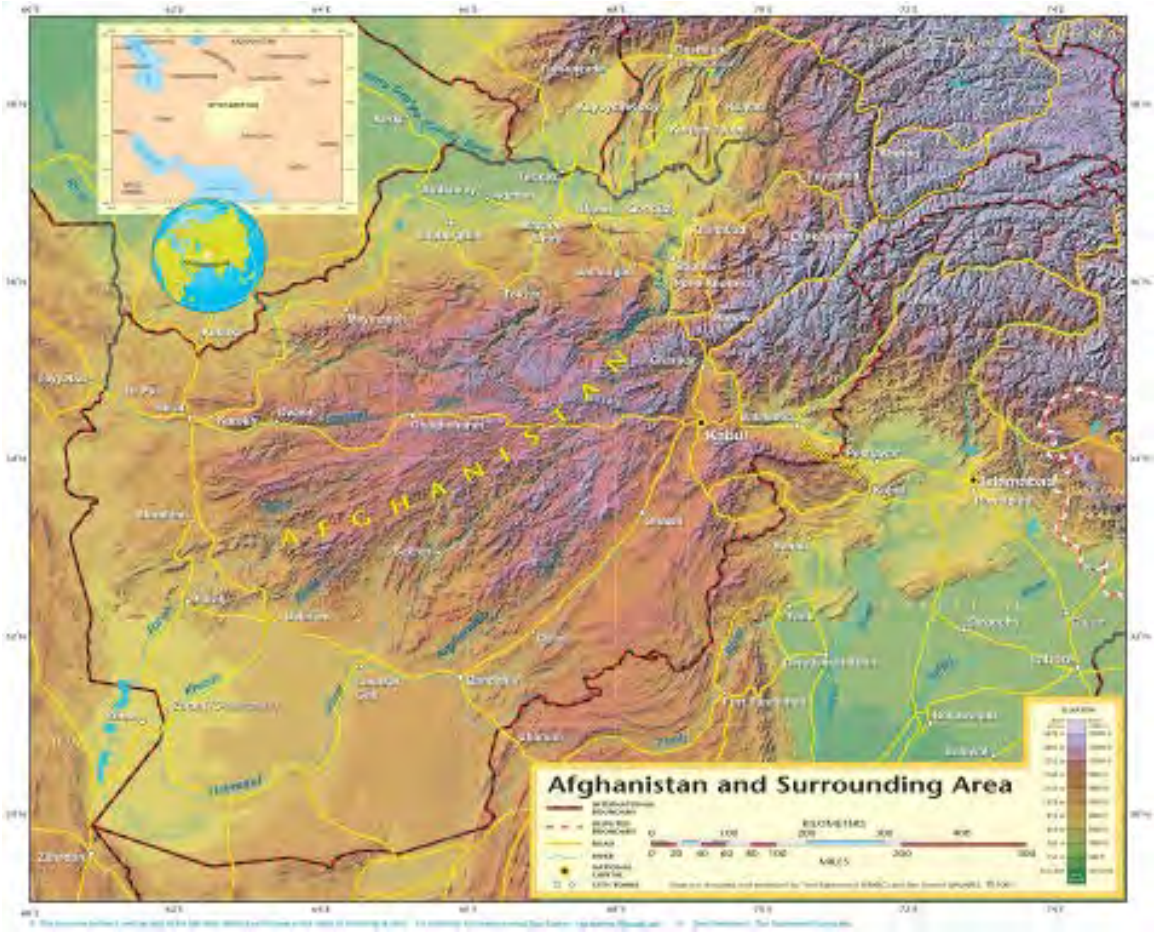

Figure 4. Detailed topography of Afghanistan. Note that Kabul lies on a valley floor surrounded by high mountains. Also note how the orientation of the mountains surrounding Kabul can (1) steer lower tropospheric winds so that they travel along approximately north-south and west-east paths and (2) force orographic lifting very near Kabul. This steering and lifting can contribute to TSTM development over and near Kabul. Image from Tradepoint Afghanistan LTD [Accessed online at: http: //www.tpeu.nl/media/img/big_map_afghanistan.jpg., March 2011].

The lowest elevations, of a few hundred meters, are found in the Margow Desert to the south and the Amu Darya riverbed valley lowlands to the north (Figures 3-4). The highest elevations are found in extreme northeastern (NE-ern) AFG where the Noshak Mountains reach 7,485 meters (m) (CIA 2011). The Hindu Kush Mountain Range, and its various branches, form three distinct

geographic regions known as the Central Highlands, the Northern Plains, and the Southwestern Plateau (Afghan Facts 2011).

The Central Highlands is an area of about 414,000 km^2 dominated by deep narrow valleys and tall mountains. The mountains reach as high as 6,400 m, with mountain passes that lie between 3,658–4,572 m (Afghan Facts 2011). Such mountain passes, like the Shebar Pass, located northwest (NW) of Kabul where the Selseleh-ye Kuh-e Baba Mountain Range meets the Hindu Kush Mountain Range (Figure 5) and the Khyber Pass (Figures 4 and 5), which leads to Pakistan, can act as paths for moisture transport into Kabul (28 OWS Kabul FRN 2010; Afghan Facts 2011). Extending eastward from the Iranian border to the foothills of Tajikistan are the Northern Plains, which slope towards the Amu Darya River, cover 103,600 km^2, and reach an average elevation of 610 m (Afghan Facts 2011). The Southwestern Plateau covers southwestern AFG in 129,500 km^2 of high plateaus and sandy deserts at an average elevation of 915 m. Within this plateau are the isolated arid salt flats of the Margow Desert. Several large rivers cross the Southwestern Plateau, among them are the Helmand River and its major tributary, the Arghandab (Figure 4; Afghan Facts 2011; 28 OWS Kabul FRN 2010).

3. Geography of Kabul, Afghanistan

Kabul is the capital of Afghanistan and sits at 1,791 m above sea level where it occupies the western center of a 1,676–1,981 m high triangular valley basin surrounded by mountains (Figure 5). Kabul is flanked to the west and NW by the Selseleh-ye Kuh-e Baba Mountain Range and to the southeast (SE) by the Selseleh-ye Spin Gahr Mountain Range, which both average 3,655–4,267 m in elevation. The most prominent mountains near Kabul, and in AFG, are the Hindu Kush Mountains to the NW, North (N), and East (E) of Kabul. Near Kabul, the Hindu Kush Mountains average between 4,575–5,180 m. Approximately 90 km to the north of Kabul, the mountains reach their peak elevation of 5,485 m. The walls of the basin rise steeply into the hills and mountains around Kabul,

which average 2,745–3,350 m in elevation. West of Kabul (72.2 km) is the Unai Pass where the Darya-I Kabul River flows through Kabul and then exits to the east past Jalalabad through the Kyber Pass into Peshawar, PAK (Figures 4–5; 28 OWS Kabul FRN 2010).

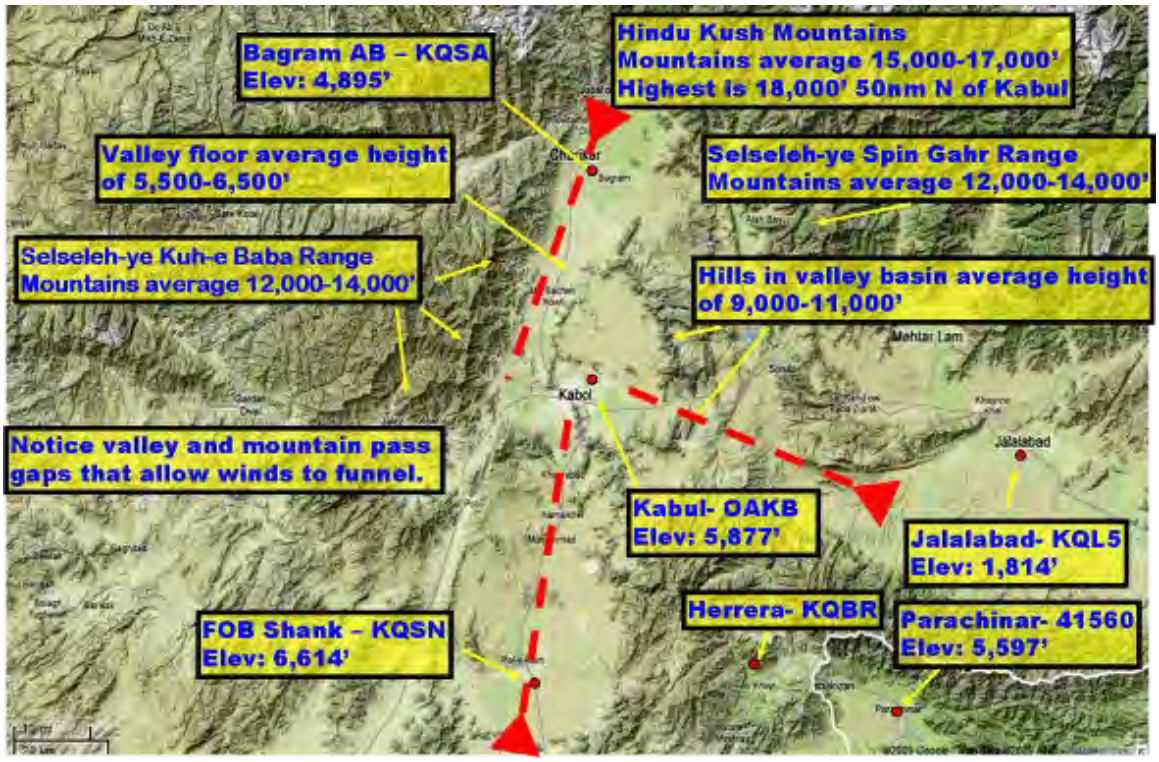

Figure 5. Topographic map of Kabul and the surrounding area. Key locations are described in blue text. Winds approaching Kabul along the valley axes are shown schematically by red arrows. Note that Kabul lies on a valley floor that is approximately 5,877 feet above sea level and is flanked on the west, north, and east by mountain ranges and hills, which can cause orographic lifting for winds approaching from the south and/or east. Also note how winds from the north-northeast can be funneled into Kabul. Image adapted from 28 OWS Kabul FRN (2010).

The orientation of these various topographic features can produce LL convergence (LLCON) of SFC winds into Kabul depending on the SFC wind direction (Figure 5; 28 OWS Kabul FRN 2010). The valleys and mountain passes can allow moisture-laden air from surrounding lower elevation regions to

interact with the topography surrounding Kabul. Subsequent moisture convergence where valleys intersect and/or orographic lifting on the upwind side of the mountains can lead to the development of convection and TSTMs (Wallace and Hobbs 2006; see also Chapter II, Section B.5.b.3).

C. LONG-TERM MEAN MARCH–MAY CLIMATOLOGY OF KABUL

1. Winter Climatology

For this study, we focused on the period of the year with the highest frequency of TSTM activity—March, April, and May (MAM). This period spans the end of winter and the beginning of spring. The rest of this section summarizes the long-term mean (LTM) conditions in Kabul during winter and spring based on the 28 OWS Kabul FRN (2010) and 14 WS (2011) documents.

During winter, the dominant climatic feature over and near Kabul is the central Asian high pressure cell characterized by cold, dry, continental polar (cP) air. The subtropical jet (STJ) and Extratropical storm track tend to lie south of Kabul. Mean high SFC temperatures in Kabul in December, January, February, and March are 7°C, 3°C, 4°C, and 13°C, respectively. Average LL winds in the winter are from the north-northwest (NNW) at 4–5 knots (kts) all winter, with southwesterly, southerly, and southeasterly winds occurring during the passage of ETCs (28 OWS FRN 2010). Winter precip and TSTM activity tend to be associated with moisture advection from the NIO, AS, AG, GoO, RS, and the GoA and orographic lifting over the Hindu Kush and Selseleh-ye Kuh-e Baba mountain Ranges (28 OWS FRN 2010). The 28 OWS FRN (2010) reports that the mean monthly precip increases from December–March, with December, January, February, and March LTM precip values of 25 mm, 25 mm, 61 mm, and 74 mm, respectively. The 28 OWS FRN (2010) also states that TSTMs are rare during December, January, and February, and that TSTMs occur on an average of only two days in March. LTM March TSTM activity is discussed in further detail in Chapter III, Section B.1.

2. Spring Climatology

The central Asian high pressure cell is also a dominant feature over and near Kabul during spring, but its strength declines from March–May. During spring, the STJ and Extratropical storm track shift to the north of Kabul. ETCs become weaker and less frequent from March–May (28 OWS Kabul FRN 2010). During spring, SFC air temperatures and TSTM activity increase. Kabul mean high SFC temperatures in March, April, and May are 13°C, 18°C, and 24°C, respectively. Precip and TSTM activity peaks in April, as the lower troposphere warms and destabilizes, and as snowmelt adds moisture to the SFC air (28 OWS Kabul FRN 2010). The large-scale SW summer monsoon regime begins to develop over the northern IO, southern PAK, and India. Occasionally, the southwesterly monsoon flow is augmented by an easterly disturbance over the AS, which can lead to enhanced northward moisture advection into, and precip and TSTM activity over, AFG (28 OWS Kabul FRN 2010). Mean monthly precip for March, April, and May are 74 mm, 112 mm, and 28 mm, respectively (28 OWS Kabul FRN 2010). Flooding is most likely to occur in April, the month with the greatest precip, the most TSTM activity, and relatively high snowmelt (28 OWS Kabul FRN 2010).

Figure 6 shows the LTM number of precip days for AFG for March, April, and May. A precip day is defined as a day with a precipitation water equivalent that is greater than the trace threshold of 0.005 inches (Capt. B. Lemke 2010, personal communication). Note a slight overall decline across AFG in the number of precip days from March–April, and a larger decline from April–May. For Kabul, there is also little change from March–April, but a notable decline from April–May.

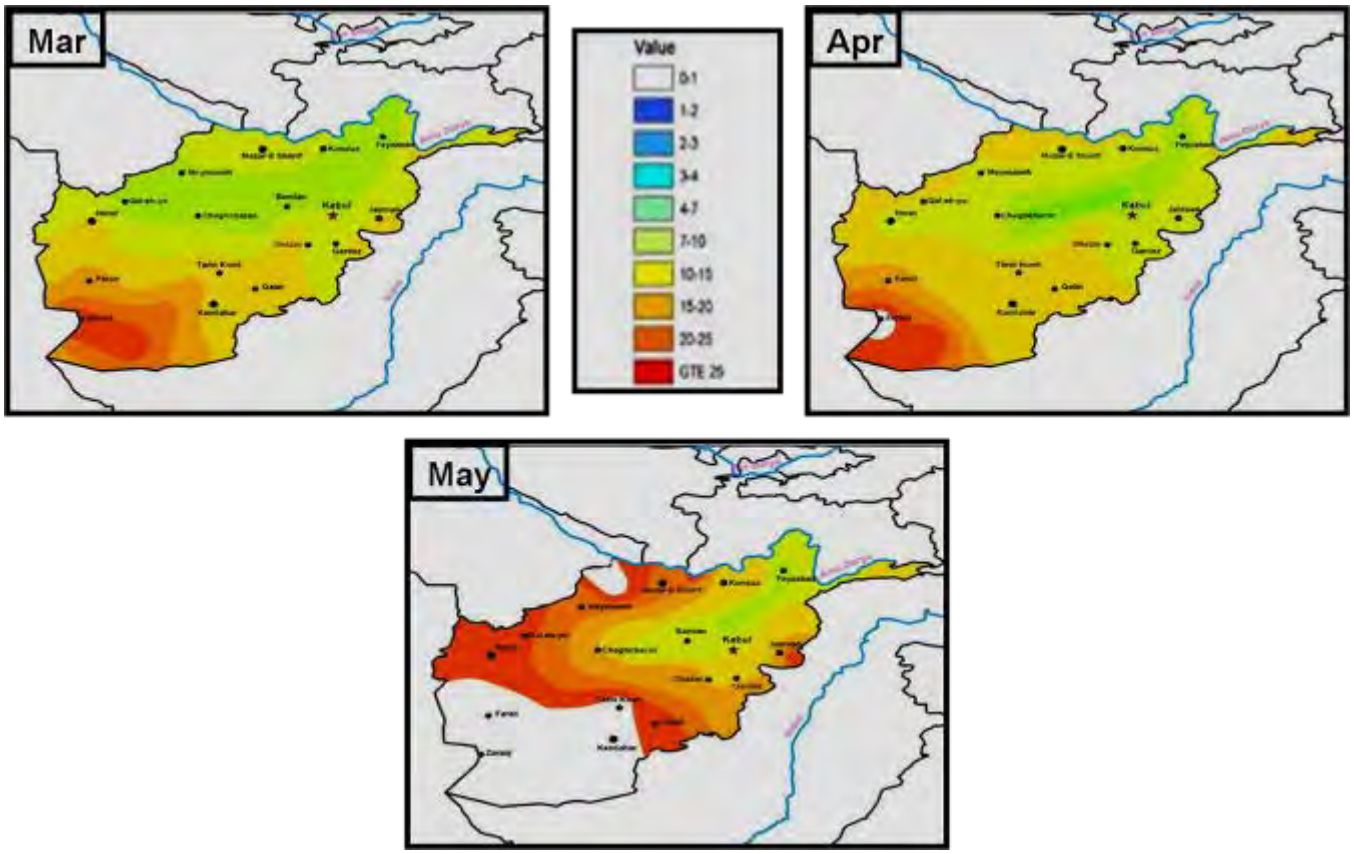

Figure 6. Long-term mean (LTM) number of Afghanistan precipitation days during March (top left), April (top right), and May (bottom) based on surface weather observations. A precipitation day is defined as a day with a precipitation water equivalent that is greater than the trace threshold of 0.005 inches. Note the increase in precipitation days from March–April, and a decrease from April–May. Data at individual observation locations are interpolated to provide continuous spatial coverage. Images from 14 WS AFG CR (1991)

Figure 7 shows the LTM number of TSTM days for AFG for March, April, and May. A TSTM day is defined as a 24-hour period in which one or more TSTMs were observed (Capt. B. Lemke 2010, personal communication). Note a large overall decline across AFG in the number of TSTM days from March–April, and a smaller decline from April–May. For Kabul, there is a large increase from 0–1 days in March to 4–7 days in April, but relatively little change from April–May.

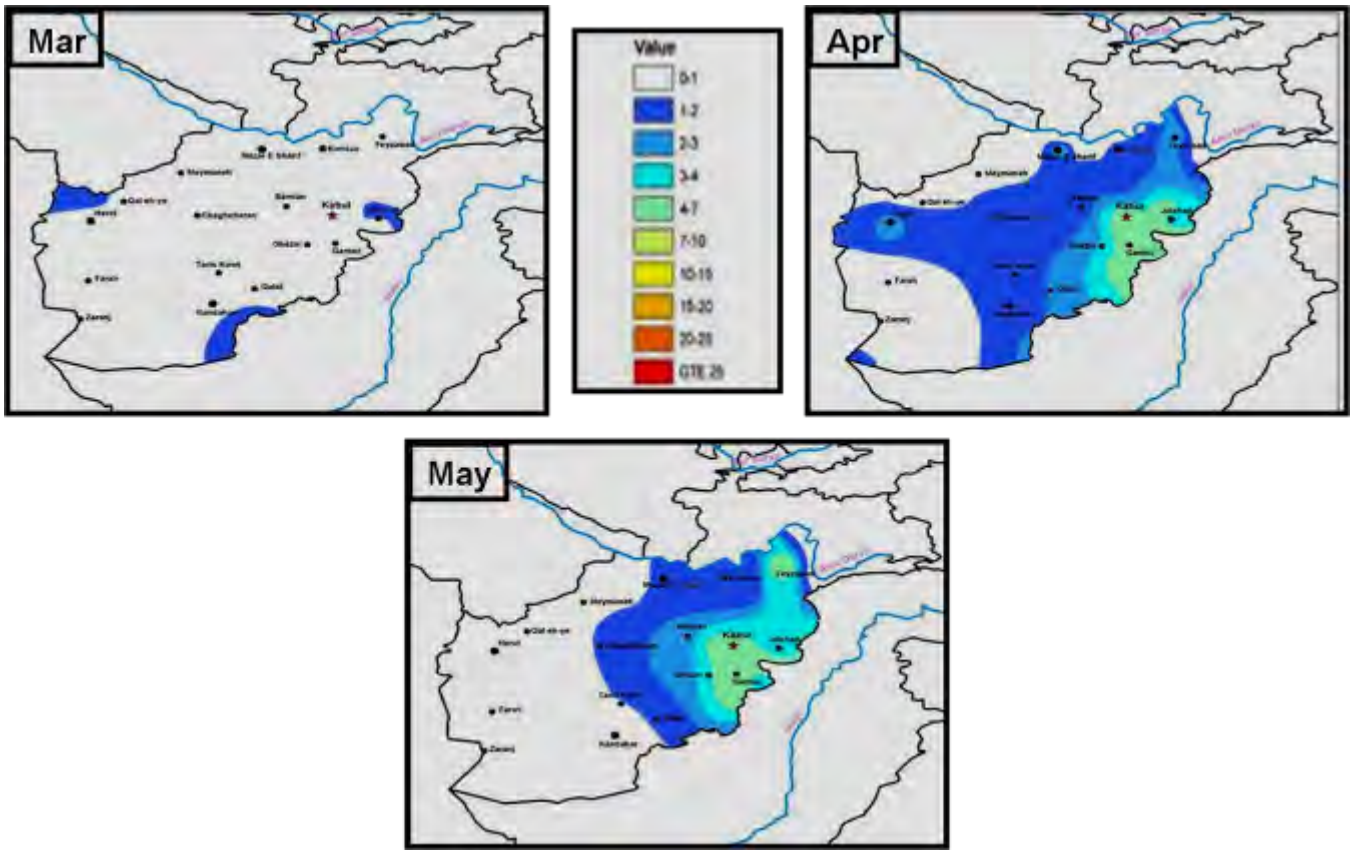

Figure 7. Long-term mean (LTM) number of Afghanistan TSTM days during March (top left), April (top right), and May (bottom) based on surface weather observations. A TSTM day is defined as a day with at least one recorded TSTM. Note the large increase in TSTM days from March–April and the large spatial extent of TSTM activity in April. Data at individual observation locations are interpolated to provide continuous spatial coverage. Images from 14 WS AFG CR (1991).

D. THUNDERSTORM FORECASTING BY 28TH 0WS FOR KABUL

The Air Force forecast reference notebooks (FRNs) provide forecasters with a detailed explanation of the local geography, seasonal climate regimes, analysis techniques, available forecasting products, and general rules of thumb (RoT) for their forecast AORs. The Kabul FRN (28 OWS Kabul FRN 2010) contains weather forecasting information for Kabul International Airport, Kabul Province, various camps located within Kabul, and the Islamic Republic of AFG. The weather forecasting information contained within the Kabul FRN accounts for geographic information, sensor details, area topography, airport imagery, climatology (climo), weather regimes, local effects, forecasting techniques, RoT, tools, products, and forecast reviews and studies. The reader is encouraged to refer to the 28 OWS website for detailed elaboration on the Kabul FRN, as it is beyond the scope of this thesis (28 OWS Kabul FRN 2010).

The Kabul FRN contains information on the hourly percentage frequency of TSTM occurrence for each month. There are two experimental RoT contained within the Kabul FRN for forecasting TSTMs in and near Kabul. The first RoT has the forecaster look for a shortwave trough moving through the area. Then, if TSTMs are forecast, the forecaster can expect a potential for LL TSTM outflows of 30–40 knots. The second RoT has the forecaster look at the Global Forecast System (GFS) 500 hectopascal (hPa) relative humidity, and if it is at least 80%, the forecaster can expect TSTMs in the region (28 OWS Kabul FRN 2010). These RoT for Kabul TSTM forecasting were developed from FRNs for nearby locations with the same, or similar, air masses, synoptic systems, and terrain features (Mr. S. Pulley 2011, personal communication).

Kabul radiosonde data are commonly used by forecasters to calculate the values of static stability indices for forecasted and actual conditions. However, radiosonde data are relatively sparse for the general Kabul region, given the large variations in atmospheric conditions associated with the extreme topographic variations in the region. Model analyzed and forecasted soundings

tend to be too dry in the LLs because of sparse observational input data to the models and the coarse horizontal and vertical resolution in the models (Capt. S. Smith 2010, personal communication). These problems with LL moisture lead to inaccurate calculations of Convective Condensation Level (CCL), Lifting Condensation Level (LCL), Convective Available Potential Energy (CAPE), Convective Inhibition (CIN), hail size, convective down rush gusts, and Convective Temperature (T_c).

Mr. S. Pulley is an experienced SWA forecaster and a primary trainer of 28 OWS forecasters (Mr. N. Triplett 2011, personal communication). Mr. Pulley told us the following about Kabul forecaster training (Mr. S. Pulley 2011, personal communication).

> There is currently no specific training received by our forecasters for Kabul. However, there is training for the SWA theater with emphasis on forecasting severe parameters based on actual and model forecast skew-T data, computer model chart interpretation, satellite imagery interpretation, [with adjustments for seasonal and regime changes] (e.g., Winter, Spring, Southwest Monsoon, Northeast Monsoon, Lut Desert Low). Rules of thumb and forecasting techniques for individual sites were developed based on months or years of observational data, in-house forecast reviews, and in-house forecast studies. Specific training is given to forecasters for their terminal aerodrome forecast (TAF) locations once their zone assignment (site, area, or region they will be producing TAFs and Advisories/Watches/Warnings for) are given. Prior to their zone assignments, standard rules for forecasting severe weather are taught to arriving personnel. The training is classroom and simulator training (on the job training using actual observations, radar data (Salerno), MIRC Chat monitoring and Advisory/Watch/Warning issuance simulations).

The standard rules for forecasting severe weather that Mr. Pulley refers to are contained within training modules for convective and severe convective weather, with additional training on the use of skew *T*- log *p* diagrams for TSTM forecasting.

The information we received about methods for forecasting TSTMs in the Kabul region indicated that the forecasting of TSTM activity in the Kabul region

would benefit from studies of: (1) the large-scale patterns and processes associated with TSTMs and NTSTMs and (2) the performance of different static stability indices when calculated from both observational data and model output. The need for such studies motivated our study.

E. NATIONAL WEATHER SERVICE METHODS FOR THUNDERSTORM FORECASTING IN HIGH ELEVATION REGIONS

At the beginning of our research, we sent e-mails to the NWS forecast offices within high elevation regions to learn how they were dealing with TSTM forecasting. We sent e-mails to NWS forecast offices in California, Wyoming, Utah, Idaho, Colorado, New Mexico, Arizona, and Nevada. We received responses from all of the offices and were referred to a paper written by Rhett Milne (2004) from the NWS forecast office in Reno, NV, titled, *A Modified Total Totals Index for Thunderstorm Potential Over the Intermountain West.*

1. The High Level Total Totals

To account for the higher topography of the western U.S., Milne (2004) adjusted the TT index to account for temperature and moisture at 700 hPa instead of 850 hPa and termed the resulting index the High Level Total Totals (HLTT). Equations 1 and 2 show how the HLTT index was created by modifying the TT index (which is a combination of the Cross Total (CT) and Vertical Total (VT) indices).

Equation 1. The Total Totals Index

$$TT = CT + VT = (T_{850} - T_{500}) + (Td_{850} - T_{500}) = T_{850} + Td_{850} - (2 * T_{500})$$

Equation 2. The High Level Total Totals Index

$$HLTT = T_{700} + Td_{700} - (2 * T_{500})$$

The HLTT index was developed using data from radiosondes launched at 0000 Coordinated Universal Time (UTC) from the NWS office in Reno, NV, during the 01 June–31 September of 1995–2003. The 0000 UTC radiosondes

were used as they represented the late afternoon environment when TSTM development was most widespread due to maximum daytime heating. The HLTT values were calculated every summer day during the nine-year period and compared to weather observations, precip amounts, and a limited lightning data set. The study revealed that the higher the value of the HLTT, the better the chance of TSTM development, especially if conditions are warm and moist at or near the 700 hPa level (Milne 2004).

Table 1 and Figure 8 show that the higher the value of the HLTT, the better the probability of receiving measurable precip, TSTMs, severe TSTMs (SVR), and Tornadoes (TOR). For example, a HLTT value of 29 was found to give a 32% chance of precip at the Reno airport, while the likelihood of precip occurring jumped sharply to 58% when the HLTT value was 31, and up to an 80% likelihood with a value of 35 or higher (Milne 2004).

Table 1. HLTT threshold values (^{o}C) and corresponding TSTM forecasts (From Milne 2004).

Forecast	High Level TT
Isolated thunderstorm possible	28-29
Isolated thunderstorms	29-30
Isolated to scattered thunderstorms	31-32
Scattered to numerous thunderstorms	>= 33

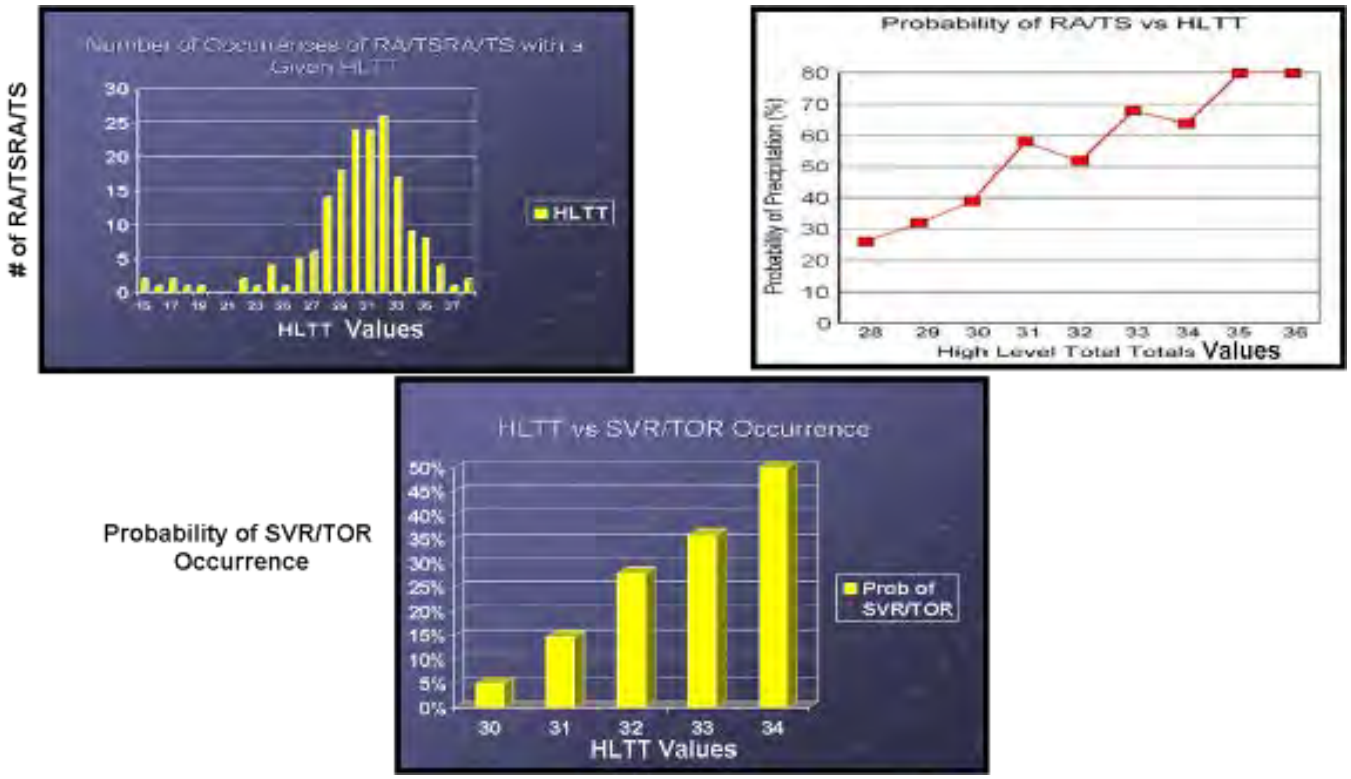

Figure 8. The relationships between the high level total totals (HLTT) instability index and precipitation (top left), TSTMs (top right), and severe TSTMs (SVR) and tornado activity (TOR) (bottom) for Reno, NV region, from Milne (2004). Note that higher values of HLTT tend to correspond to higher precipitation, TSTMs, and severe weather. For details, see Milne (2004).

2. Other NWS Elevated Thunderstorm Forecast Methods

Jim Wallmann from the NWS forecast office in Reno, NV, has stated that, "One of the main tools we use to assess instability is the 500–300 hPa lapse rate. Since many of our cloud bases can be at 600 hPa or above, it is really that layer which will determine if we get deep convection or capped cumulus in our drier environments" (J. Wallmann 2010, personal communication).

Ryan Knutsvig from the NWS forecast office in Elko, NV, says the following about how they forecast TSTMs in their area.

> Indices that are frequently used at our office (Elko, NV) for basic convection forecasting include standard Lifted Index (LI), LI 400 (uses 400 hPa instead of 500 hPa), Convective Available Potential Energy (CAPE), and precipitable water (PW). Since the Convective Condensation Level (CCL) is at or around 500 hPa, quite often it is important to look at the sounding and not just take the standard LI. That is why the LI 400 can be helpful. Also, a key factor is an acceptable low-level moisture (surface dew point mixing ratio) forecast. (R. Knutsvig 2010, personal communication)

Stan Czyzyk from the NWS forecast office in Las Vegas, NV, says the following about forecasting TSTMs in his area.

> Tools like the LI, CAPE, and Convective Inhibition (CIN) work fairly well for low desert regions. The recent addition of Integrated Precipitable Water sensors and Geostationary Operational Environmental Satellite (GOES) soundings as well as additional surface sensors has improved our forecasting capability and model guidance. One other parameter we use is theta-e (850–500 hPa or 850–700 hPa). Generic trends seem to work well. For instance, 342 Kelvin (K) is the value that we typically see convection initiate, but utilizing the value from today's convection to forecast tomorrow's works quite well. (S. Czyzk 2010, personal communication)

Dr. Thomas Warner from the UCAR in Boulder, CO, says the following about TSTM forecasting in an elevated desert environment.

> A colleague at the National Center for Atmospheric Research (NCAR), Mike Chapman, has done forecasting in Saudi Arabia. He (Mike Chapman) says that 'significant convection results only when easterly waves disturb the capping inversion.' Given the terrain contrasts in Afghanistan and the strength of the solar forcing, I wonder if there are also elevated mixed layers (such as in the U.S. High Plains) that can inhibit convection. Their strength in a region could depend on wind direction and other factors. (Dr. T. Warner 2010, personal communication)

F. OTHER REGION SPECIFIC INSTABILITY INDEX STUDIES

In a study by Stratton (2006), eighteen convective indices were calculated for five central and western North Pacific sites, which were then evaluated for their ability to predict the onset and intensity of deep convection. Using SFC observations and blended rain rate estimates from the Naval Research Laboratory, each of the eighteen indices was evaluated for predictive skill in terms of seasonality and location. The indices that had significant skill were used to define an experimental multivariate tropical convective index, which was also tested for performance during different seasons and locations. Stratton (2006) determined that the experimental multivariate index performed reasonably well during summer in the tropical western North Pacific but no better than the highest ranked single indices. For the central North Pacific, the multivariate index was not able to delineate convective from non-convective environments.

In a study done by Cercone (2007), a climatology was developed for convection over Laughlin Air Force Base in Texas based on radiosonde data and data for several corresponding indices (K-Index (KI), LI, Showalter Index (SI), TT, Severe Weather Threat Index (SWEAT), CAPE, mean layer CAPE (MLCAPE), most unstable CAPE (MUCAPE), 0-2 and 0-6 km bulk shear, 700–500 hPa lapse rate, lifted condensation level (LCL), and mean layer LCL heights). Cloud-to-ground lighting data, SFC observations, and severe weather reports from the Storm Prediction Center were used to categorize the radiosonde soundings as either non-convective, light convection, convection within the vicinity, moderate

severe convection, or severe convection. Cercone (2007) found that the 0–6 km bulk shear along with the MLCAPE and LCL height provided some discrimination between moderate and severe convection. The most favorable results came from calculating the product of the 0–6 bulk shear and MLCAPE, in conjunction with the 0–6 bulk shear versus the MLCAPE and the 700–500 hPa lapse rate.

The two prior studies by Stratton (2006) and Cercone (2007) convey the importance of developing location specific convective indices that account for the processes that are most important in determining convection in the location. This includes accounting for factors related to the location's terrain, regional climate setting, seasonal variations, and climate variations (cf. Stratton 2007).

G. RESEARCH MOTIVATION AND SCOPE

1. Specific Problems that Limit Skill in Forecasting Thunderstorms in Kabul

a. Failure of CONUS-Based Static Stability/Instability Indices

When we began this research, our initial discussions with the 28 OWS forecasters revealed some of the problems they were having with TSTM forecasting in AFG. Capt. S. Smith, U.S. Air Force (USAF), former Flight Commander for the 28 OWS, said that, "There is an approximate 50% false alarm rate for severe TSTM events in AFG, yielding missed lead times for watches, warnings and advisories (WWAs)" (Capt. S. Smith 2010, personal communication). Additionally, we were informed that the operational forecasters for Kabul, AFG, were using static stability/instability indices (e.g., CAPE, TT, LI) that were developed for use in the CONUS. The CONUS-developed indices use the 850 hPa level in their equations to account for LL temperature and moisture (Equation 1 for TT calculation). From the analysis of our radiosonde data from Kabul, the average SFC pressure during MAM TSTM events is 818 hPa, and for the NTSTM events, it is 819 hPa. Kabul's elevation is 1,791.8 m (5,877 feet)

above sea level. This equates to a SFC pressure of approximately 820 hPa when assuming a standard atmosphere (Wallace and Hobbs 2006). From this analysis, it becomes clear that there is no 850 hPa pressure level in Kabul. Thus, a major problem identified with using CONUS-based static stability/instability indices is that they use pressure levels that occur too low within the lower troposphere to capture the SFC temperature and moisture characteristics in the high elevations in and near Kabul.

b. Inadequate Observational Data Used for Research and as Inputs to Instability Analyses and Forecast Models

From our research, it has become evident that factors such as the rugged terrain and unstable political/military environment of the war-afflicted region in AFG have resulted in a lack of observational data. In particular, an inadequate network of SFC and radiosonde observations can reduce the value of weather analyses and the performance of forecast models, by, for example, providing insufficient information on moist layers located at different levels, elevated mixed layers, and circulations that disrupt inversions (cf. Dr. T. Warner 2010, personal communication). Kabul was chosen as the focus region for our study because it had the best long-term observational data set available within AFG. However, the observational records for Kabul have a number of temporal discontinuities and other shortcomings, which made our research more challenging (for more on these issues, see Chapter II, Sections A.1, A.2, and A.3).

c. Lack of Documented Empirical Studies

During our investigation into previous related studies, it became evident that there have not been many, if any, documented empirical studies on the occurrence, or forecasting, of TSTMs in AFG. There were also relatively few such studies for other high elevation regions. Of these, Milne (2004) was the most useful.

2. Scientific Motivations

These shortcomings in prior studies, and the operational need for accurate TSTM forecasts, led us to conduct a study on the patterns and processes associated with TSTM and NTSTM periods in the Kabul region, and on forecasting those periods. Specifically, we wanted to evaluate if there were distinct atmospheric or oceanographic regimes that tended to lead to the occurrence of TSTM or NTSTM events in or near Kabul, and how to exploit information about such regimes to improve TSTM forecasting. We hope that our study will contribute to improved forecasting of TSTMs in Kabul, and perhaps in similar environments elsewhere in the world.

3. Operational Motivations

TSTMs, and their associated phenomena, lead to some of the most dangerous operational environments for our troops. Flight operations, ground troop movements, and base security are all negatively affected by TSTM events. TSTM associated phenomena such as, lighting, turbulence, strong winds, heavy precip, flooding, and dust storms, to name a few, create potential operational hazards (AFI 15-128 2010 and AFMAN 15-129 2010). By improving TSTM forecasting in Kabul, AFG, we hope to mitigate some of these hazards. Meeting this need for improved TSTM forecasting capabilities in Kabul will add significant value to the support the METOC community provides for DoD operations, which could save resources, money, and lives.

4. Research Questions and Hypotheses

The main mission of our research is to provide an empirically based scientific study that improves TSTM forecasting in and near Kabul. In order to complete this task we designed our study to address the following questions:

(1) What are the temporal and spatial weather and climate patterns and processes that characterize TSTM and NTSTM periods, at local, regional, and hemispheric scales?

(2) What indices can be developed to analyze the occurrence of conditions favorable for TSTM and NTSTM periods?

(4) How can the answers to the prior questions be used to improve long and short range TSTM forecasting?

Our study was also designed to test the following hypotheses:

(1) Favorable conditions for TSTM and NTSTM activity are determined by local, regional, and hemispheric conditions operating at short, medium, and long lead times.

(2) Variations in low-level winds are especially important in creating those favorable conditions because of circulation impacts on temperature and moisture advection, and moisture convergence.

(3) Comparisons between characteristic TSTM and NTSTM conditions can be especially useful in developing stability/instability indices, and the identification of potential precursors and predictors.

5. Thesis Outline

Chapter II presents our data and analysis methods. Chapter III presents our results. Chapter IV contains a summary of our results, conclusions, and suggestions for future research.

THIS PAGE INTENTIONALLY LEFT BLANK

II. DATA AND METHODS

A. DATA SETS

1. 14th Weather Squadron Kabul Surface Observations

a. Description of Data Set

The SFC meteorological observation data set that we used for this research was provided by the 14 WS (formerly known as the Air Force Combat Climatology Center (AFCCC)). This data set spans the period from 04 March 2002–31 July 2010 and contains data collected at the Kabul International Airport. The data set includes the station name, site identifier, year, month, day, total observation hours recorded for the day, precip hours observed, and TSTM hours observed. Specific information about maximum or minimum observing distance thresholds (e.g., the maximum distance a TSTM can be from a station in order for that station to officially observe and report the TSTM) varies from base to base and is dependent on the operational situation. Due to the unclassified nature of this thesis those specific details will not be discussed. The reader is referred to the AFMAN 15-111 (2010) for a description of the weather observing practices within the USAF. It should be noted that both human and automated observation methods were used to develop this data set. All weather observing and reporting procedures are based on agreements with the World Meteorological Organization (WMO), International Civil Aviation Organization, NWS, Federal Aviation Administration, international and domestic aviation interests, and other civil weather services (AFMAN 15-111 2010).

b. Strengths

The 14 WS Kabul SFC observation data set is temporally continuous with no gaps in the data set for 04 March 2002–31 July 2010. The

average daily observed hours for the entire record is 23.23 hours out of a 24-hour period, or 97% of the total hours in a day that could be observed. Considering the previously discussed unstable nature of the METOC observation network in this region, we were very satisfied with this temporal continuity. The data set include information needed to determine precip and TSTM frequency, timing, and duration.

c. Limitations

Unfortunately, this SFC data set does not contain information about the amount of precip that was recorded. It also does not contain the detailed information that a Meteorological Terminal Air Report (METAR) would have, such as wind direction and speed, weather condition, sky condition, SFC and dew point temperatures, and observation remarks. It needs to be noted that the 14 WS did provide us with METAR records for the period from 31 March 2002–29 September 2010. However, these METAR records have too many temporal gaps to be useful for our study and therefore they were not used in our research. One last limitation of this SFC data set is its short period of record of 9.3 years. A climatological data set is typically 30 years or longer in length (Dr. T. Murphree 2010, personal communication). Despite these limitations, we decided that this SFC data set was suitable for use in conducting an initial study of TSTM activity.

2. 14th Weather Squadron Kabul Radiosonde Observations

a. Description of Data Set

The radiosonde data set provided by the 14 WS spans the period from 24 February 2003–30 June 2010. The data were collected from the Kabul International Airport and include the station name, site identifier, year, month, day, and time of sounding launch. Most sounding launch times were consistent with the WMO standard of 0000 and 1200 UTC during the period of record from 2006–2010. However, during the period from 2003–2005 the 0000 UTC launch

times do vary from as early as 1700–2300 UTC, and as late as 0100 UTC. For the 1200 UTC launch times the deviation from the standard runs plus or minus two hours (e.g., 1000, 1100, 1300, and 1400 UTC). OEF-A operations were in their early stages during this period, and this could possibly explain the wide range of sounding times, as base operations may not have been as secure or established as they were during the later years of the war. Data were reported for the mandatory levels of 700, 500, 400, 300, 200, and 100 hPa, along with SFC observations, and reports were also made for significant levels that lie between the mandatory levels. The data recorded at mandatory and significant levels included height in meters, pressure in hPa, air and dew point temperatures in $^{\circ}$C, wind direction in degrees clockwise from true north, and wind speed in meters per second. Not all of these variables were recorded during every sounding for every mandatory and significant level. For example, most dew point temperatures were not recorded above 300 hPa as the radiosonde hygristors seemed to fail at these high altitudes. The temperature and wind information also experienced random gaps in their recording. The reader is referred to the USAF Air Weather Service Manual (AWS/TR-79/006; 1979) for a description of radiosonde discontinuities in sampling.

b. Strengths

The 14 WS radiosonde data set contains all of the standard information that a sounding should have, and is one of the few upper air data sets available for AFG. It is also the most temporally continuous upper air data set available for the region.

c. Limitations

Not every mandatory or significant level had a measurement recorded for each variable. This limitation cannot be avoided due to the nature of the radiosonde sensors and sampling methods. There are significant temporal gaps in the data set. For example, during 28 February–02 June 2004, the

radiosonde network was apparently not in operation and no radiosonde data are available for that period. This gap occurred during the MAM period when TSTM activity tends to be especially high. So this radiosonde data set represents only seven years of data for the most active period. There are also random gaps within this data set on the order of a day to a few days that are too numerous to account for in this thesis. If the reader is interested in using this data set for research, we suggest they contact us for a copy of the data set and further discussion about its temporal characteristics.

3. 14th Weather Squadron Kabul Static Data on Stability Indices and Thermodynamic Levels

a. Description of Data Set

The 14 WS uses a computer program to calculate various static stability indices and thermodynamic levels based on the 14 WS radiosonde data set previously discussed. The resulting data set includes the station identifier, year, month, day, hour of the sounding (e.g., 0000 or 1200 UTC), and information on the following indices: TT, KI, KO-index (KO), LI, SI, and CAPE. The following thermodynamic levels were calculated: CCL pressure and temperature in hPa and $^{\circ}$C, respectively, and T_c. The only static stability indices that were routinely calculated for this data set were the LI and CAPE. The other stability indices listed above were not routinely calculated due to the high elevation of Kabul and surface pressure that was usually lower than 850 hPa.

b. Strengths

This data set is very useful for comparisons to other calculations of these indices and levels, for example, those calculated and made available in the University of Wyoming (UWY) radiosonde data set (see next section).

c. Limitations

The main limitation of this data set is the temporal gaps.

4. University of Wyoming Kabul Radiosonde Observations

a. Description of Data Set

This radiosonde data set was based on the same radiosonde observations as the 14 WS data set described previously, but it has additional parameters computed and interpolated values between levels. Thus, the UWY radiosonde data set spans the period from 24 February 2003–24 August 2010. The data was collected at the Kabul International Airport and includes the station name, site identifier, year, month, day, and time of sounding launch. All mandatory and significant levels are reported. The major difference between the UWY radiosonde data set and the 14 WS radiosonde data set is the amount of information available. The following is a list of what the UWY radiosonde data set contains: pressure in hPa, height in m, temperature and dew point in °C, relative humidity in %, mixing ratio in g/kg, wind direction in degrees, wind speed in knots, potential temperature in Kelvin (K), equivalent potential temperature in K, and the potential temperature using virtual temperature in K. In addition, the following information is also provided: station latitude and longitude, station elevation, LI, LI computed using virtual temperature, CAPE, CAPE computed using virtual temperature, CIN, CIN computed using virtual temperature, Bulk Richardson Number (BRN), BRN computed using virtual temperature, temperature of the LCL in K, pressure of the LCL in hPa, mean mixed layer potential temperature in K, mean mixed layer ratio, 1000–500 hPa thickness, and precipitable water (PW) for the entire sounding in millimeters (mm). Therefore, the UWY radiosonde data set provides much more information than the 14 WS radiosonde data set. All of the report times for the UWY soundings comply with the WMO standard of 0000 and 1200 UTC. However, there are random times when some soundings are not available. For example, the large gap in data during 2004 that was found in the 14 WS data set was also found in the UWY data set during the same period in 2004.

b. Strengths

This data set contains additional types of information, and additional soundings, which are not available in the 14 WS radiosonde data set. This allowed us to fill in temporal gaps in the 14 WS data set.

c. Limitations

Unfortunately, this data set also has a number of random gaps in coverage of up to several days in duration, plus the extended loss of coverage in 2004 previously mentioned. As was the case in the 14 WS data set, the UWY data set experiences the same random fallouts in the temperature, dew point, and wind speed and direction parameters.

5. NCEP/NCAR Reanalysis 1

a. Description of Data Set

We used the global atmospheric and surface retrospective analysis, or reanalysis, produced by the U.S. Department of Commerce National Oceanic and Atmospheric Administration (NOAA) National Centers for Environmental Prediction (NCEP) and the National Center for Atmospheric Research (NCAR), also referred to as the Reanalysis I (R1) data set (Kalnay et al. 1996). Online access to this data set is provided by the NOAA Earth Systems Research Laboratory (ESRL) Physical Sciences Division. The R1 data set spans from January 1948–the present. The R1 data set was developed from in situ and remote observations that are extensively quality controlled. A data assimilation system and forecast model that were kept unchanged over the entire reanalysis period were used to produce reanalysis values of atmospheric and surface variables on a regular horizontal grid, at regular vertical levels, and at 6 hour intervals (Kalnay et al. 1996).

b. Strengths

The R1 data set is easily accessible and it enables us to analyze variations on a wide range of time scales (e.g., daily, intraseasonal, interannual) and on local to global scales. The R1 variables used in our research are discussed within this Chapter, Section B.4.a-i. We were able to evaluate R1 data within a period that was consistent with the 14 WS Kabul SFC observation data set from 04 March 2002–31 July 2010.

c. Limitations

The R1 data set with which we worked has a 2.5^{o} spatial resolution, at standard tropospheric and stratospheric levels, and at a daily temporal resolution. This limited our ability to capture the mesoscale and sub-daily features that occur within the complex topography of the AFG mountain ranges.

6. Comments on Data Availability

a. Data Sets Not Used and Why

The 14 WS provided us with SFC observation data sets for Bagram and Kandahar, AFG, along with a radiosonde data set for Kandahar. The 14 WS Bagram SFC data set spans the period from 22 March 2002–07 July 2010. However, this data set is temporally very discontinuous and similar to the corresponding Kabul data set, since Bagram is close to Kabul and, at 4,895 m, is only 982 m lower than Kabul. Thus, we did not use the Bagram data set.

The 14 WS Kandahar SFC data set spans the period from 01 March 2002–09 September 2010 and is temporally continuous. However, the Kandahar radiosonde data set only spanned a four-year period from 18 February 2007–30 June 2010, which was too short for the purpose of our study.

The UWY provided radiosonde data for Herat and Kandahar, AFG. The Herat data set covers the years from 1978–81, and 1985–88. The Herat

data set is temporally very discontinuous, and thus was not used. The Kandahar radiosonde data set spans the period from 1979–88, 1991, and 2003–2010. The quality of these data before 2003 is problematic. However, the data during 2003–2010 may be acceptable and should be considered for future studies similar to ours for the Kandahar region

The UWY also provides radiosonde data for Kabul from 1973–74, 1976, and 1978–92. These periods have a lot of temporal discontinuity both between and within the years represented in the data set. The quality of the data is also problematic for these periods. Thus, we did not use this data.

b. Data We Wished Existed but Does Not

The only reliable, multi-year radiosonde data available for AFG are for Kabul and Kandahar. We would have liked to have worked with much more spatially and temporally extensive data sets for AFG. We hope that the current and planned military involvement in AFG by the U.S. and allied nations will lead to the long-term collection of METOC observations from a network spanning the key regions of AFG. A robust data set of observations would contribute significantly to the improvement of operational forecasting for AFG and SWA in general.

B. ANALYSIS METHODS

1. Selection of Kabul TSTM and NTSTM Surface Observation Data Sets and Time Periods Used

The focus of this thesis was on the MAM period in Kabul, AFG, because it has the highest frequency of TSTM occurrence (see Chapter III, Section B.1 and Figure 9). The Kabul TSTM SFC observation data set provided the number of TSTM hours observed (see Chapter II, Section A.1.a). We identified as TSTM days those during which one or more TSTM hours were recorded during the day. Using this method, we identified 129 TSTM days from the MAM period within the

entire Kabul SFC data set. March had 27 TSTM days, April had 52, and May had 50. These 129 MAM TSTM days became our Kabul TSTM data set. We used this set to help characterize TSTM periods.

To select the NTSTM data set, we identified prolonged periods within MAM that had no precip and TSTM activity. For example, if there was a period of a week, or several weeks, in which no precip and TSTMs were recorded, then we would identify as a NTSTM day the days in the middle of the period. Using this method, we constructed a NTSTM data set composed of periods of up to 11 days without precip and TSTM activity. This led us to identify from the Kabul SFC data set 27 NTSTM days in March, 52 NTSTM days in April, and 50 NTSTM days in May. With these techniques, we constructed a 129-day MAM NTSTM data set for Kabul. We used the NTSTM data set to help characterize NTSTM periods. We identified more than 129 NTSTM days, but limited the NTSTM data set to 129 days to facilitate the comparison of TSTM and NTSTM conditions.

2. Selection of Kabul TSTM and NTSTM Radiosonde Observation Data Sets and Time Periods Used

We then selected the Kabul TSTM and NTSTM radiosonde data sets by using the 129 TSTM dates and 129 NTSTM dates to find corresponding radiosonde data for each of those dates. In general, we used the 1200 UTC soundings (or in some cases soundings close to 1200 UTC) to represent the pre-convective and convective conditions in Kabul, because 1200 UTC is close to the peak time of the day for TSTM activity in Kabul in MAM (see Chapter III, Section B.3). However, for six of the TSTM dates (4.7% of the total 129 TSTM dates), we used soundings from 0000 UTC soundings, because stability index and thermodynamic level data was not available at 1200 UTC for these six dates (see following section). For the NTSTM radiosonde data set, we used soundings from 1200 UTC (or in some cases soundings close to 1200 UTC) to represent NTSM conditions in Kabul in MAM. Due to the gaps within the radiosonde data record, there were no soundings to match with 39 of the SFC TSTM days. Thus, we

limited our TSTM and NTSTM data sets for MAM to a total of 90 days (129 – 39 = 90). For these 90 days, March had 22 TSTM and NTSTM days, April had 37, and May had 31. The number of NTSTM days for each of these months was the same.

3. Selection of Kabul TSTM and NTSTM Static Stability Indices and Thermodynamic Levels Data Sets and Time Periods Used

We identified 67 (76) of the 90 TSTM (NTSTM) radiosonde data set dates for MAM for which stability index and thermodynamic level data were available. For the MAM TSTM data set, 11 dates were from March (with all soundings from 1200 UTC), 32 were from April (with 31 soundings from 1200 UTC and one from 0000 UTC), and 24 from May (with 21 soundings from 1200 UTC and 3 from 0000 UTC). For the MAM NTSTM data set, March had 14 dates, April had 36 dates, and May had 26 dates (with all the soundings for the NTSTM dates from 1200 UTC). We used this data set based on 67 TSTM dates and 76 NTSTM dates to characterize the stability index and thermodynamic level values associated with TSTM and NTSTM periods.

4. Variables Used for TSTM and NTSTM Conditional Composite Anomalies, Correlations, and Teleconnections

Using the R1 data set, we examined the local and regional physical patterns and processes that characterized TSTM and NTSTM periods in Kabul in MAM. We analyzed TSTM and NTSTM conditional composite means and anomalies of a range of atmospheric and oceanic variables for the 129 TSTM and 129 NTSTM dates identified in the 14 WS Kabul SFC observation data set. From this analysis, we were able to analyze correlations and teleconnections among the different variables and gain a better understanding of the conditions that lead to TSTM and NTSTM events in Kabul. Table 2 lists the variables that we analyzed, their abbreviations, and units. In sections a-i, we discuss our reasons for choosing these variables.

Table 2. TSTM and NTSTM conditional composite anomaly variables, abbreviations, and units.

Variable	Abbreviation	Units
200 hPa geopotential height	Z200	geopotential meter (gpm)
850 hPa geopotential height	Z850	geopotential meter (gpm)
850 hPa air temperature	T850	degree Celsius (°C)
850 hPa specific humidity	SH850	kilogram per kilogram (kg/kg)
Precipitable water	PW	kilogram per meter squared (kg/m^2)
Precipitation rate	PR	millimeter per day (mm/day)
Outgoing longwave radiation	OLR	Watt per meter squared (W/m^2)
500 hPa Omega	ω500	Pascal per second (Pa/s)
Sea surface temperature	SST	degree Celsius (°C)
Lifted index	LI	degree Celsius (°C)

a. 200 hPa Geopotential Height

We analyzed the 200 hPa Geopotential Height (Z200) to characterize the upper level (UL) circulation and large-scale teleconnections.

b. 850 hPa Geopotential Height

We analyzed the 850 hPa geopotential height (Z850) to characterize the LL circulation and temperature and moisture transports.

c. 850 hPa Air Temperature

We analyzed the 850 hPa air temperature (T850) to enable us to characterize the thermodynamic properties of the air masses that were being advected into AFG.

d. 850 hPa Specific Humidity

We analyzed the 850 hPa specific humidity (SH850) to characterize moisture transports into AFG.

e. Precipitable Water

Precipitable water (PW) gave us information about the moisture content of the entire vertical column of air from the SFC–top of the atmosphere (Amer. Meteor. Soc. GoM 2011). The SFC value used for the R1 data set is 1000 hPa and the top of the atmosphere value used is 10 hPa (Kalnay et al. 1996).

f. Precipitation Rate

We analyzed precipitation rate (PR) because of its connections to moisture transports, moisture convergence, and TSTM activity, and as an indicator of latent heating.

g. Outgoing Longwave Radiation

We used outgoing longwave radiation (OLR) as an indicator of convection, clouds, precip, and latent heating (Libmann et al. 1996).

h. 500 hPa Omega

We used 500 hPa omega (ω500) to assess upward and downward vertical motion (UVM and DVM) and as an indicator of conditions favorable for TSTM or NTSTM activity.

i. Sea Surface Temperature

We analyzed sea surface temperature (SST) as an indicator of heat and moisture sources for driving atmospheric circulations and associated temperature and moisture transports.

j. Lifted Index

We used the R1 LI values to assess regional patterns of atmospheric stability/instability. Negative (Positive) values of LI indicate unstable (stable) conditions (Djuric 1994).

5. TSTM and NTSTM Analysis Methods

a. Necessary Ingredients for Thunderstorm Development

We analyzed the SFC, sounding, and R1 data to characterize the weather to climate scale, and local to hemispheric scale, conditions that characterize TSTM and NTSTM periods. These analyses involved compositing TSTM days and NTSTM days, and calculating the corresponding composite mean and composite climate anomaly patterns and implied processes.

Climate anomalies are commonly used in climate analysis, especially in the study of climate variations, to highlight how actual conditions differ from LTM conditions, which can be very useful in determining the causes and the predictability of climate variations (e.g., Moss 2007; DeHart 2011). A climate anomaly is defined as average (or LTM) conditions minus actual conditions for a given variable, period, and location (e.g., T850 anomaly for MAM in AFG). LTM conditions are for a given base period, which in our study was 1968–1996, the base period used by ESRL for the R1 data set.

We focused our analyses on variables that are known to be favorable and unfavorable to deep convection and TSTM activity. Wallace and Hobbs (2006) note that the necessary conditions for the occurrence of deep convection are:

(1) Instability from the existence of a conditionally unstable lapse rate, or potential instability, in which the environmental lapse rate (ELR) is less than the dry adiabatic lapse rate (DALR) and greater than the moist adiabatic lapse rate (MALR).

(2) Substantial LL moisture that increases the potential instability via latent heat release mechanisms. The amount of LL moisture varies widely in comparable storms in different geographical locations.

(3) LLCON, or a lifting mechanism, that is sufficient to release the potential instability. To overcome the stability that can exist near the SFC, represented by CIN, a lifting mechanism is required to lift an air parcel to the level of free convection (LFC) or CCL. At this point, the air parcel will respond to the temperature and moisture stratification to produce convective clouds. Common lifting mechanisms include orographic lift (cf. Djuric 1994).

(4) UL divergence and outflow from the convective region to allow continued UVM.

For our study, we focused on analyzing (a) the regional scale factors that contribute to favorable and unfavorable conditions for convection and TSTM activity, especially LL temperature and moisture advection, LL moisture convergence, UL divergence; and (b) sounding data as represented in skew T-log p diagrams for TSTM and NTSTM periods.

b. Skew T – Log P Analyses

We used skew T – log p analyses of Kabul sounding data to characterize the patterns and processes associated with TSTM and NTSTM conditions in Kabul.

CAPE: We used convective available potential energy (CAPE) as an indicator of stability/instability. On a skew T – log p sounding, CAPE is the area bounded by the environmental temperature (ELR) on the left and a moist adiabat (MALR) on the right from the lower boundary denoted by the LFC for the lifted parcel method, or CCL for the heated SFC parcel method, to the upper boundary denoted by the equilibrium level (EL) for both the heated and lifted methods. The numerical value for CAPE is given in Joules per kilogram (J/kg)

and is calculated as an integration of the bounded area (Wallace and Hobbs 2006). CAPE is calculated by conducting the following integration:

Equation 3. The Convective Available Potential Energy Integration

$$CAPE = \int_{LFC}^{EL} (F / \rho')dz$$

Here, *F* is the upward buoyancy force per unit volume on the rising air parcel due to the temperature difference between the parcel and its environment, and ρ' is the density of the air parcel (Wallace and Hobbs 2006). For CAPE to become available to the air parcel, a lifting mechanism (heating, mechanical forcing) is needed to get the parcel to its LFC (or CCL) (Wallace and Hobbs 2006). Table 3 shows CONUS values of CAPE associated with different levels of stability/instability.

Table 3. CONUS based CAPE threshold values and corresponding atmospheric stability or instability. CAPE values adapted from Wallace and Hobbs (2006).

CAPE Value in J/kg	Indicated Stability or Instability
0	Stable
0 – 1000	Marginally unstable
1000 - 2500	Moderately unstable
2500 - 4000	Strongly unstable
> 4000	Extremely unstable

CIN: Convective inhibition (CIN) is the amount of energy needed to lift a parcel to its LFC, and is measured in J/kg. It is represented on a skew T – log p sounding as the area bounded by the SFC pressure on the bottom, the LFC at the top, the ELR on the right, and on the left by a line parallel to the dry

adiabat from the SFC to the LCL, then upwards on a line parallel to the MALR to the LFC. CIN is analyzed using the SFC lifted air parcel method or the heated SFC air parcel method. The numerical value for CIN is calculated using the following integration (*Amer. Meteor. Soc. GoM* 2011):

Equation 4. The Convective Inhibition Integration

$$CIN = -\int_{p_i}^{p_f} R_d (T_{vp} - T_{ve}) d \ln p$$

Here, p_i is the pressure at the level where the air parcel originates, p_f is the pressure at the LFC, R_d is the specific gas constant for dry air (287.058 J/(kg - K), T_{vp} is the virtual temperature of the lifted air parcel, and T_{ve} is the virtual temperature of the environment. It is assumed that the environment is in hydrostatic balance and that the pressure of the air parcel is the same as that of the environment.

For typical CONUS conditions, CIN values over 50 J/kg are generally associated with little or no convection, unless lifting mechanisms are strong.

LI: The lifted index (LI) is a static stability index based on the difference between the temperatures (T) of a parcel lifted from the SFC–500 hPa and the T of the environment at 500 hPa. The parcel T is determined by assuming the parcel starts from the SFC with the sounding's SFC T and a SFC-850 hPa average weight, and then rises dry adiabatically to its LCL, and then rises wet adiabatically to 500 hPa: LI = $T_{500} - T_{parcel}$. Table 4 shows CONUS values of LI associated with different levels of stability/instability.

Table 4. CONUS based LI threshold values and corresponding atmospheric stability or instability. LI values adapted from Weather Prediction Education and Resources [Accessed online at: http://www.theweatherprediction.com, March 2011].

LI Value in °C	Indicated Stability or Instability
> 6	Very stable conditions
1 to 6	Stable conditions, TSTMs not likely
0 to -2	Slightly unstable, TSTMs possible, with lifting mechanism (i.e., cold front, daytime heating)
-2 to -6	Unstable, TSTMs likely, some severe with lifting mechanism
> -6	Very unstable, severe TSTMs likely with lifting mechanism

c. Static Stability/Instability Indices

We used the TSTM and NTSTM composite data to develop and test stability/instability indices for analyzing and forecasting TSTM conditions in Kabul. These indices were based primarily on sounding data, and were focused on the major differences in the composite soundings for TSTM and NTSTM periods.

d. TSTM and NTSTM Anomaly Regime Indices

Due to the importance of large-scale weather pattern recognition in the analysis and forecasting process and the impact of the regional circulation on the development of TSTM events, we developed indices based on large-scale patterns in the TSTM and NTSTM composite anomalies. In particular, we used the Z850 circulation and moisture anomaly fields to develop TSTM and NTSTM indices that could be used for short, medium, and long-range forecasting (e.g., 1–5 days, 5–15 days, > 15 days).

THIS PAGE INTENTIONALLY LEFT BLANK

III. RESULTS

A. THUNDERSTORM AND PRECIPITATION TIME SERIES ANALYSIS

1. Seasonal Cycle of Thunderstorm and Precipitation Activity (Monthly and Bi-weekly)

We examined the entire 14 WS Kabul SFC observation data set to determine what time of the year TSTMs were most frequent. We discovered that the MAM period represents the highest frequency of TSTM activity during any given year (Figure 9). There were a total of 215 days when one or more TSTM hours were observed during our study period of 04 March 2002–31 July 2010. Out of these 215 TSTM days, 129 (60%) of them occurred during MAM. Figure 9 shows that for the MAM period, March had 27 TSTM days, followed by April with 52 TSTM, and May with 50 TSTM days. Notice how March marked the beginning of the TSTM season after a minimum in TSTM activity during December–February. From May–June TSTM activity decreased by more than 50%. There were 21 TSTM days in June, similar to the 27 days in March. However, we chose to focus our study on March–May, rather than March–June because of (1) strong similarities in the regional circulation patterns during March, April, and May; and (2) clear differences between the patterns for those three months and the corresponding patterns during June (not shown).

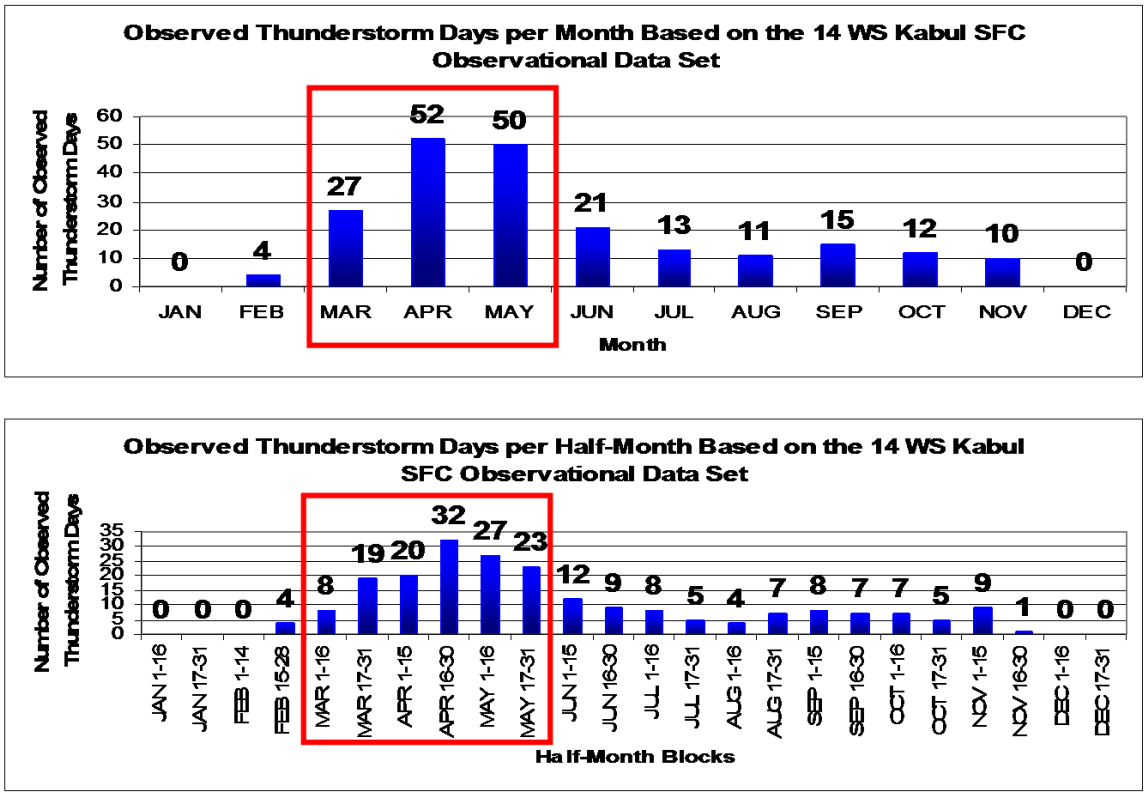

Figure 9. Observed Kabul TSTM days for each month of the year (top) and each half-month block of the year (bottom). Based on Kabul TSTM observations during the study period of 04 Mar 2002–31 Jul 2010. A TSTM day is defined as a day that has at least one observed TSTM. Note that March, April, and May (MAM, red box) account for 60% of the TSTM days during the study period. Note the gradual increase in TSTM day frequency beginning during early March and peaking in the middle of April, which is then followed by a gradual decrease as spring transitions to summer during late May.

When we break down the 12 months of a year into 24 half-month blocks, we achieve better resolution on the distribution of TSTM days. The bottom of Figure 9 shows that there is a significant increase in TSTM activity from the first half of March to the second half of March. Peak TSTM activity occurs during the second half of April with 32 TSTM days, which is followed by a gradual decrease in activity towards the end of May, leading into the less active summer months.

Figure 10 shows that there is an overall positive correlation between TSTM and precip activity, especially during the MAM period. Note in particular that when the TSTM activity peaks in MAM, so does precip activity. The precip observations are based on the U.S. Air Force threshold definition of precip greater than 0.005 inches (in) in an hour. Thus, for example, the zero precip for January indicates that there were no hours during which the threshold was exceeded in January, but it does not mean that there was no January precip during the study period.

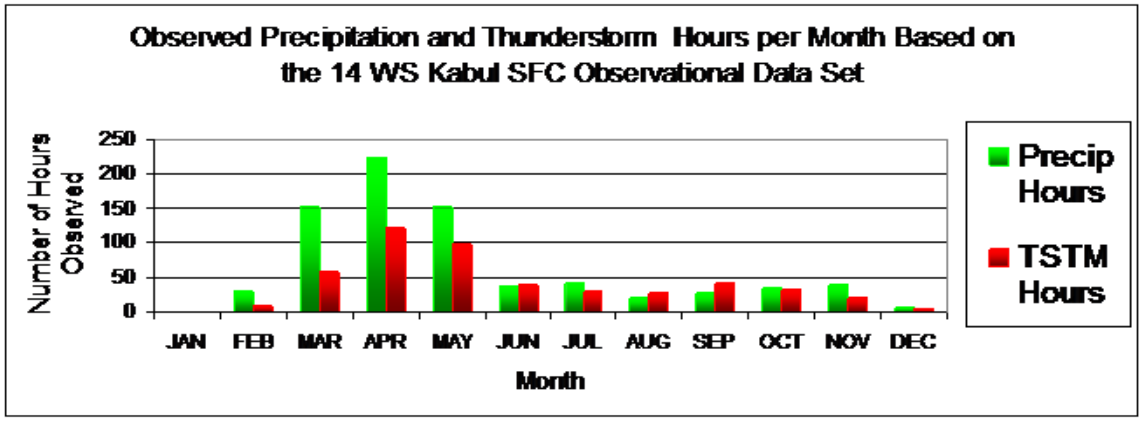

Figure 10. Observed Kabul monthly precip and TSTM hours. Based on Kabul precip and TSTM observations during the study period of 04 Mar 2002–31 Jul 2010. A precip hour is defined as an hour with a precipitation water equivalent greater than the trace threshold value of 0.005 inches. A TSTM hour is defined as an hour with at least one TSTM. Note: (1) the largest number of both precip hours and TSTM hours in March-April-May (MAM); and (2) the indications of an overall positive correlation on a monthly basis between precip hours and TSTM hours.

Figure 11 shows the number of precip hours and TSTM hours in half-month blocks for MAM. The precip and TSTM hours tend to vary in similar ways, but the variations in precip hours tend to lead those in TSTM hours by about two to four weeks.

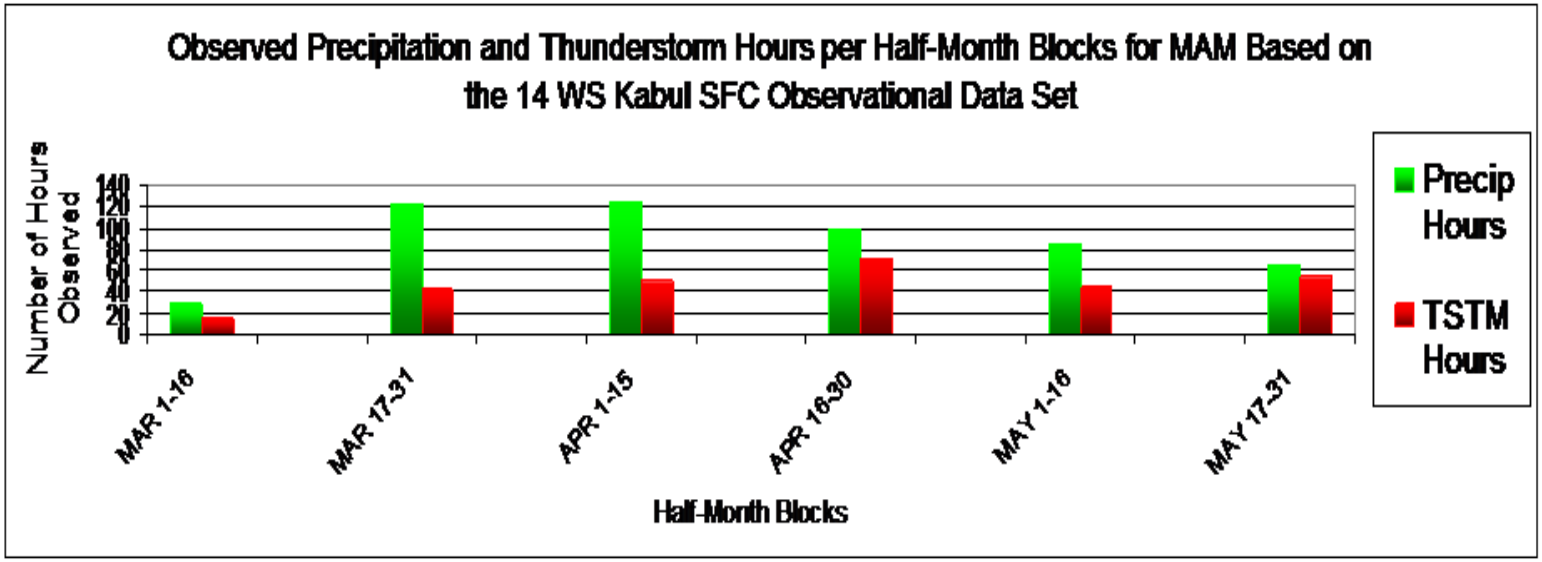

Figure 11. Observed Kabul half-monthly precipitation hours and TSTM hours during March-April-May (MAM). Based on Kabul precipitation and TSTM observations during the study period of 04 Mar 2002–31 Jul 2010. A precipitation hour is defined as an hour with a precipitation water equivalent greater than the trace threshold value of 0.005 inches. A TSTM hour is defined as an hour that has at least one TSTM. Note that there is a general correspondence between precipitation hours and TSTM hours, but that the peak in precipitation hours occurs in the second half of March and first half of April, about two to four weeks prior to the peak in TSTM hours in the second half of April.

2. Hourly Variations in Thunderstorm Activity

An important factor in analyzing and forecasting TSTMs is determining what time of the day or night they are most likely to occur. For this discussion, it is useful to refer to Kabul Local Time (KLT), which is UTC plus 0430 hours. The daily peak TSTM activity occurs during: (1) 1630–2330 KLT, with a peak at 1830 KLT, for January–December; and (2) 1230–2030 KLT, with a peak at 1630 KLT, for MAM (Figure 12).

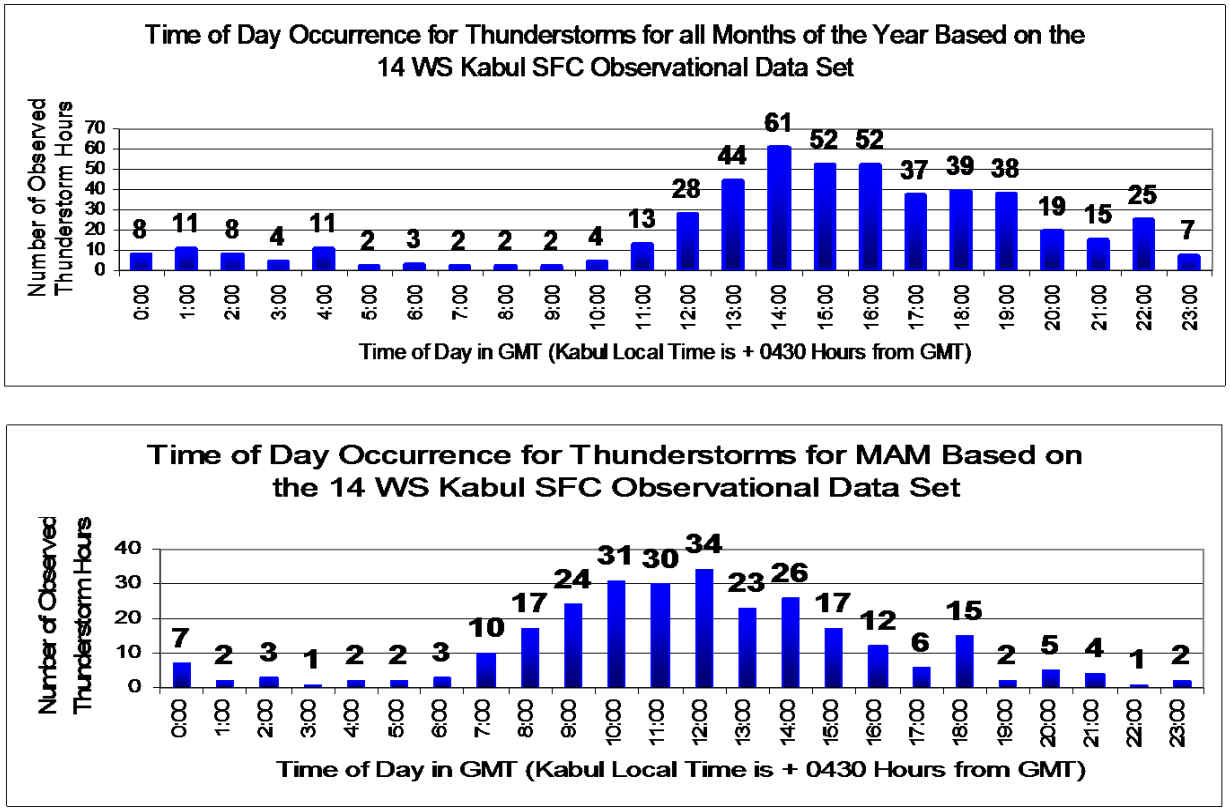

Figure 12. Time of day when Kabul TSTMs occur for: (top) all months of the year and (bottom) March-April-May (MAM). Based on Kabul TSTM observations during the study period of 04 Mar 2002–31 Jul 2010. Note that, when averaged over all months, the peak time of day for TSTM activity is approximately 1400 UTC/1830 Kabul local time (KLT). But, when averaged over only MAM, the peak time of day for TSTM activity is approximately 1200 UTC/1630 KLT.

Figures 13–15 shows the hourly TSTM distributions for March, April, and May, respectively, for each month as a whole, and for the first and second halves of each month. Note the general tendency for TSTM activity to occur over a wider range of hours, and to peak slightly later in the day, as the season progresses from March–May.

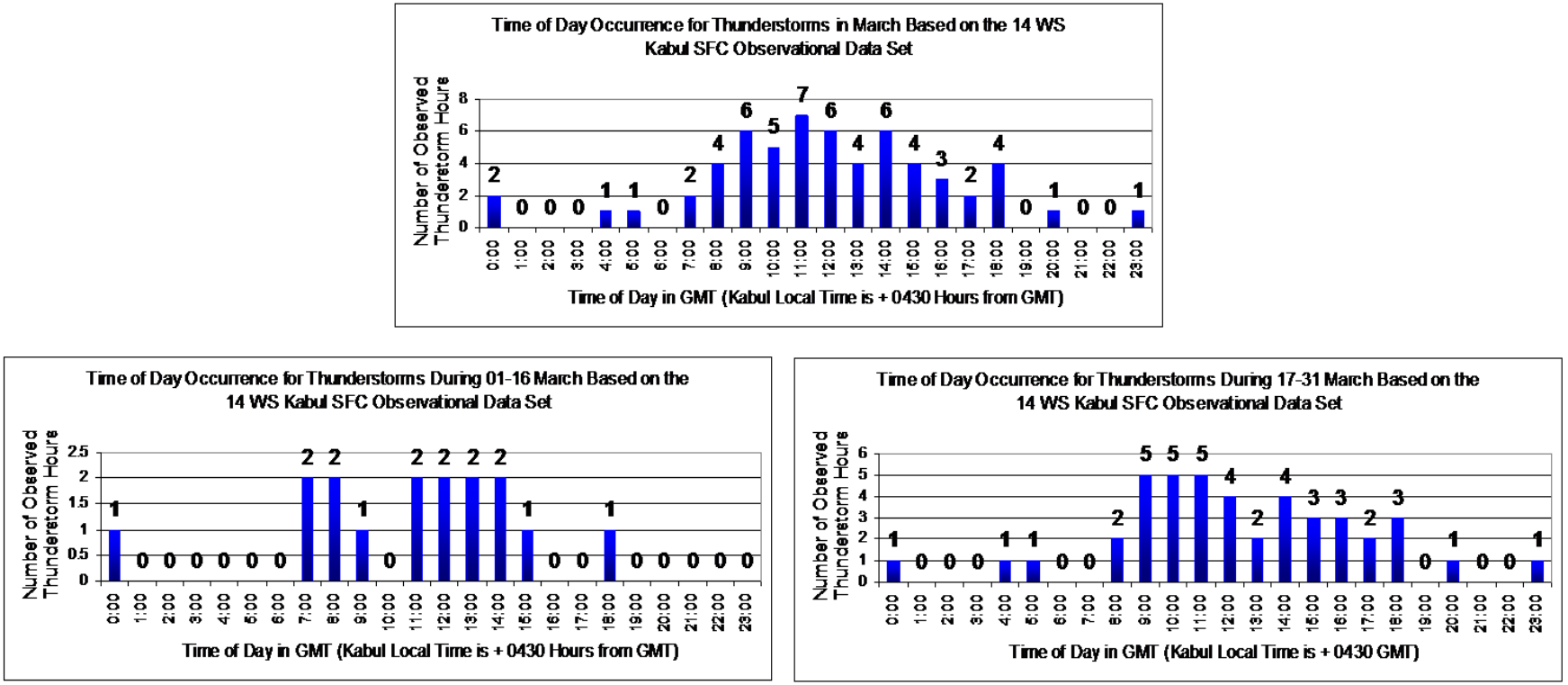

Figure 13. Time of day when Kabul TSTMs occur for: (top) March; (bottom left) 01–16 March; and (bottom right) 17–31 March. Based on Kabul TSTM observations during the study period of 04 Mar 2002–31 Jul 2010. Note that the March peak in TSTM activity is at approximately 0900–1400 UTC/1330–1830 KLT.

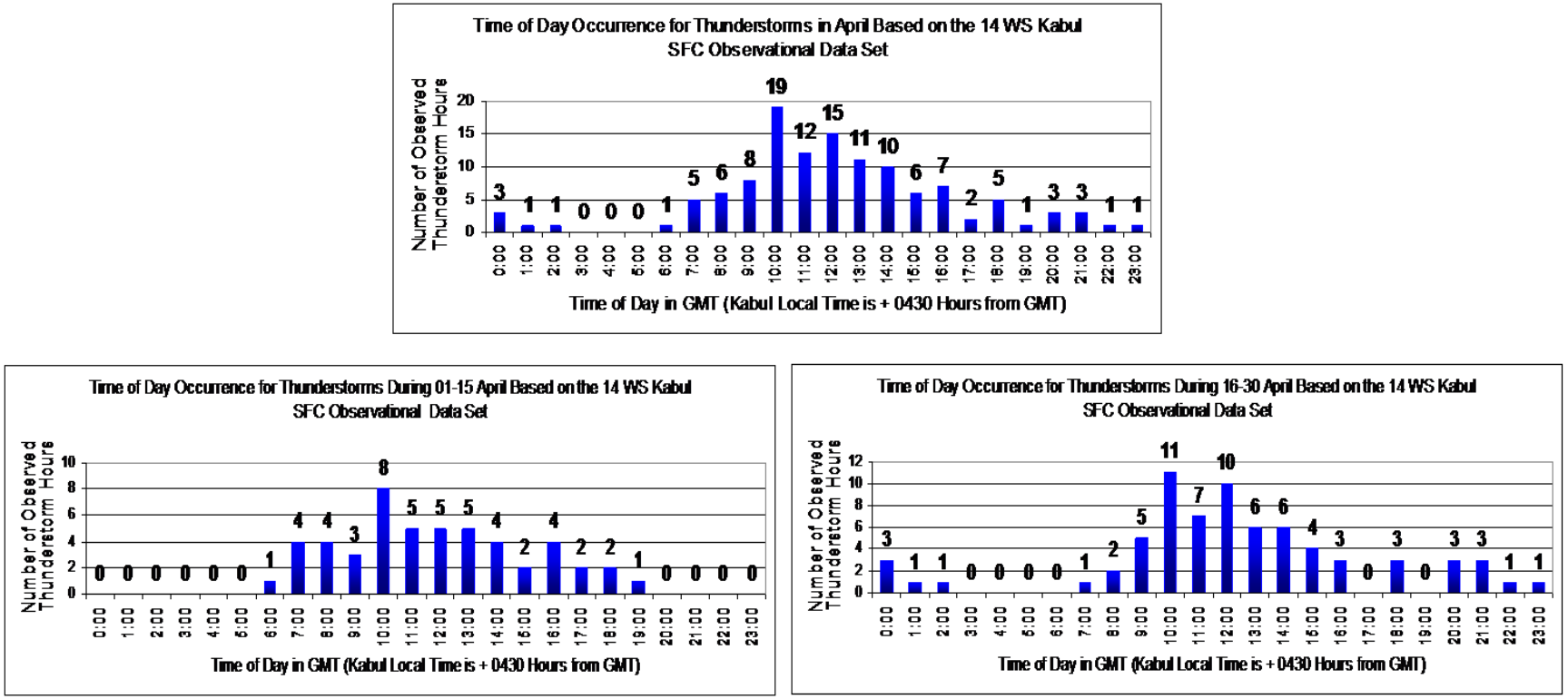

Figure 14. Time of day when Kabul TSTMs occur for: (top) April; (bottom left) 01–15 April; and (bottom right) 16–30 April. Based on Kabul TSTM observations during the study period of 04 Mar 2002–31 Jul 2010. Note that the April peak in TSTM activity is at approximately 0700–1600 UTC/1130–2030 KLT.

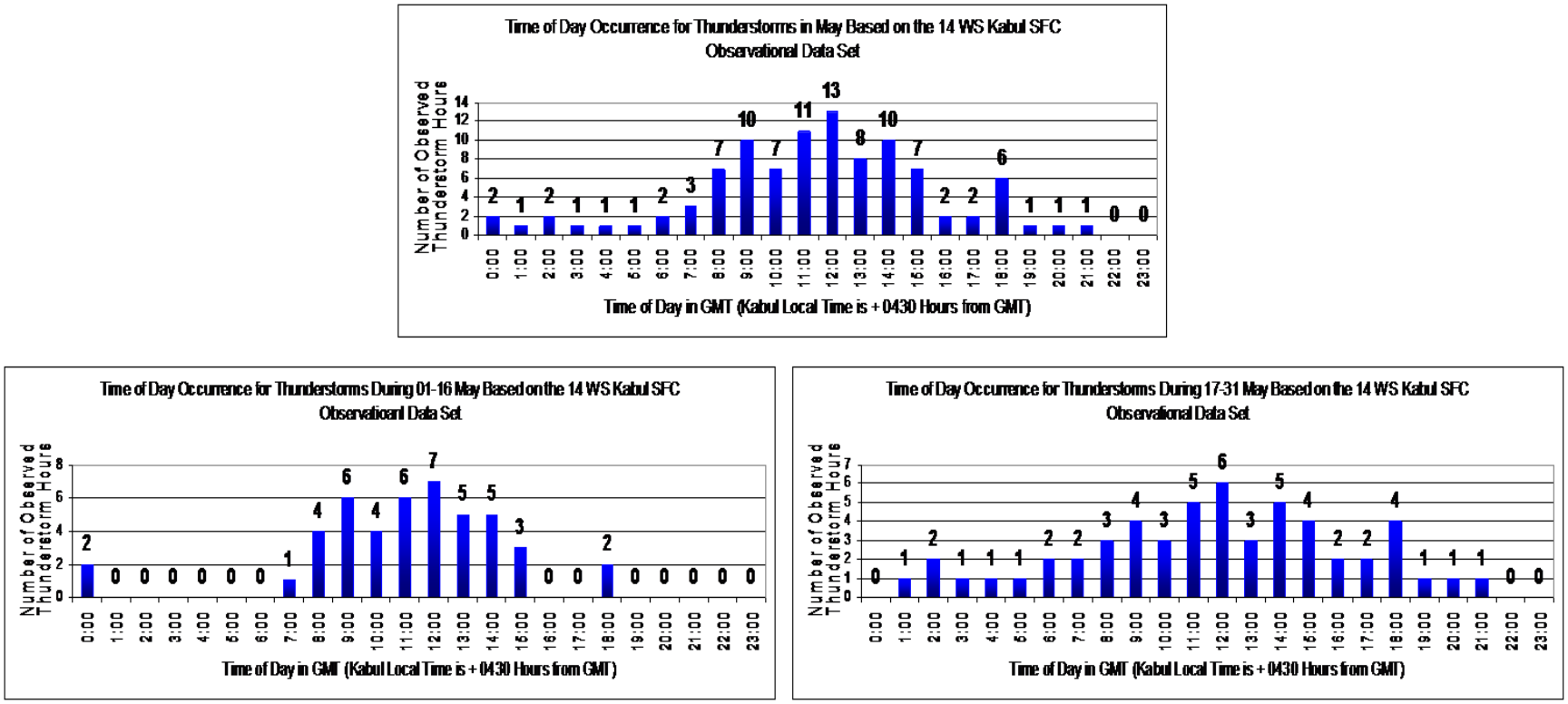

Figure 15. Time of day when Kabul TSTMs occur for: (top) May; (bottom left) 01–16 May; and (bottom right) 17–31 May. Based on Kabul TSTM observations during the study period of 04 Mar 2002–31 Jul 2010. Note that the May peak in TSTM activity is at approximately 0800–1500 UTC/1230–1930 KLT.

3. Intraseasonal and Interannual Variations in Thunderstorm Activity

Figure 16 shows the intraseasonal and interannual variations in MAM TSTM days. These results are based on just the 9.3 years of data in the study period, so they cannot represent long-term interannual or decadal scale changes. However, they do reveal large interannual variations on shorter interannual time scales, as well as large intraseasonal variations. The large intraseasonal variability in the number of observed TSTM days can be readily identified by comparing any given March, April, or May to the other MAM months in the same year. For example, in 2009, March had 1 TSTM day, April had 10 TSTM days, and May had 7 TSTM days. In general, the number of TSTM days in any given month in MAM does not seem to be related to the number of TSTM days in the other MAM months of that year. The large interannual variability in the number of observed TSTM days can be readily identified by comparing any given month to the same month in other years. For example, May had 4 TSTM days in 2004, 7 in 2005, and 0 in 2006. In general, the number of TSTM days in any given month and year do not seem to be related to the number of TSTM days in the preceding or following years. The large intraseasonal variations in TSTM activity suggest that TSTM activity in AFG may be related to larger scale intraseasonal climate variations, especially the Madden-Julian Oscillation (MJO). Such variations have been shown to affect AFG and nearby regions (e.g., Vorhees 2006; Moss 2007; DeHart 2011). This in turn indicates that TSTM activity may be predictable at medium to long lead times based on information about precursor climate variations (e.g., tropical OLR changes associated with MJO).

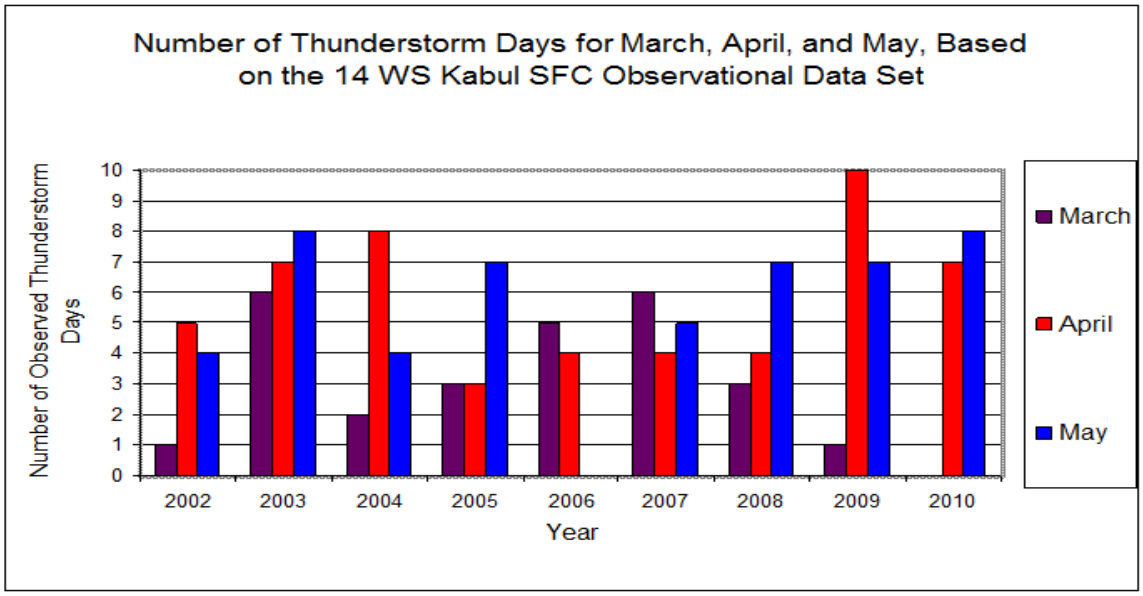

Figure 16. Observed Kabul TSTM days in March, April, and May (MAM) during 2002–2010. Based on Kabul TSTM observations during the study period of 04 Mar 2002–31 Jul 2010. A TSTM day is defined as a day that has at least one TSTM. Note the large intraseasonal and interannual variability in March–May TSTM activity, and the absence of TSTM days during May 2006 and March 2010.

When we apply a smooth fit to the individual monthly values and add a trend line, more information about the interannual variations in TSTM activity during MAM becomes evident. Figures 17–18 show the results of these analyses of TSTM activity in terms of TSTM days (Figure 17) and TSTM hours (Figure 18). Figure 17 shows that (1) March has an apparent four-year period of interannual variation with an overall decreasing linear trend in time; (2) April has an apparent five-year period of interannual variation with an overall increasing linear trend in time; and (3) May has an apparent four-year period of interannual variation with an overall increasing linear trend in time. Figure 18 shows similar results, except that there are no significant long-term trends for April and May.

The results shown in Figures 17–18 concerning interannual variations are preliminary, since our data set for these results is only 9.3 years long. However, these results strongly indicate that TSTM activity in AFG is affected by interannual climate variations. Such variations tend to be related to large-scale

regional, hemispheric, and/or global scale climate phenomena, such as El Nino–La Nina (ENLN) and the Indian Ocean Zonal Mode (IOZM), that have been shown to influence temperature, winds, and precipitation in AFG and nearby regions (e.g., Vorhees 2006; Moss 2007; DeHart 2011). This in turn indicates that TSTM activity may be predictable at medium to long lead times based on information about precursor climate variations (e.g., tropical SST changes associated with ENLN or IOZM).

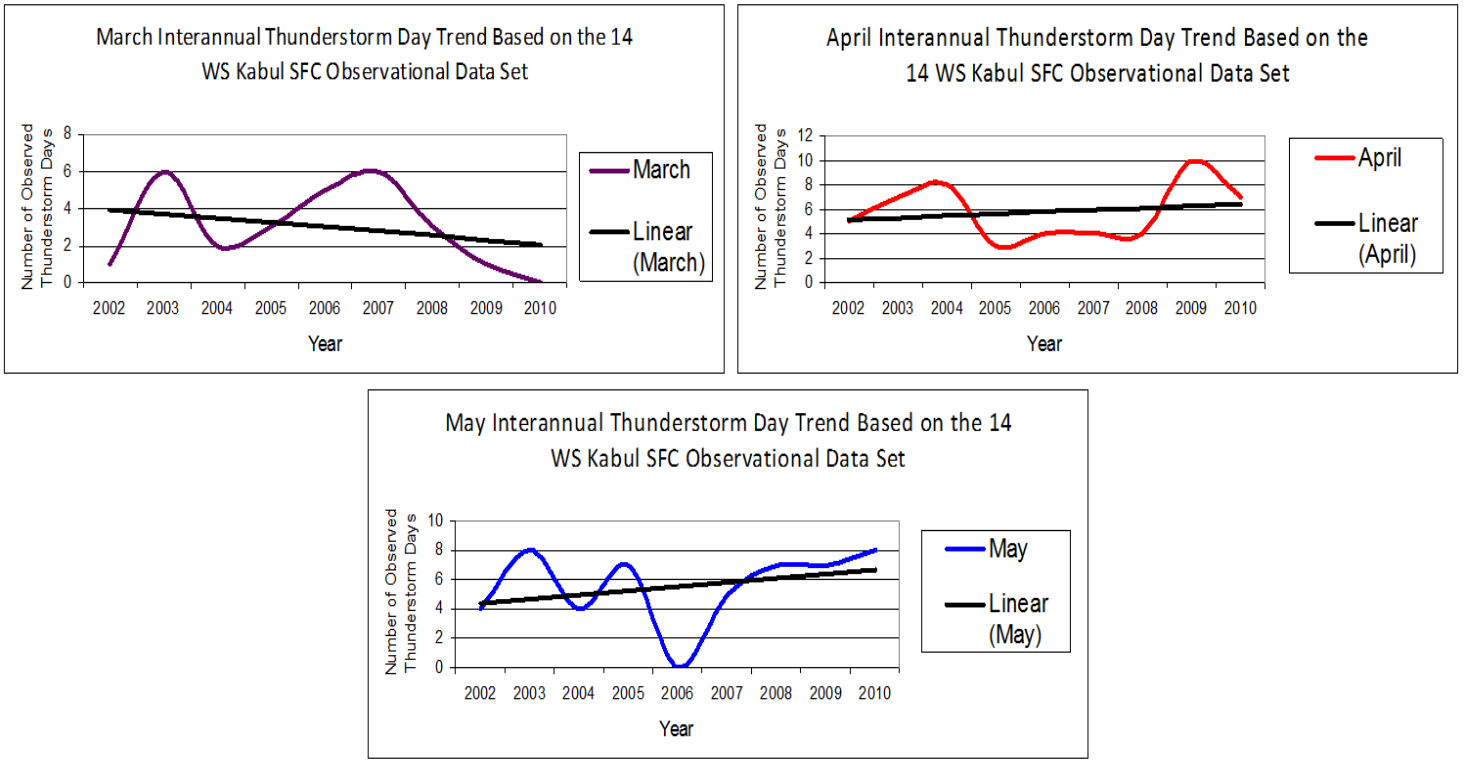

Figure 17. Observed Kabul TSTM days in March (top left), April (top right), and May (bottom) during 2002–2010. Based on Kabul TSTM observations during the study period of 04 Mar 2002–31 Jul 2010. A TSTM day is defined as a day that has at least one TSTM. Note the large percentage interannual variability in March– May TSTM activity, and the absence of TSTM days during May 2006 and March 2010. The curves in each panel represent a smooth fit to the individual monthly values (Figure 16). The straight black lines represent nine-year linear trends. Note that: (1) March shows a decreasing linear trend and evidence of an interannual variation with a four-year period; (2) April shows an increasing linear trend and evidence of an interannual variation with a five-year period; and (3) May shows an increasing linear trend and evidence of an interannual variation with a four- year period.

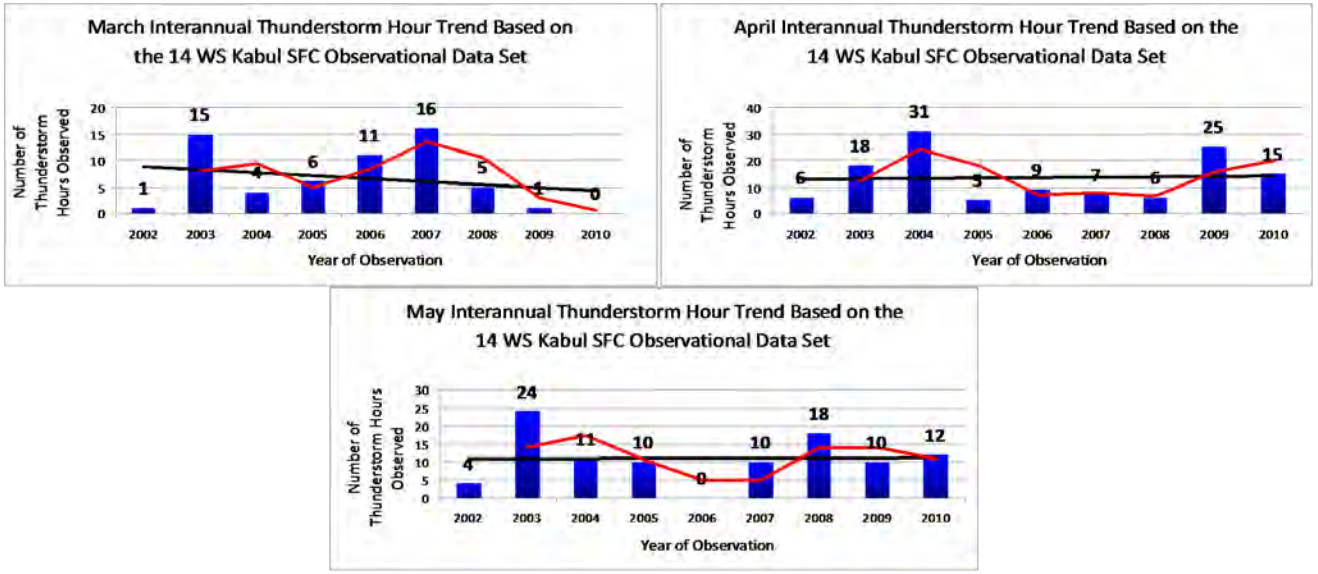

Figure 18. Observed Kabul TSTM hours in March (top left), April (top right), and May (bottom) during 2002–2010. Based on Kabul TSTM observations during the study period of 04 Mar 2002–31 Jul 2010. A TSTM hour is defined as an hour that has at least one TSTM. Note the large interannual variability in March–May hourly TSTM activity, and the absence of TSTM hours during May 2006 and March 2010. The red lines in each panel represent a moving average based on the previous two-year average value of TSTM hours observed. The straight black lines represent nine-year linear trends. Note that each month shows evidence of interannual variations with periods of about 4–5 years, and that March shows a decreasing linear trend. Comparison of Figures 13–18 provides evidence of a positive correlation between the number of TSTM days and the number of TSTM hours for March and April (MA) and a negative correlation between the number of TSTM days and the number of TSTM hours for May. Thus, when MA has a large (small) number of TSTM days they also tend to have a large (small) number of TSTM hours. When May has a large (small) number of TSTM days, it tends to have a smaller (larger) number of TSTM hours.

B. LONG-TERM MEAN (LTM) REGIONAL CLIMATE

1. LTM MAM SST, T850, Z850, Z200, SH850, OLR, and PR

Figures 19–21 show LTM SST, and air temperature and specific humidity at 850 hPa (T850, SH850), in the large-scale region surrounding AFG during MAM. These LTM conditions are useful in assessing the patterns and processes that affect TSTM activity in AFG. Figure 19 shows that warm tropical and subtropical waters reside to the south and east of AFG, with cooler waters to the north and west in the Mediterranean, Caspian, Black, and Aral Seas. Figure 20 shows relatively warm (cool) T850 to the south (north) of AFG, and large T850 gradients to the north of AFG. Figure 21 shows relatively high SH850 values over the tropics and Southeast Asia, and relatively low SH850 over most of SWA, India, and the northwestern IO. The high SH850 values over and near Tibet and the Himalayas and nearby mountain ranges, are likely a result of the elevated surface with large amounts of year-round snow. The SST, T850, and SH850 patterns in Figures 19–21 indicate that (1) large-scale, LL southerly (northerly) flow into AFG would tend to be favorable for the advection of warm moist (cool dry) air into AFG; and (2) the convergence of southerly (warm moist) and northerly (cool dry) flows over AFG would favor instability over AFG.

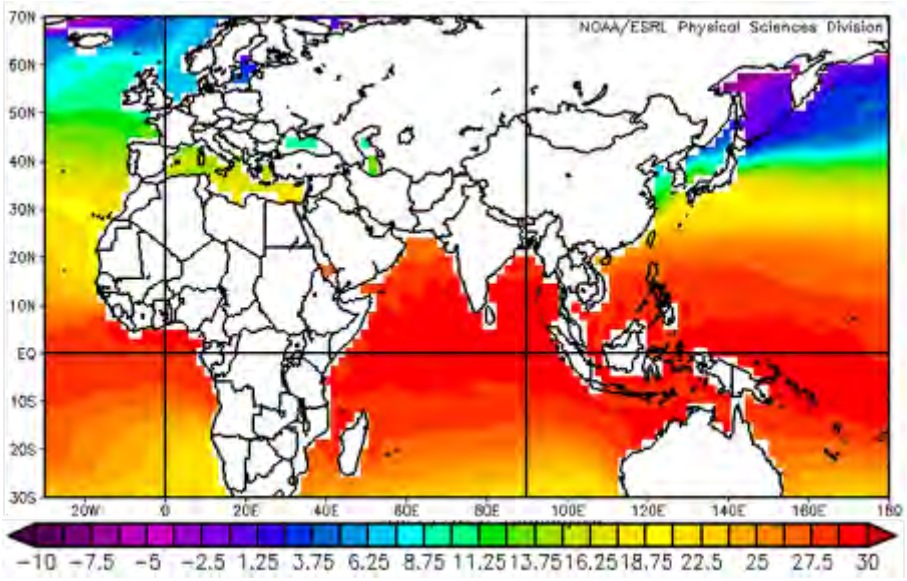

Figure 19. Long-term mean (LTM) sea surface temperature (SST; °C) for March-April-May (MAM). Note the warm tropical and subtropical waters to the south and east of AFG and the cooler waters in the Mediterranean, Caspian, Black, and Aral Seas to the north and west of AFG. LTM base period: 1968–1996.

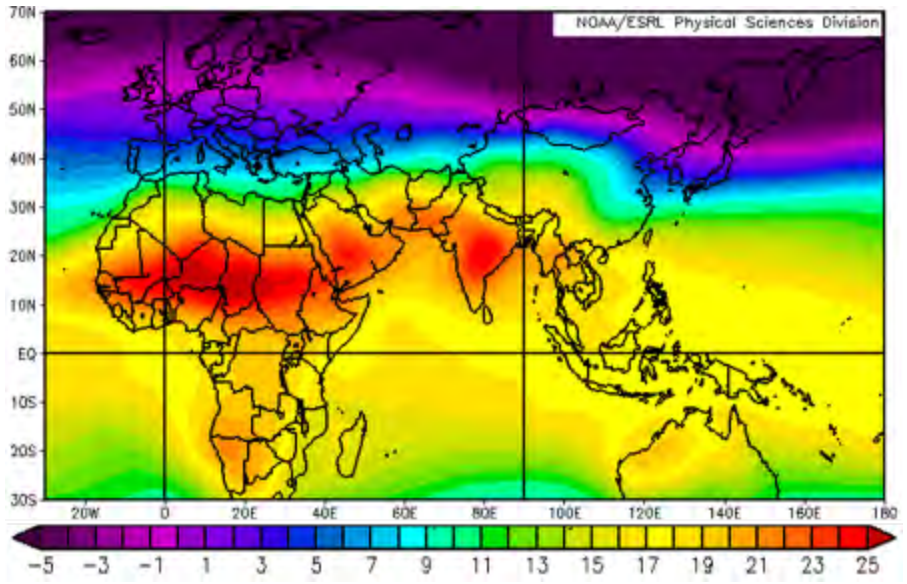

Figure 20. Long-term mean (LTM) 850 hPa (Z850) air temperature (T850; °C) for March-April-May (MAM). Note the warm (cool) air to the south (north) of Afghanistan and the large temperature gradients to the north of Afghanistan. LTM base period: 1968–1996.

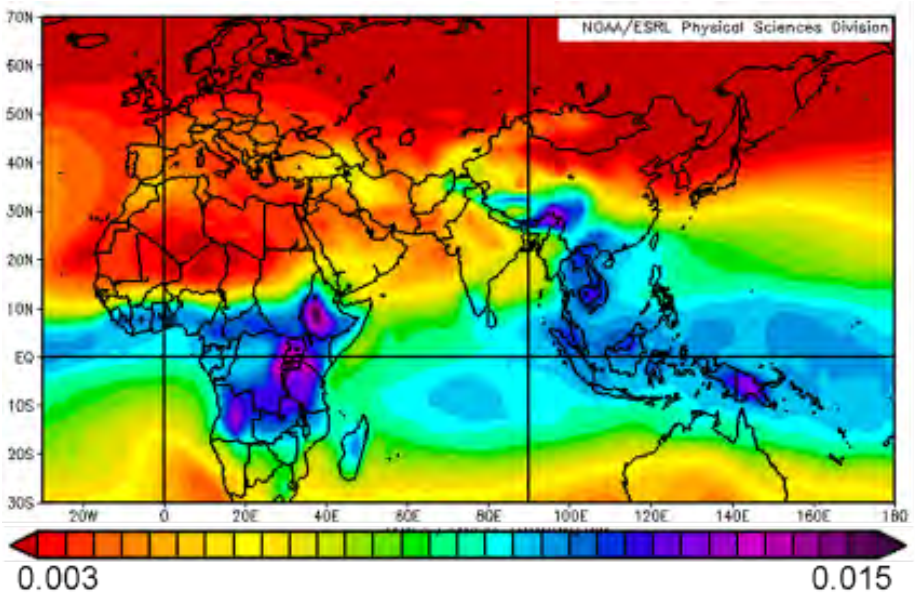

Figure 21. Long-term mean (LTM) 850 hPa specific humidity (SH850, kg/kg) for March-April-May (MAM). The contour interval is 0.0004 kg/kg. Note the generally high SH850 in the tropics and southeast Asia extending into northern Pakistan and northeast Afghanistan, and the generally low SH850 over SWA and most of India. LTM base period: 1968–1996.

Figure 22 shows the LTM MAM 850 hPa geopotential heights (Z850). AFG is located within a trough that extends across Iran, AFG, PAK, and northern India. Ridges are located to the southwest of AFG centered over Saudi Arabia and to the east centered over western China. Together, these height patterns indicate a tendency for low-level cyclonic flow centered over or near AFG, with northwesterly flow in southern AFG and southeasterly flow over northern AFG. This LTM low-level circulation is favorable for the development of convection over and near AFG.

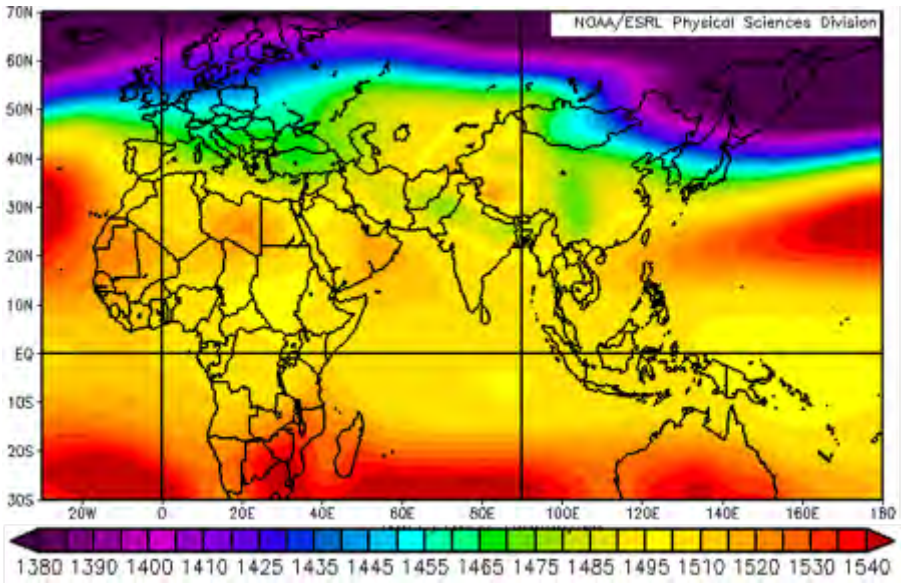

Figure 22. Long-term mean (LTM) 850 hPa geopotential height (Z850, gpm) for March-April-May (MAM). Note the ridging centered near the Arabian Peninsula and western China, with a trough extending southeastward from Iran, across AFG, Pakistan, and north India. LTM base period: 1968–1996.

Figure 23 shows the LTM MAM 200 hPa (Z200) geopotential heights. AFG generally lies under the STJ (as indicated by its position beneath a strong Z200 gradient), and is bounded by a broad trough centered over southern Europe and a broad ridge centered over western China. This LTM upper level circulation is favorable for the transiting of ETCs over and near AFG, and upper level divergence and the development of convection over and near AFG.

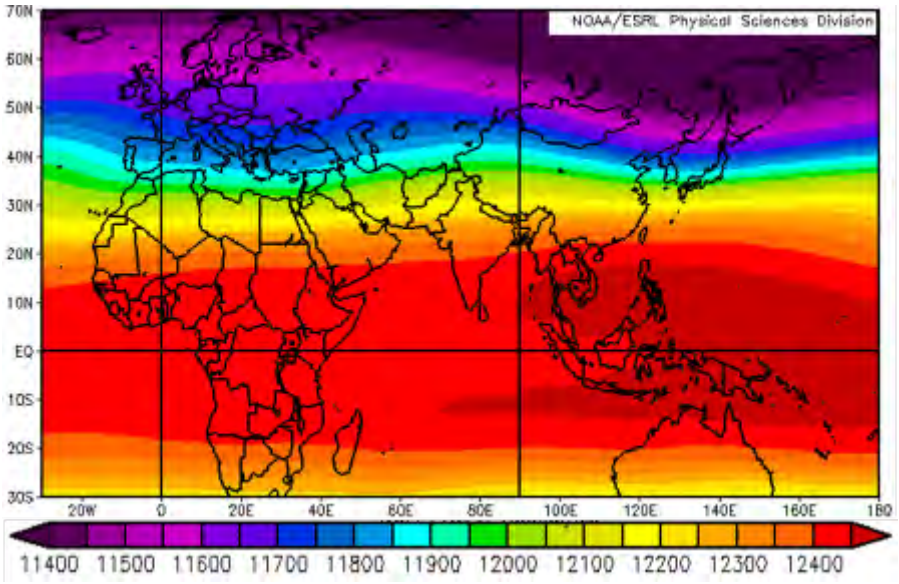

Figure 23. Long-term mean (LTM) 200 hPa geopotential height (Z200, gpm) for March-April-May (MAM). Note that AFG lies to the east of a broad trough centered over southern Europe and to the west of broad ridge centered over western China. LTM base period: 1968–1996.

The LTM MAM OLR is depicted in Figure 24. Note the high values of OLR over northern Africa, the Arabian Peninsula, the northwestern Indian Ocean (IO), and most of India. These high OLR values indicate a tendency for subsidence and are consistent with the high T850, low SH850, and high Z850 in this area shown in Figures 20–22. AFG lies on the northern edge of this subsidence region, which indicates that deep convection over and near AFG is sensitive to small changes in the location and strength of the subsidence region.

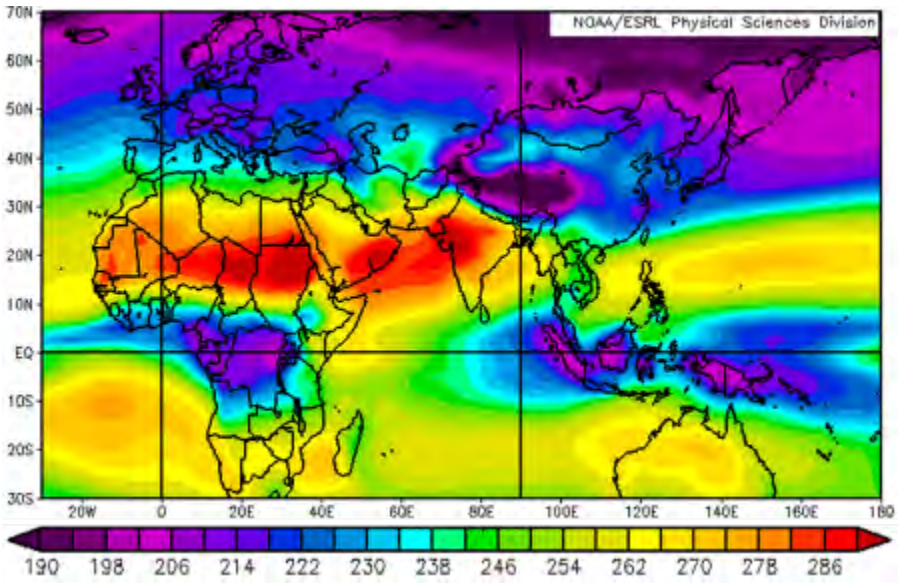

Figure 24. Long-term mean (LTM) outgoing longwave radiation (OLR, W/m^2) for March-April-May (MAM). Note: (1) the generally high OLR over the NIO, indicating low levels of non-convective activity; and (2) the generally low OLR over western-central China, northern AFG, and west of the Caspian Sea, indicating cold surface and lower tropospheric temperatures and/or low levels of deep convective activity. LTM base period: 1968–1996.

Figure 25 shows the LTM MAM PR. PR is generally: (1) low over northern Africa, SWA, and most of India; and (2) high over much of the tropics, Southeast Asia, and northern AFG and PAK. These results are consistent with the results shown in Figures 20–24. Note too that the high precip values over the western tropical Pacific and maritime continent are consistent with the high SSTs, high specific humidity, persistent deep convection, and low OLR in that region. Intraseasonal to interannual variations in convection in this region have been shown to influence circulations and temperature and moisture advection over and near SWA, including over AFG and PAK (Vorhees 2006; Stepanek 2006; Moss 2007; DeHart 2011).

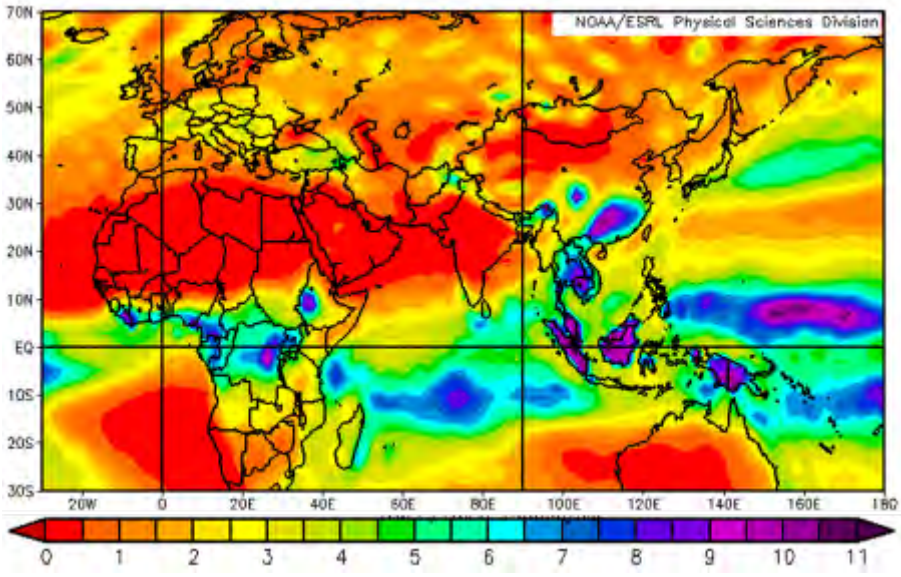

Figure 25. Long-term mean (LTM) precipitation rate (PR, mm/day) for March-April-May (MAM). Note: (1) the low PR over northern Africa, SWA, and most of India; and (2) the relatively high PR over much of the tropics, Southeast Asia, and northern Afghanistan and Pakistan. LTM base period: 1968–1996.

C. CLIMATE VARIATION ANALYSIS

1. TSTM Conditional Composite Anomaly Results

The actual conditions for our anomaly calculations were those for the 129 MAM TSTM days and 129 MAM NTSTM days in Kabul that we identified in our study period. Our analyses focused on 129-day composites of anomalous TSTM (NTSTM) conditions to highlight the deviations from LTM conditions that characterize and are potentially favorable (unfavorable) for TSTM activity. All of our discussions of climate variations in this report are based on analyses of 129-day composite anomalies for TSTM and NTSTM conditions, unless otherwise stated. The information on LTM conditions presented in Figures 19–25 was used to infer the impacts of anomalous conditions (e.g., positive temperature and moisture advection anomalies associated with northward low-level wind anomalies from the AS into AFG were inferred from the LTM MAM T850 and

SH850 information in Figures 20–21). Our climate variation analyses focused on large-scale mechanisms occurring over the full MAM period, since climate variations tend to be associated with processes occurring over large regions and extended periods (e.g., basin, hemispheric, or global scales, and several months). This large-scale perspective helps describe the regional context within which variations in Kabul TSTM and NTSTM activity occur. Thus, in this section, much of the focus is on conditions over AFG and nearby regions of PAK, as opposed to conditions over and near Kabul.

a. Z850 Anomalies

Figure 26 shows the Z850 TSTM composite anomalies for March, April, and May. Note the similar pattern in each month: a L centered near central Asia (in the vicinity of Turkmenistan, Uzbekistan, Tajikistan, Kyrgyzstan, and Kazakhstan—referred to as the Stans from here on), a L centered near southeastern Saudi Arabia, a high pressure cell (H) centered near and east of the Caspian Sea; and a H centered near Tibet. This pattern indicates that during TSTM periods there is a tendency for anomalous: (1) warm-moist air advection (WMAA) from the AS and BoB, and cold-dry air advection (CDAA) from central Eurasia just east of the Caspian Sea, into AFG; (2) LLCON of these different air masses over AFG. The similar patterns for these three months indicate that (1) similar processes are operating during each of the three months to produce TSTM activity near Kabul and (2) the large-scale circulation anomalies that lead to Kabul TSTMs in MAM can be represented well by three-month, MAM, composite anomalies.

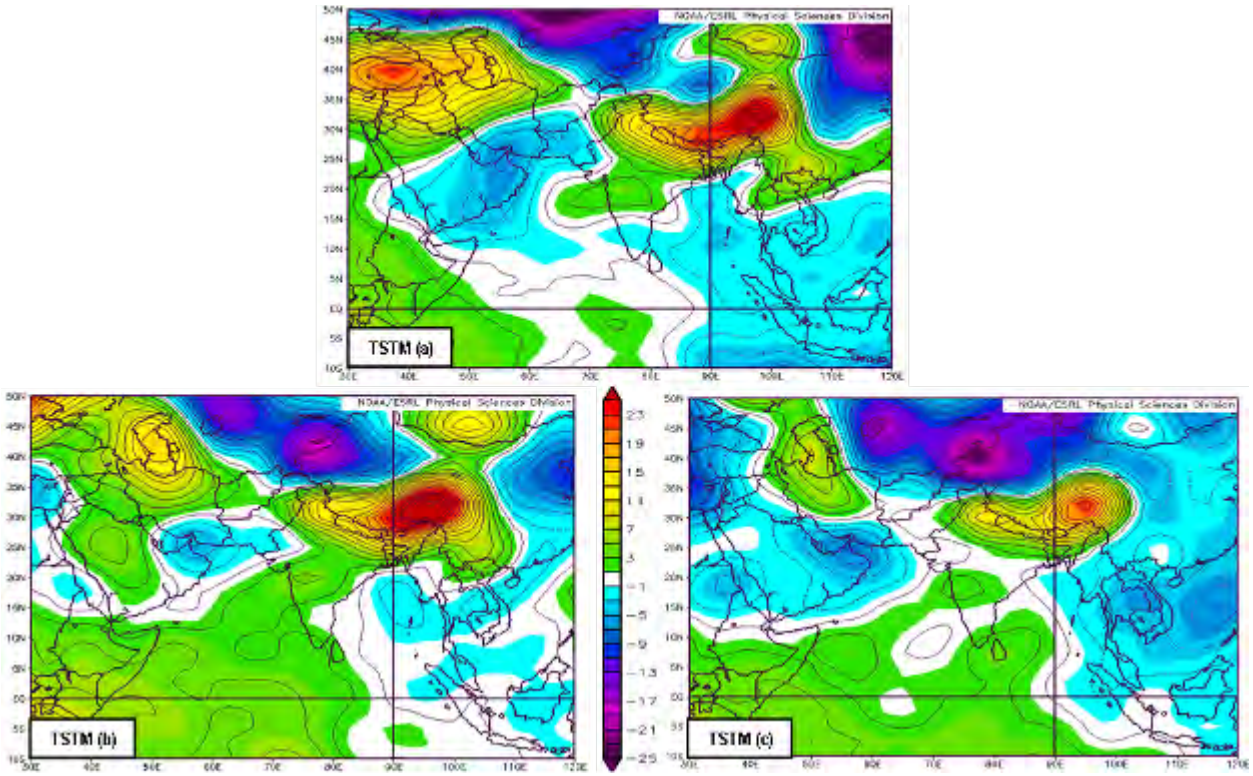

Figure 26. TSTM conditional composite anomalies of 850 hPa geopotential height (Z850; gpm) for: (a) Mar, (b) Apr, and (c) May. Based on Kabul TSTM observations during 04 Mar 2002–31 Jul 2010. Note the similar patterns for the three months, especially the anomalous four-part pattern with a: (1) L centered near central Asia; (2) L centered near southeastern Saudi Arabia; (3) H centered near and east of the Caspian Sea; and (4) H centered near Tibet. This pattern is favorable for anomalous warm-moist air advection (WMAA) from the southeast and cold-dry air advection (CDAA) from the northwest into AFG. This leads to anomalous LLCON over AFG—for example, anomalous WMAA from the Arabian Sea and Bay of Bengal, and CDAA from central Eurasia east of the Caspian Sea.

Compositing the three anomalies shown in Figure 26 produces the Z850 TSTM composite anomalies for MAM shown in Figure 27. As expected, the anomaly patterns are similar to, and simpler than, those in Figure 26. The net implied impact of these height anomalies is anomalous LLCON of cold dry air advected toward AFG from the northwest with warm moist air advected toward AFG from the southeast. These anomalies are useful in determining the regional climate regimes and physical processes that are favorable for TSTM activity near Kabul.

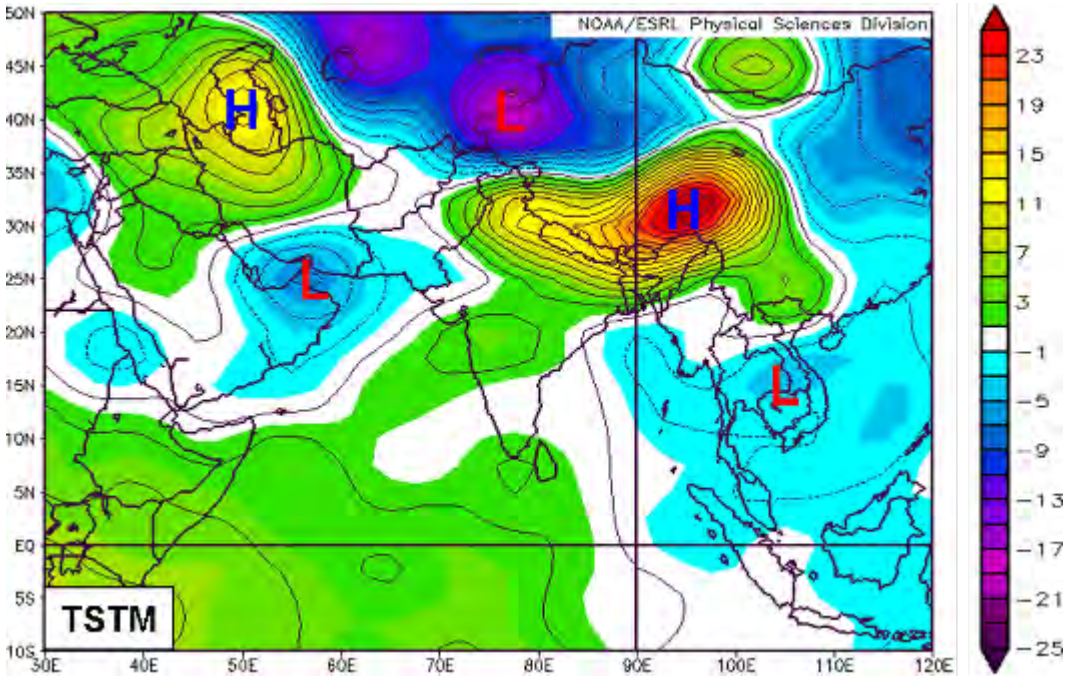

Figure 27. TSTM conditional composite anomalies of 850 hPa geopotential height (Z850; gpm) for MAM. Based on Kabul TSTM observations during 04 Mar 2002–31 Jul 2010. Note: (1) the anomalous L centered over the Strait of Hormuz and the anomalous H centered over Tibet that together support anomalous WMAA into AFG; and (2) the anomalous H centered over the Caspian Sea and the anomalous L centered over central Asia that together support anomalous CDAA toward AFG. The net effect is anomalous LLCON over AFG of CDA from the north and WMA from the south. These anomaly patterns help identify the regional climate regimes and physical mechanisms that are favorable for TSTM activity over AFG.

Figure 28 shows the same information presented in Figure 27, except for a larger region and schematic arrows that indicate the main LL anomalous circulations (inferred from the height anomalies). These arrows indicate a general anomalous convergence of air over AFG, with anomalous transports into AFG originating well to the north, south, and east of AFG (e.g., cP air from central Russia, and mT air from the AS, BoB, and South China Sea). This indicates that AFG TSTM activity is related to remote circulation, and temperature and moisture advection and convergence anomalies.

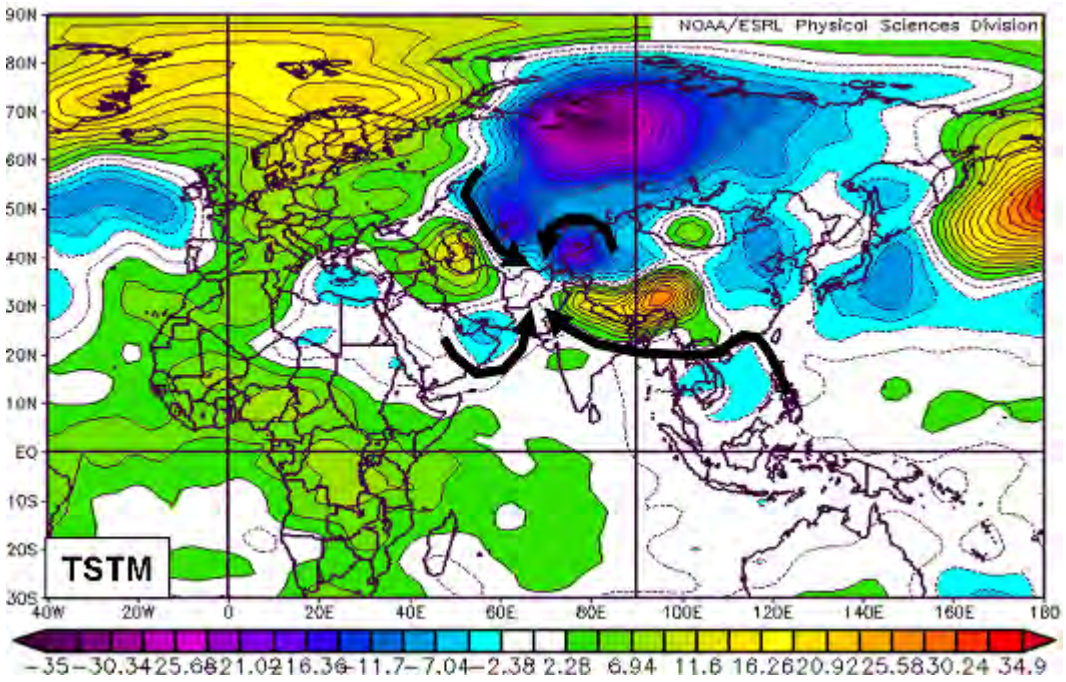

Figure 28. TSTM conditional composite anomalies of 850 hPa geopotential height (Z850; gpm) for MAM. Based on Kabul TSTM observations during 04 Mar 2002–31 Jul 2010. Black arrows represent corresponding Z850 anomalous winds. Note the indications of anomalous advection of: (1) mT air from the Arabian Sea, Bay of Bengal, and South China Sea; (2) cP air from central Russia; and (3) LLCON of mT air and cP air over AFG.

b. T850 Anomalies

Figure 29 shows the T850 TSTM composite anomalies for MAM. These anomalies are consistent with the corresponding prior LTM T850 and circulation anomaly results (Figures 20, 26–28). In particular: (1) the negative T850 anomalies to the NW of AFG are consistent with the temperature advection anomalies implied by the northwesterly flow anomalies to the northwest of AFG; and (2) the positive T850 anomalies to the southeast of AFG are consistent with the temperature advection anomalies implied by the southeasterly flow anomalies to the southeast of AFG (see Figures 20 and 28).

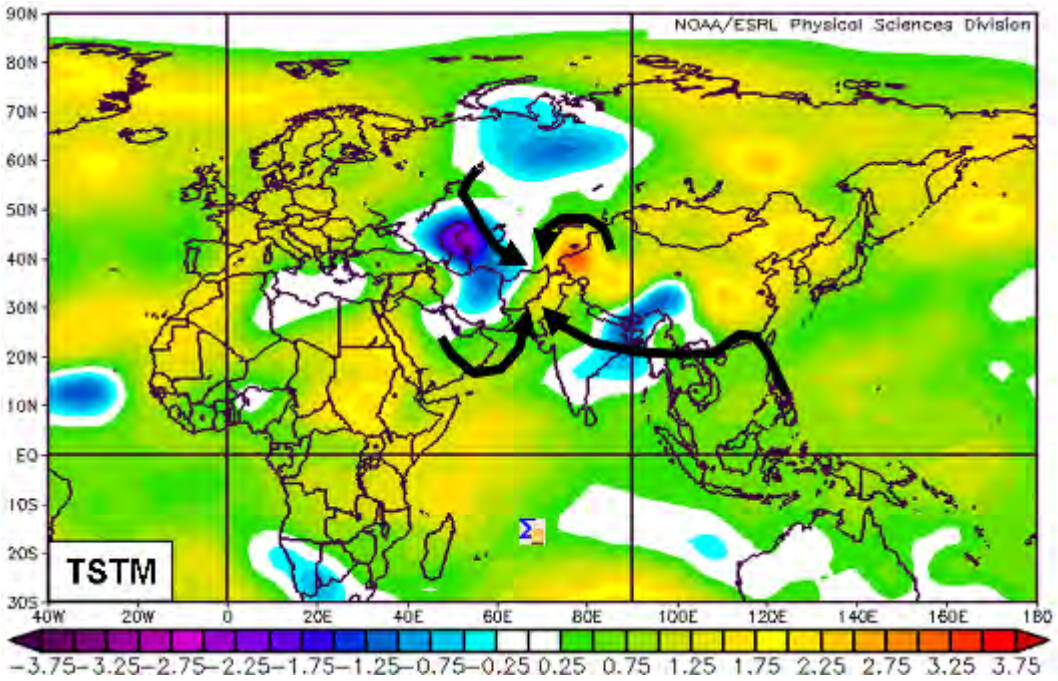

Figure 29. TSTM conditional composite anomalies of 850 hPa air temperature (T850; °C) for MAM. Based on Kabul TSTM observations during 04 Mar 2002–31 Jul 2010. Black arrows represent corresponding Z850 anomalous winds (see Figure 28). Note the indications of: (1) cool anomalies to the northwest of AFG associated with the anomalous northwestward flow from Russia; and (2) warm anomalies to the southeast of AFG associated with the anomalous southward flow from the Arabian Sea and Bay of Bengal.

c. SH850 Anomalies

Figure 30 shows the SH850 TSTM composite anomalies for MAM. These anomalies are consistent with the corresponding prior LTM SH850 and circulation anomaly results (Figures 21, 26–28). In particular, note the positive SH850 anomalies over the GoA, NIO, northern India, BoB, and AFG are consistent with the WMAA from the southeast toward AFG indicated by the corresponding Z850 and T850 anomaly results (Figures 28–29). The correspondence is less clear to the northwest of AFG, but Figure 30 does indicate weakly negative SH850 anomalies to west and northwest of AFG (over the south Caspian Sea and western Iran), consistent with the northerly circulation anomalies from Russia.

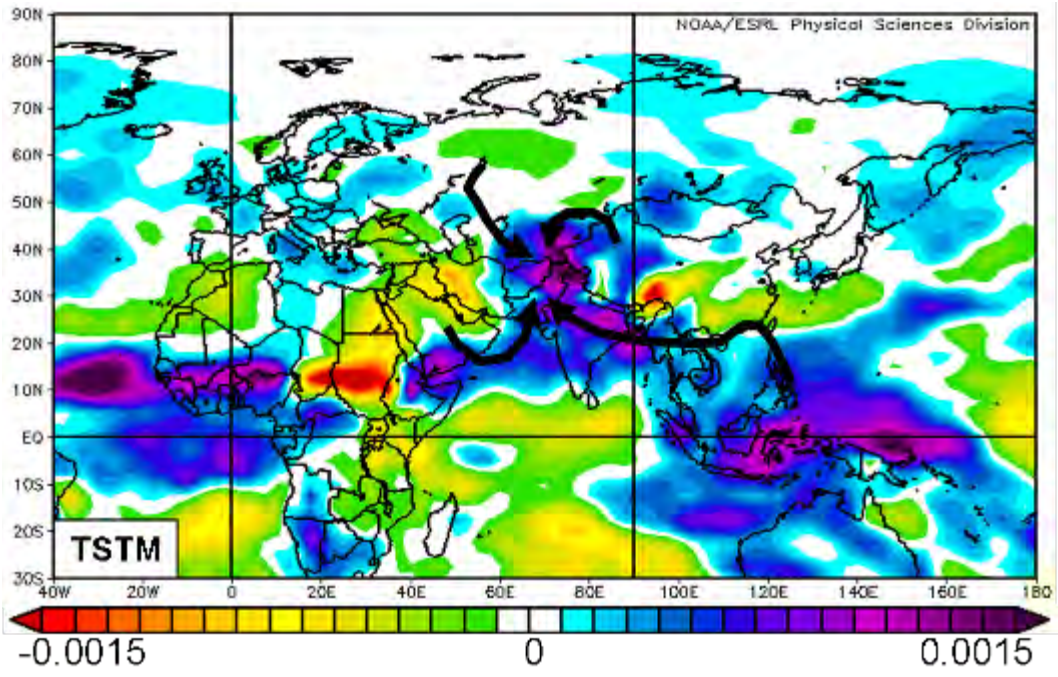

Figure 30. TSTM conditional composite anomalies of 850 hPa specific humidity (SH850; kg/kg) for MAM. Based on Kabul TSTM observations during 04 Mar 2002–31 Jul 2010. The contour interval is 0.0001 kg/kg. Black arrows represent corresponding Z850 anomalous winds (Figure 28). Note that the positive SH850 anomalies over the GoA, NIO, northern India, BoB, MC, and AFG are consistent with the WMAA from the south toward AFG indicated by the corresponding Z850 and T850 anomalies (Figures 28–29).

d. PW Anomalies

Figure 31 shows the PW TSTM composite anomalies for MAM. These anomalies are similar to and consistent with the corresponding prior SH850 anomaly results (Figure 30). One notable difference is that near the Himalayas, northern PAK, and eastern AFG, the SH850 anomalies are more widespread than the PW anomalies. This is likely due to the PW accounting for moisture throughout the atmosphere while SH850 accounts only for moisture at 850 hPa.

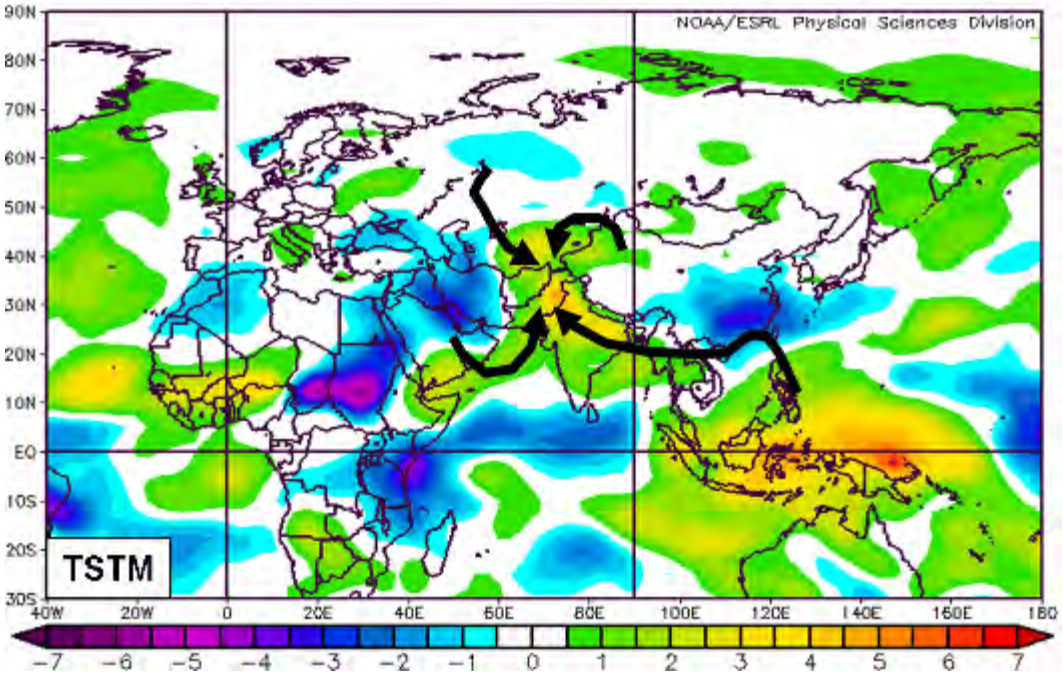

Figure 31. TSTM conditional composite anomalies of precipitable water (PW; kg/m^2) for MAM. Based on Kabul TSTM observations during 04 Mar 2002–31 Jul 2010. Black arrows represent corresponding Z850 anomalous winds (Figure 28). The PW anomalies are very similar to the SH850 anomalies (Figure 30). For example, both the SH850 and PW anomalies indicate that there is anomalous positive moisture advection into AFG from the NIO, northern India, and BoB.

e. OLR Anomalies

Figure 32 shows the OLR TSTM composite anomalies for MAM. Note the maximum negative OLR anomalies (OLRA), indicating anomalous deep convection, over northern AFG and the southern Stans region. Also, note the positive OLRA to the west and east of AFG over SWA and western China, respectively. These negative and positive OLRAs together are consistent with DVM associated with LL Hs to the east and west of AFG. Figures 27–31 support these conclusions about the circulation patterns associated with TSTMs over AFG. There are also widespread negative OLRAs over the western tropical Pacific Ocean, BoB, and NIO. These tropical OLRAs indicate that AFG TSTM activity may be linked to remote tropical convection anomalies, such as those that develop as part of climate variations such as the MJO, IOZM, and ENLN, perhaps via anomalous teleconnections involving Rossby and Kelvin waves (cf. Vorhees 2006; Moss 2007; Stepanek 2006; DeHart 2011).

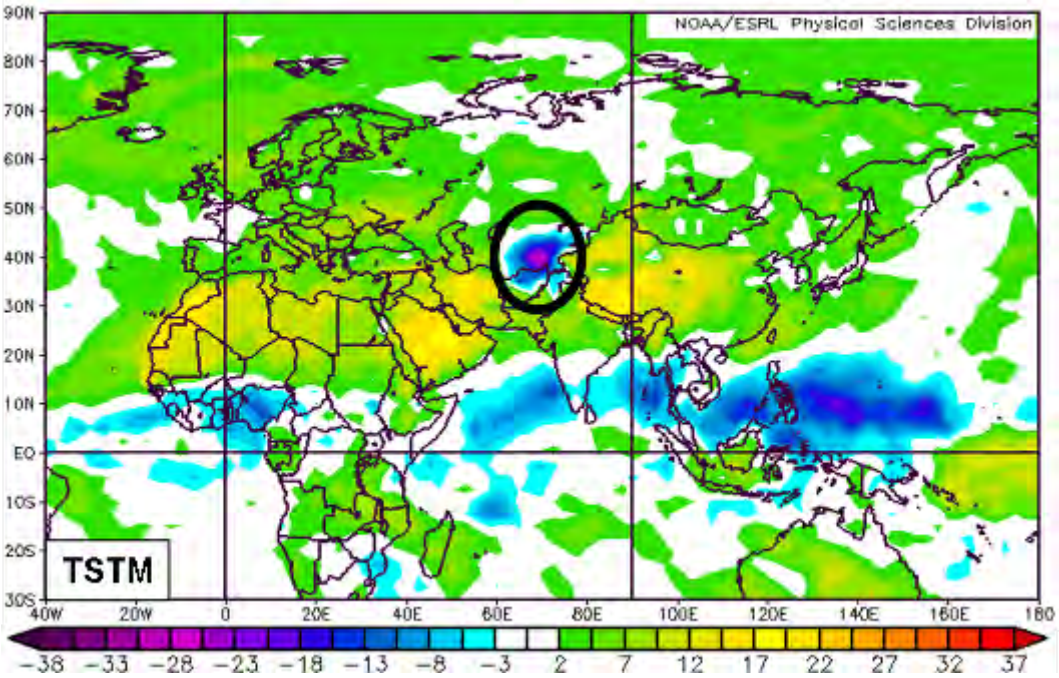

Figure 32. TSTM conditional composite anomalies of outgoing longwave radiation (OLR; W/m^2) for MAM. Based on Kabul TSTM observations during 04 Mar 2002–31 Jul 2010. Note the maximum negative OLR anomalies, consistent with anomalous deep convection, over northern AFG and the southern Stans region. Also, note the widespread negative OLR anomalies over the western tropical Pacific Ocean, BoB, and NIO. These tropical OLR anomalies indicate that AFG TSTM activity may be linked to remote tropical convective anomalies (e.g., those associated with climate variations, such as the Madden-Julian Oscillation, Indian Ocean Zonal Mode, and El Nino – La Nina).

f. Z200 Anomalies

Figure 33 shows the Z200 TSTM composite anomalies for MAM. Note the anomalous UL trough-ridge pattern over south-central Asia and centered near AFG. This UL pattern indicates anomalous UL divergence, UVM, and positive vorticity advection (PVA), all of which are (1) consistent with the results in Figures 28–32 and (2) favorable for instability, deep convection, and TSTM development over AFG.

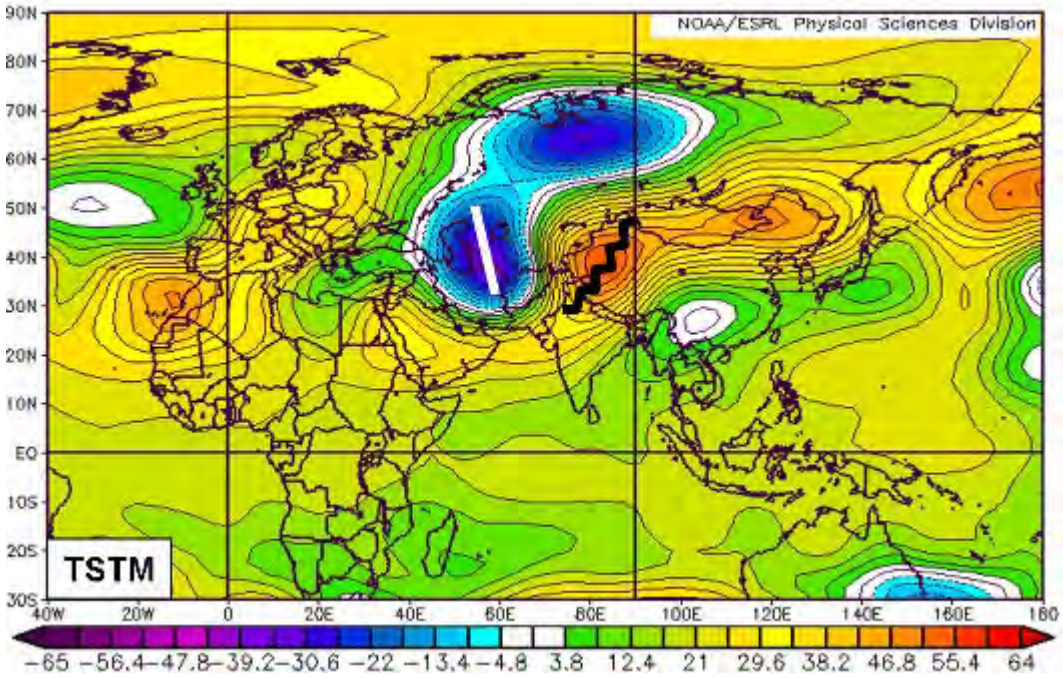

Figure 33. TSTM conditional composite anomalies of 200 hPa geopotential height (Z200; gpm) for MAM. Based on Kabul TSTM observations during 04 Mar 2002–31 Jul 2010. The anomalous upper level trough-ridge pattern over south-central Asia and centered near AFG indicates anomalous upper level divergence, upward vertical motion, and positive vorticity advection—all favorable for TSTM development over AFG.

g. ω500 Anomalies

Figure 34 shows the ω500 and OLR TSTM composite anomalies for MAM. The negative (positive) ω500 values, indicating strong UVM (DVM), over northern AFG and PAK (SWA and Tibet), are consistent with the results in Figures 28–33 (e.g., the negative OLRA over AFG). In particular, anomalous LLCON into the UVM region leads to rising warm moist air over AFG that cools adiabatically as it rises until saturation and condensation are achieved, which leads to latent heat release and additional instability to the air column, all of which is favorable for deep convection and TSTM activity over AFG. The region of DVM over Tibet favors the development of positive Z850 anomalies in that

region and anomalous low level flow along the southern flank of this positive height anomaly into AFG (see Figure 28).

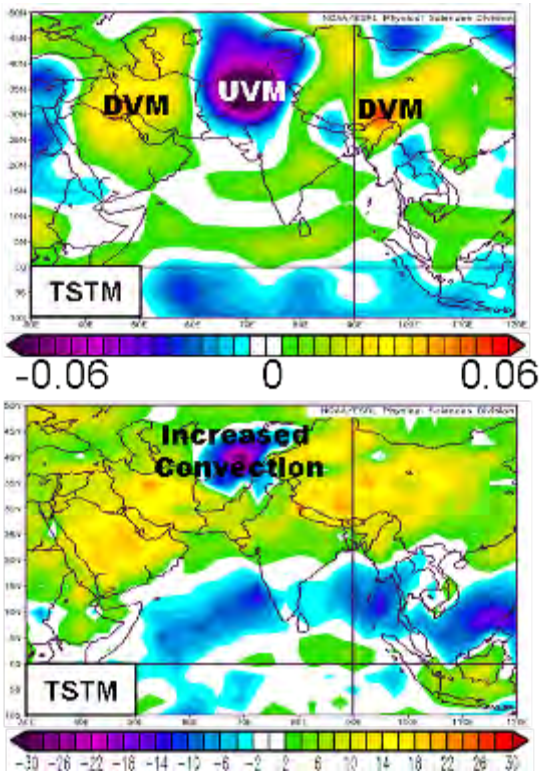

Figure 34. TSTM conditional composite anomalies of 500 hPa omega (ω500; Pa/s) (top) and OLR (W/m^2) anomalies (bottom) for MAM. Based on Kabul TSTM observations during 04 Mar 2002–31 Jul 2010. The ω500 contour interval is 0.004 Pa/s. Note that the results in these two panels are consistent with each other and with prior TSTM composite figures in indicating anomalous LLCON of warm moist air, UVM, and deep convection over AFG and PAK during TSTM periods (Figures 28–33).

h. PR Anomalies

Figure 35 shows the ω500 and PR TSTM composite anomalies for MAM. The positive (negative) PR anomalies over northern AFG and PAK (SWA and Tibet), are consistent with the results in Figures 28–34 (e.g., the negative OLR and UVM anomalies over AFG).

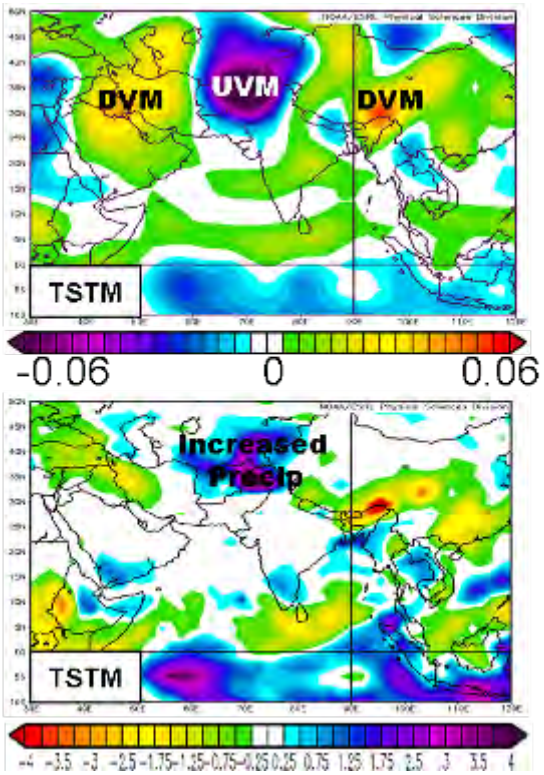

Figure 35. TSTM conditional composite anomalies of 500 hPa omega (ω500; Pa/s) (top) and precipitation rate (PR; mm/day) anomalies (bottom) for MAM. Based on Kabul TSTM observations during 04 Mar 2002–31 Jul 2010. The ω500 contour interval is 0.004 Pa/s. The anomalous UVM and positive PR anomalies over AFG are consistent with the corresponding circulation and implied advection anomalies (Figures 28–34) and with enhanced TSTM activity near AFG.

i. LI Anomalies

Figure 36 shows the LI TSTM composite anomalies for MAM. Negative (Positive) values of LI indicate unstable (stable) conditions. The negative (positive) LI anomalies over northern AFG and PAK (SWA and Tibet), are consistent with the results in Figures 28–35 (e.g., the negative OLR and positive PR anomalies over AFG).

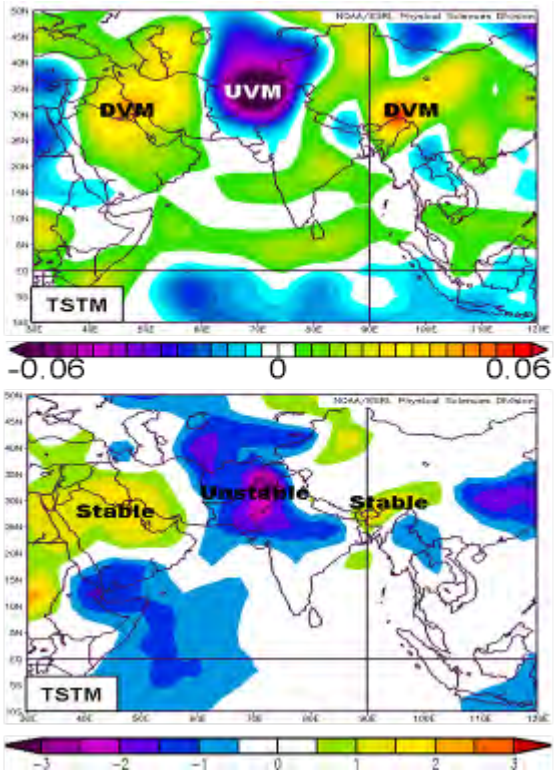

Figure 36. TSTM conditional composite anomalies for MAM of: (top) 500 hPa omega (ω500; Pa/s) and (bottom) LI (°C). Based on Kabul TSTM observations during 04 Mar 2002–31 Jul 2010. The ω500 contour interval is 0.004 Pa/s. Note the general correspondence between UVM (DVM) and negative (positive) values of LI, indicating instability (stability), especially near AFG and PAK (SWA and Tibet).

j. SST Anomalies

Figure 37 shows the Z850 and SST TSTM composite anomalies for MAM. The positive SST anomalies in the AS, BoB, tropical IO, and South China Sea (SCS) are broadly consistent with the corresponding T850 and SH850 anomalies (Figures 29–30) and prior indications of LL temperature and moisture advection anomalies. Figure 37 suggests that tropical SST anomalies may contribute to the corresponding T850 and SH850 anomalies, and thereby to WMAA into AFG.

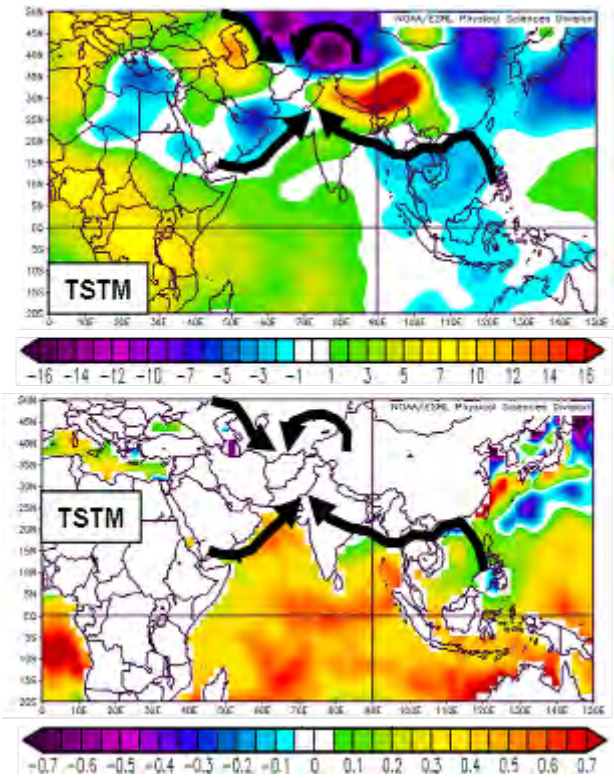

Figure 37. TSTM conditional composite anomalies of Z850 (gpm) (top) and Sea Surface Temperature Anomalies (SSTAs) (°C) (bottom) for MAM. Based on Kabul TSTM observations during 04 Mar 2002–31 Jul 2010. Black arrows represent corresponding Z850 anomalous winds (Figure 28). Note that winds converging toward AFG from the south may be anomalously warm and moist due to positive SSTAs in the NIO, AS, BoB, and SCS. Anomalously warm moist air converging with cool dry air from the north over AFG would lead to enhanced instability.

2. NTSTM Conditional Composite Anomaly Results

In this section, we present the results of our NTSTM climate variation analyses based on 129-day composites of anomalous NTSTM conditions. The same conditions apply to this NTSTM section as applied to the TSTM section (see the beginning of Chapter II, Section C.1).

a. Z850 Anomalies

Figure 38 shows the Z850 NTSTM anomalies for March, April, and May. Note the similar patterns for the three months, especially the anomalous Hs across central Asia extending into SWA. The anomalous clockwise anticyclonic flow around this H is associated with anomalous (1) CDAA into AFG from the northeast and (2) blocking of WMAA into AFG from tropical regions to the south. The similar patterns for these three months indicate that similar processes are operating to produce NTSTM activity over and near Kabul, and that NTSTM anomalous circulations would be well represented by MAM composite anomalies.

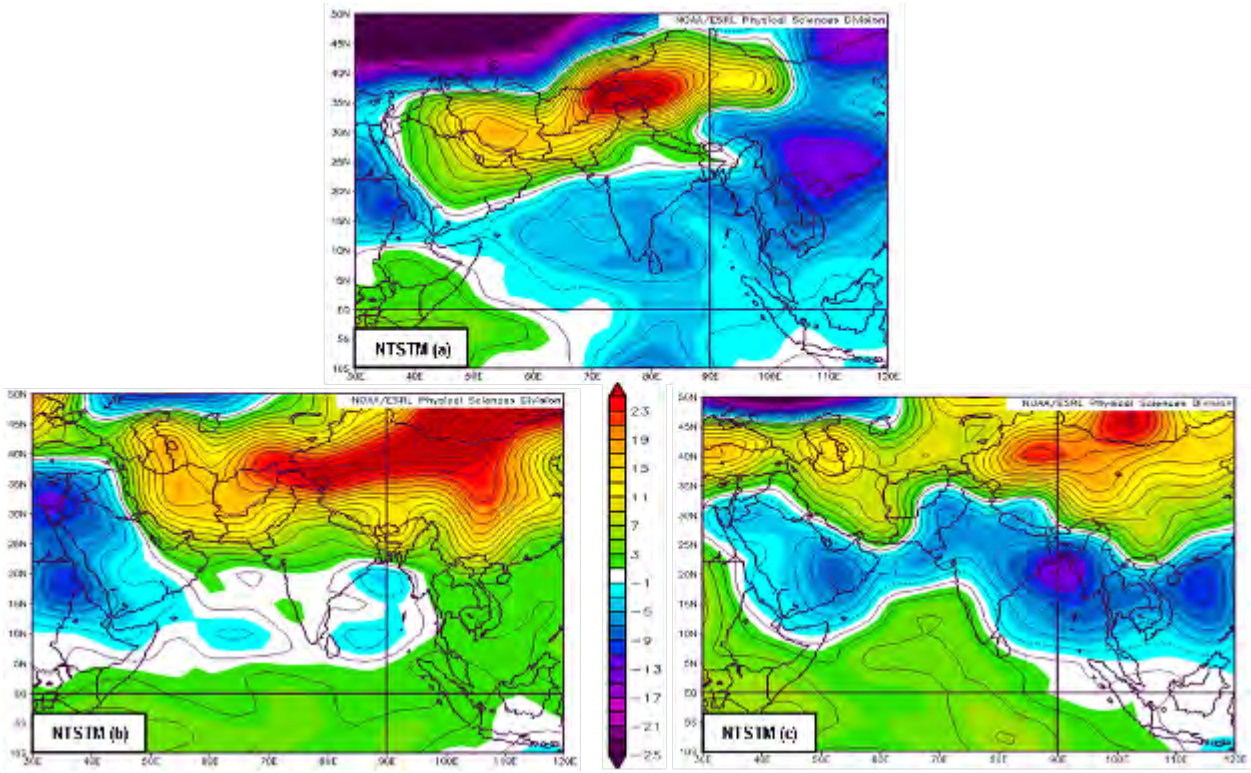

Figure 38. NTSTM conditional composite anomalies of 850 hPa geopotential height (Z850; gpm) for: (a) Mar, (b) Apr, and (c) May. Based on Kabul NTSTM observations during 04 Mar 2002–31 Jul 2010. Note the similar patterns for the three months, especially the anomalous Hs across central Asia extending into SWA, leading to anomalous CDAA from the northeast into AFG and anomalous blocking of WMAA into AFG from the south.

Figure 39 shows the Z850 NTSTM anomalies for MAM. As expected, the results are similar to, and somewhat simpler than, those in Figure 38. Note that the NTSTM Z850 anomalies are not the opposite of the TSTM Z850 anomalies, but the impacts on LL temperature and moisture advection into AFG are approximately opposite (compare Figures 27 and 39).

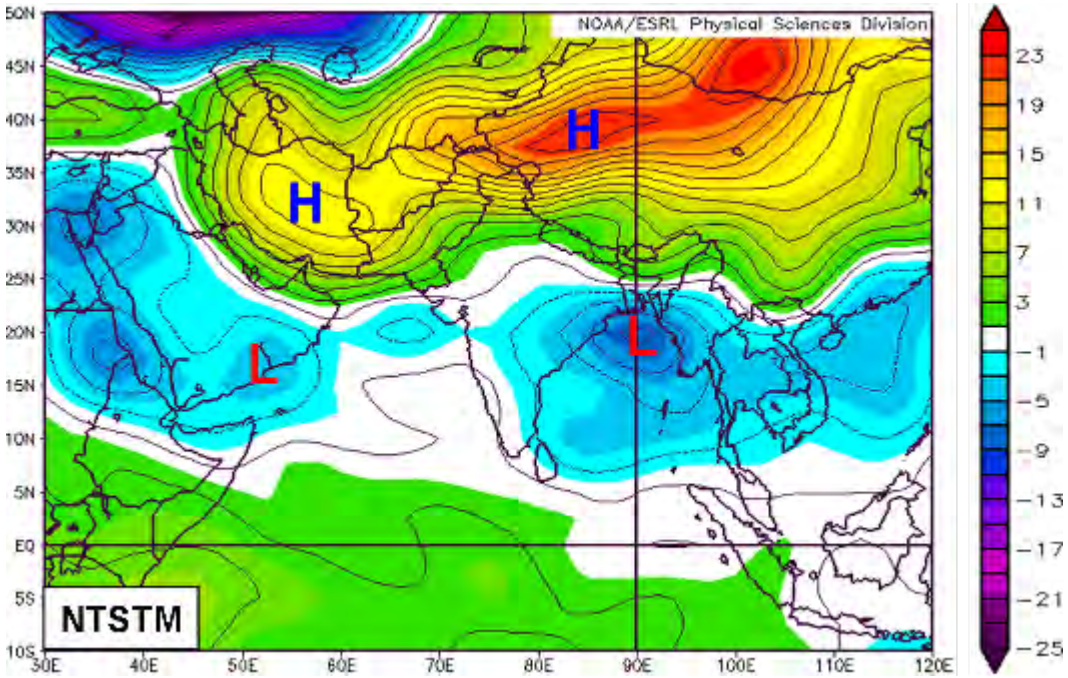

Figure 39. NTSTM conditional composite anomalies of 850 hPa geopotential height (Z850; gpm) for MAM. Based on Kabul NTSTM observations during 04 Mar 2002–31 Jul 2010. Note the anomalous H centered over central Asia and extending to Iraq indicating anomalous CDAA into AFG from the northeast and anomalous blocking of WMAA into AFG from the south. These anomaly patterns help identify the climate regimes and physical mechanisms that are favorable for NTSTM activity near Kabul.

Figure 40 shows the same information presented in Figure 39, except for a larger region and with arrows indicating the corresponding anomalous circulation. Note: (1) the indications over and near AFG of the anomalous advection of cP air from northern Europe southward and eastward into SWA and from northern and central Asia toward AFG and (2) the anomalous blocking of ETCs approaching from the west and of WMA from the south. Both of these factors contribute to anomalous stability over AFG and nearby areas.

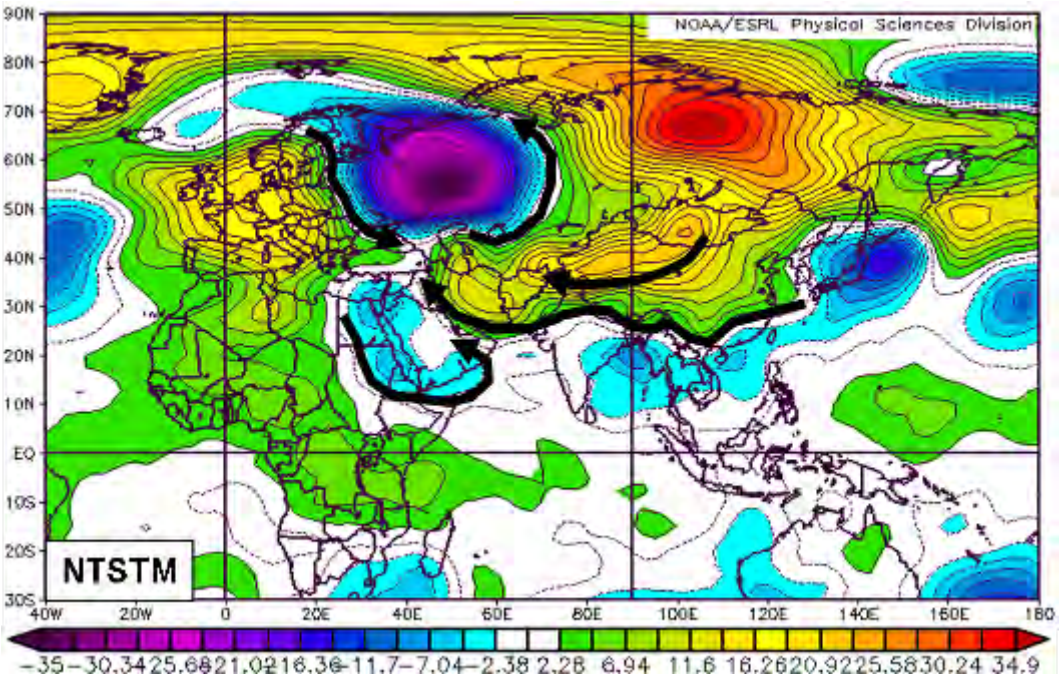

Figure 40. NTSTM conditional composite anomalies of 850 hPa geopotential height (Z850; gpm) for MAM. Based on Kabul NTSTM observations during 04 Mar 2002–31 Jul 2010. Black arrows represent corresponding Z850 anomalous winds. Note the indications over and near AFG of anomalous: (1) advection of cP air from central and northern Asia toward AFG: and (2) blocking by the anomalous H over south-central Asia of ETCs and advection of mT from the tropics into AFG.

b. T850 Anomalies

Figure 41 shows the T850 NTSTM anomalies for MAM. The major anomalies in western and south-central Asia are generally consistent with the anomalous T850 advection implied by the Z850 anomalies (Figure 40). In particular, the positive (negative) T850 anomalies to the west (east) of AFG are consistent with anomalous WAA (CAA) from the south (northeast) into SWA (northern India and western China). The T850 anomalies are likely also due in part to anomalous vertical motions and corresponding impacts on adiabatic

warming/cooling and insolation (e.g., the positive T850 anomalies that are co-located with positive Z850 anomalies and centered over northern Iran - western AFG, and over north-central Russia).

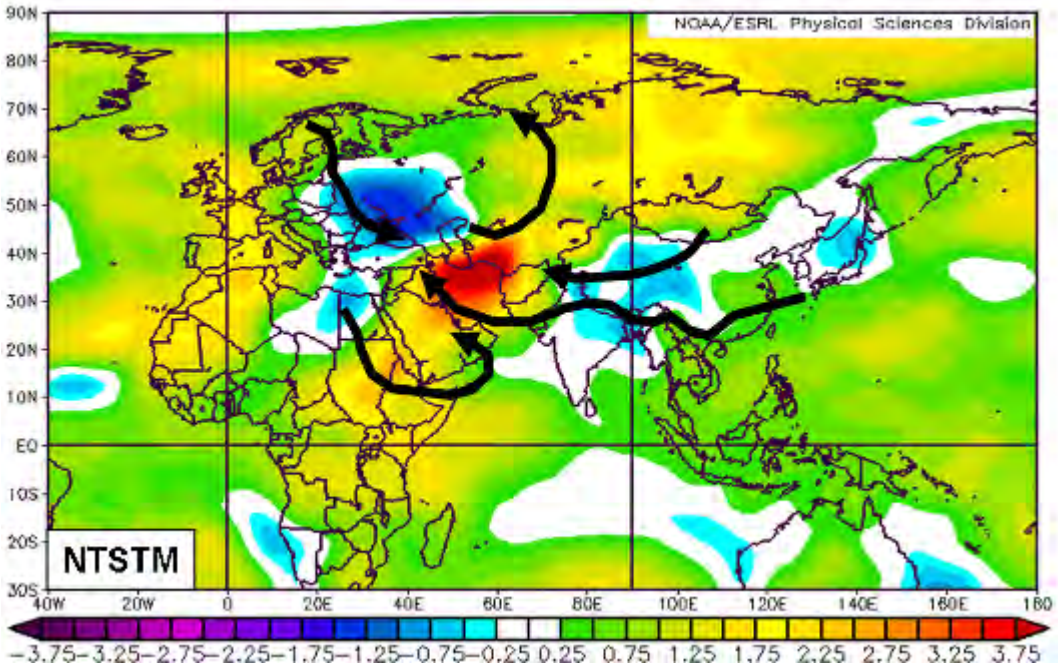

Figure 41. NTSTM conditional composite anomalies of 850 hPa air temperature (T850; °C) for MAM. Based on Kabul NTSTM observations during 04 Mar 2002–31 Jul 2010. Black arrows represent corresponding Z850 anomalous winds (Figure 40). Note that the T850 anomalies over much of Asia are broadly consistent with the anomalous advection and/or vertical motion implied by the corresponding LTM T850 and anomalous Z850 (Figures 20 and 40).

c. SH850 Anomalies

Figure 42 shows the SH850 NTSTM anomalies for MAM. Note the widespread zonal band of negative SH850 anomalies extending to the west and east of AFG, and consistent with the corresponding anomalies in LL heights and winds. These negative anomalies support the conclusion that the blocking H over south-central Asia (Figure 40) has a significant impact on moisture over and near AFG.

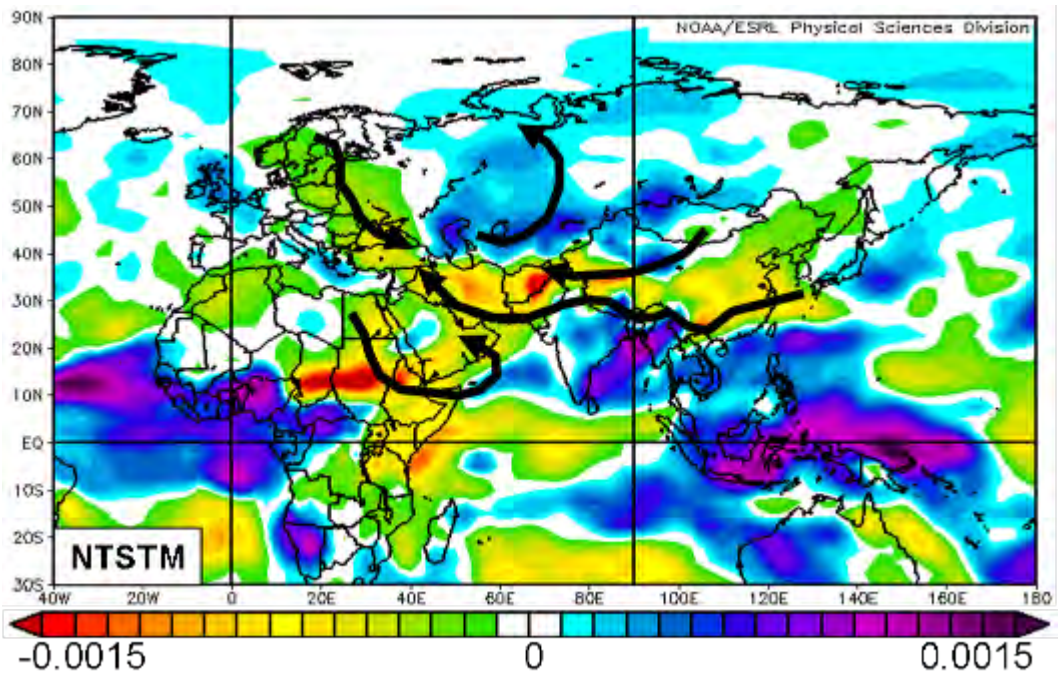

Figure 42. NTSTM conditional composite anomalies of 850 hPa specific humidity (SH850; kg/kg) for MAM. Based on Kabul NTSTM observations during 04 Mar 2002–31 Jul 2010. The contour interval is 0.0001 kg/kg. Black arrows represent corresponding Z850 anomalous winds (Figure 40). Note the band of negative SH850 anomalies extending from SWA across AFG and central China, consistent with the corresponding anomalous 850 hPa heights and winds.

d. PW Anomalies

Figure 43 shows the PW NTSTM anomalies for MAM, which are very similar to the SH850 anomalies. Note in particular the anomalous low PW over AFG-PAK and the northern AS in Figures 42–43. These anomalously dry conditions, coupled with the anomalously cool conditions shown in Figure 41, favor anomalously stable conditions over AFG.

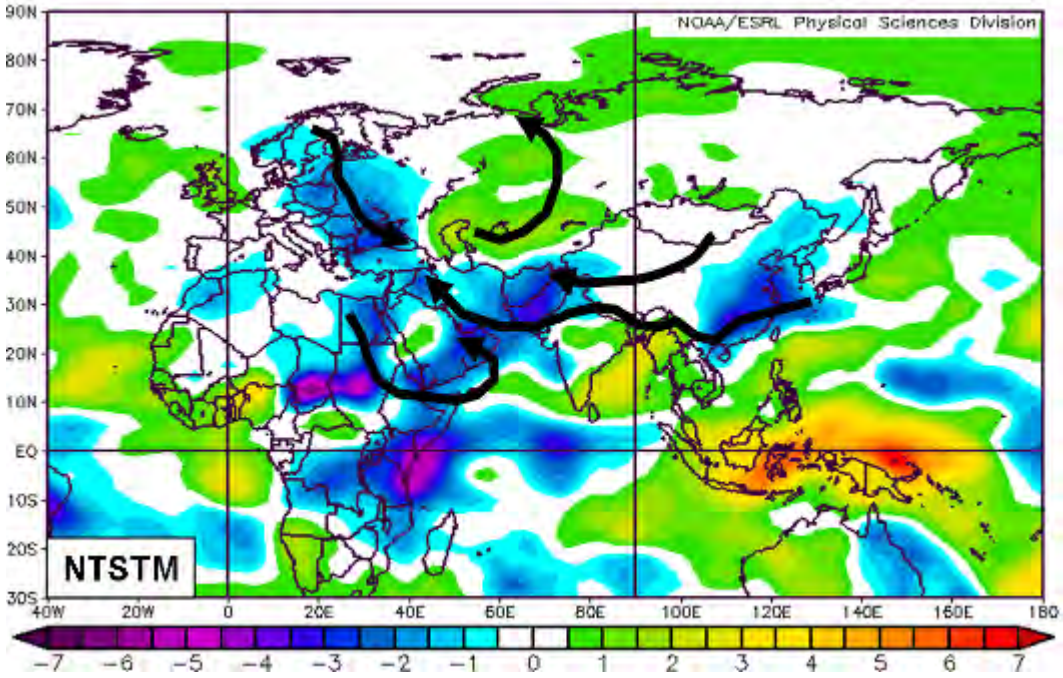

Figure 43. NTSTM conditional composite anomalies of precipitable water (PW; kg/m^2) for MAM. Based on Kabul NTSTM observations during 04 Mar 2002–31 Jul 2010. Black arrows represent corresponding Z850 anomalous winds (Figure 40). The PW anomalies are similar to the SH850 anomalies (Figure 42) and provide additional evidence of anomalously negative moisture advection into AFG and nearby areas.

e. OLR Anomalies

Figure 44 shows the OLR NTSTM anomalies for MAM. The positive OLRAs over AFG-PAK indicate anomalously weak convection in that area, consistent with the prior NTSTM results (Figures 38–43), especially the indications of DAA into, and blocking and subsidence over, AFG-PAK. The widespread negative OLRAs over much of the tropical NIO, western tropical Pacific Ocean, and South Pacific Ocean Convergence Zone (SPCZ) suggest that anomalies in remote tropical convection may be related to AFG NTSTM activity. Tropical anomalies such as these are often part of intraseasonal to interannual climate variations (e.g., MJO, ENLN, IOZM), and can lead to impacts on SWA, and AFG in particular, via anomalous teleconnections involving Rossby and Kelvin waves (cf. Vorhees 2006; Moss 2007; Stepanek 2006; DeHart 2011).

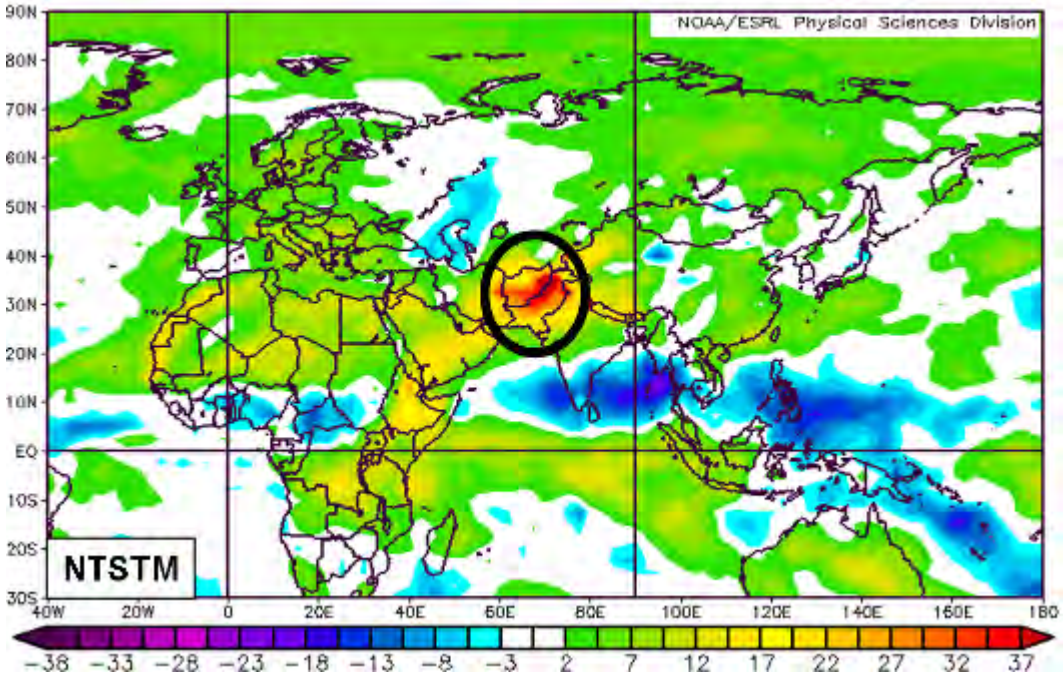

Figure 44. NTSTM conditional composite anomalies of outgoing longwave radiation (OLR; W/m^2) for MAM. Based on Kabul NTSTM observations during 04 Mar 2002–31 Jul 2010. Note the positive OLR anomaly area centered near AFG-PAK and indicating anomalously weak convection. Also, note the widespread negative OLR anomalies over much of the NIO, western tropical Pacific Ocean, and South Pacific Convergence Zone (SPCZ). These tropical OLR anomalies indicate that AFG NTSTM activity may be linked to remote tropical convective anomalies (e.g., those associated with climate variations, such as the Madden-Julian Oscillation, Indian Ocean Zonal Mode, and El Nino–La Nina).

f. Z200 Anomalies

Figure 45 shows the Z200 NTSTM anomalies for MAM. Note the anomalous UL trough-ridge-trough pattern centered over Iran and the Stans. This anomalous circulation is favorable for ULCON, DVM, and negative vorticity advection (NVA) over and near the AFG-PAK area, and is thus unfavorable for TSTM development in that area.

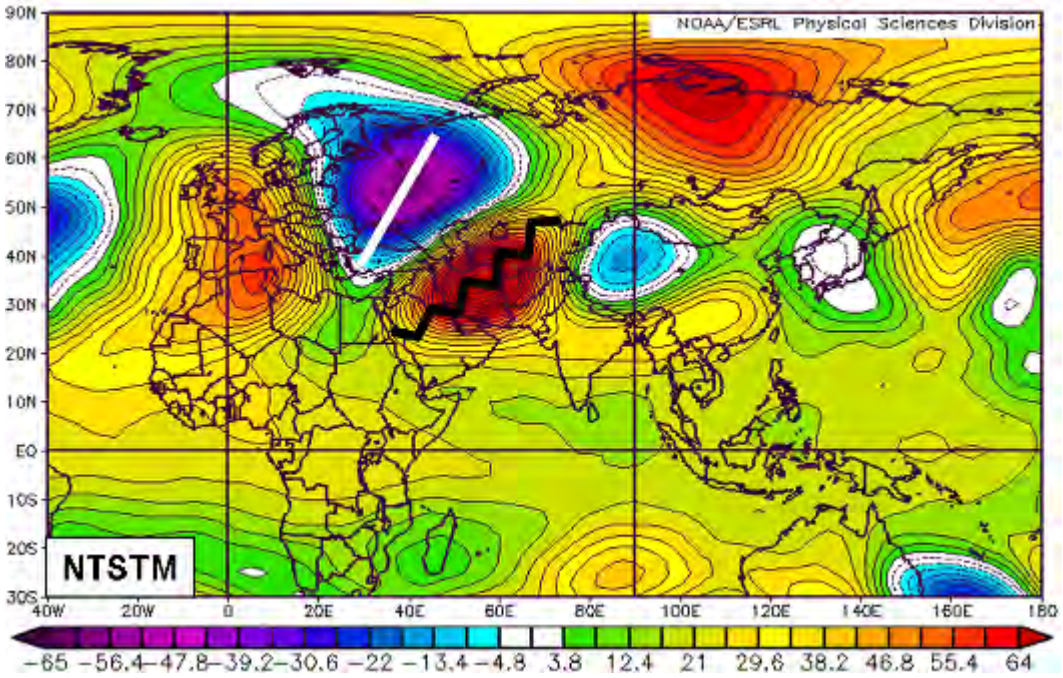

Figure 45. NTSTM conditional composite anomalies of 200 hPa geopotential height (Z200; gpm) for MAM. Based on Kabul NTSTM observations during 04 Mar 2002–31 Jul 2010. The anomalous upper level trough-ridge-trough pattern over western Russia, SWA, and western China indicates anomalously unfavorable conditions over AFG-PAK for deep convection and TSTM development.

g. ω500 Anomalies

Figure 46 shows the ω500 and OLR NTSTM anomalies for MAM. Note the DVM and positive OLRA over the AFG-PAK area, which support the prior indications of blocking and CDAA over the area that lead to anomalously low convection and stable conditions in the area.

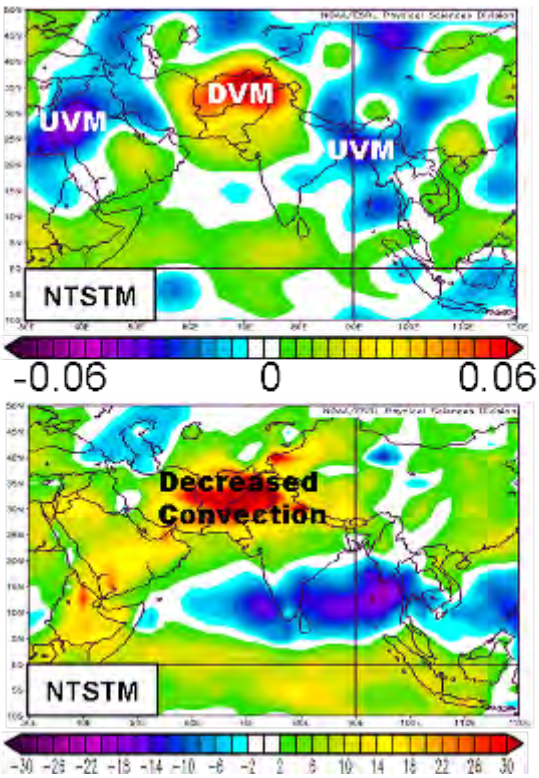

Figure 46. NTSTM conditional composite anomalies of 500 hPa omega (ω500; Pa/s) (top) and OLR (W/m^2) anomalies (bottom) for MAM. Based on Kabul NTSTM observations during 04 Mar 2002–31 Jul 2010. The ω500 contour interval is 0.004 Pa/s. Note that the results in these two panels are consistent with each other and with prior NTSTM conditional composite figures in indicating anomalous blocking of warm moist air, DVM, and weak or absent convection over AFG and PAK during NTSTM periods (Figures 40–45).

h. PR Anomalies

Figure 47 shows the ω500 and PR NTSTM anomalies for MAM. DVM and negative PR anomalies occur over AFG-PAK, consistent with the prior NTSTM anomaly results (Figures 40–46).

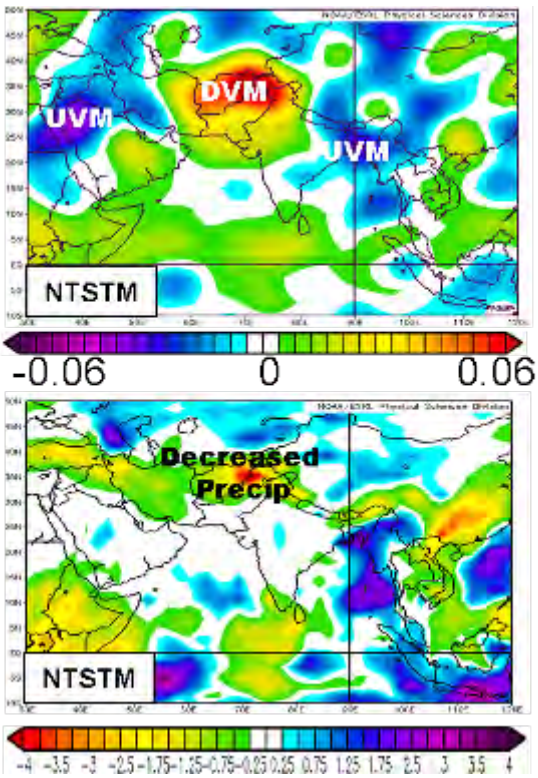

Figure 47. NTSTM conditional composite anomalies of 500 hPa omega (ω500; Pa/s) (top) and precipitation rate (PR; mm/day) anomalies (bottom) for MAM. Based on Kabul NTSTM observations during 04 Mar 2002–31 Jul 2010. The ω500 contour interval is 0.004 Pa/s. The anomalous DVM and negative PR anomalies over and near AFG and PAK are consistent with enhanced NTSTM activity near Kabul.

i. LI Anomalies

Figure 48 shows the ω500 and lifted index (LI) NTSTM composite anomalies for MAM. The positive LI anomalies over AFG-PAK support the other NTSTM results and indicate anomalously stable conditions over AFG-PAK.

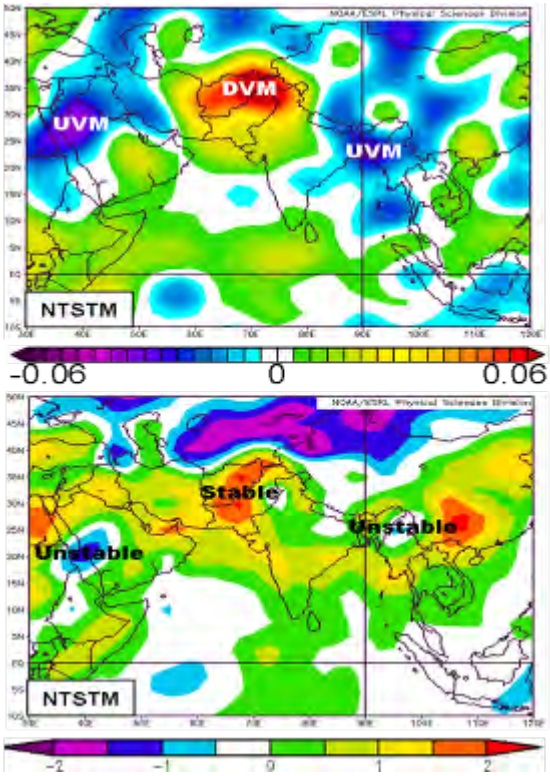

Figure 48. NTSTM conditional composite anomalies for MAM of: (top) 500 hPa omega (ω500; Pa/s) and (bottom) LI. Based on Kabul NTSTM observations during 04 Mar 2002–31 Jul 2010. The ω500 contour interval is 0.004 Pa/s. Note the DVM and positive values of LI, indicating stability over AFG and PAK.

j. SST Anomalies

Figure 49 shows the Z850 and SST NTSTM composite anomalies for MAM. Positive SSTAs occur in the NIO, but: (1) the NTSTM tropical SSTAs are 20–50% less positive than those in the corresponding TSTM composite (Figure 37); and (2) the NTSTM LL circulation anomalies over south-central Asia block the advection of tropical air into AFG, thus minimizing the impacts of the NTSTM SSTAs on, and favoring stable conditions over, AFG.

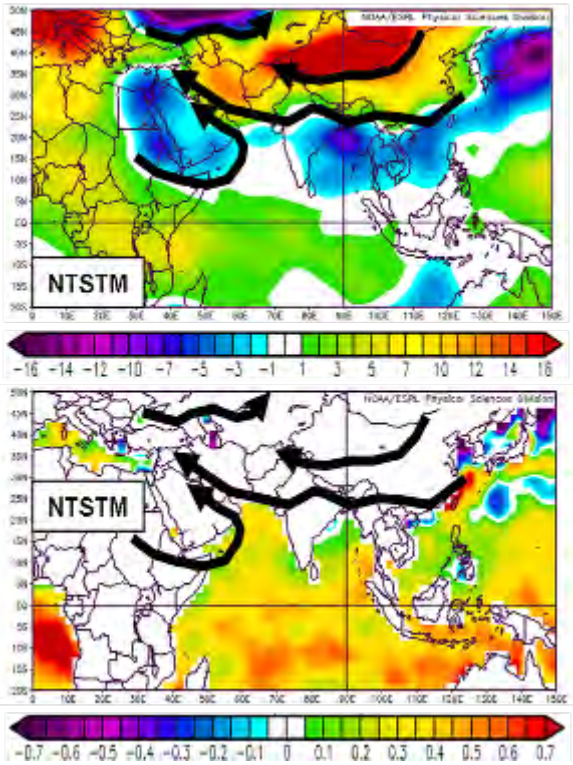

Figure 49. NTSTM conditional composite anomalies of Z850 (gpm) (top) and SSTAs (°C) (bottom) for MAM. Based on Kabul NTSTM observations during 04 Mar 2002–31 Jul 2010. Black arrows represent corresponding Z850 anomalous winds. Note the positive SSTAs in the NIO and the indications of anomalous blocking of flow from the tropics toward AFG (see Figure 40). Compare with corresponding TSTM anomalies (Figure 37).

3. Comparison of Select TSTM and NTSTM Conditional Composite Anomaly Results

Direct comparisons of TSTM and NTSTM composite anomalies are useful in highlighting the processes that contribute to TSTM and NTSTM conditions in AFG.

a. Z850 TSTM and NTSTM Anomalies

The Z850 anomalies are especially useful in summarizing the differences between the regional scale processes associated with TSTM and

NTSTM conditions. This is because the Z850 anomalies can be a relatively direct indicator of anomalies in momentum, energy, and mass distributions.

Figure 50 shows clear differences in the TSTM and NTSTM anomalies in 850 hPa circulation, and in the implied temperature and moisture advection anomalies. In particular, the TSTM anomalies indicate anomalous convergence over AFG of CDA from the north and WMA from the south, while NTSTM composite indicates anomalous advection of CDA into AFG and blocking of ETCs and tropical WMA over AFG. The net results are large-scale regional conditions that are anomalously favorable (unfavorable) for TSTM development in the TSTM (NTSTM) composite.

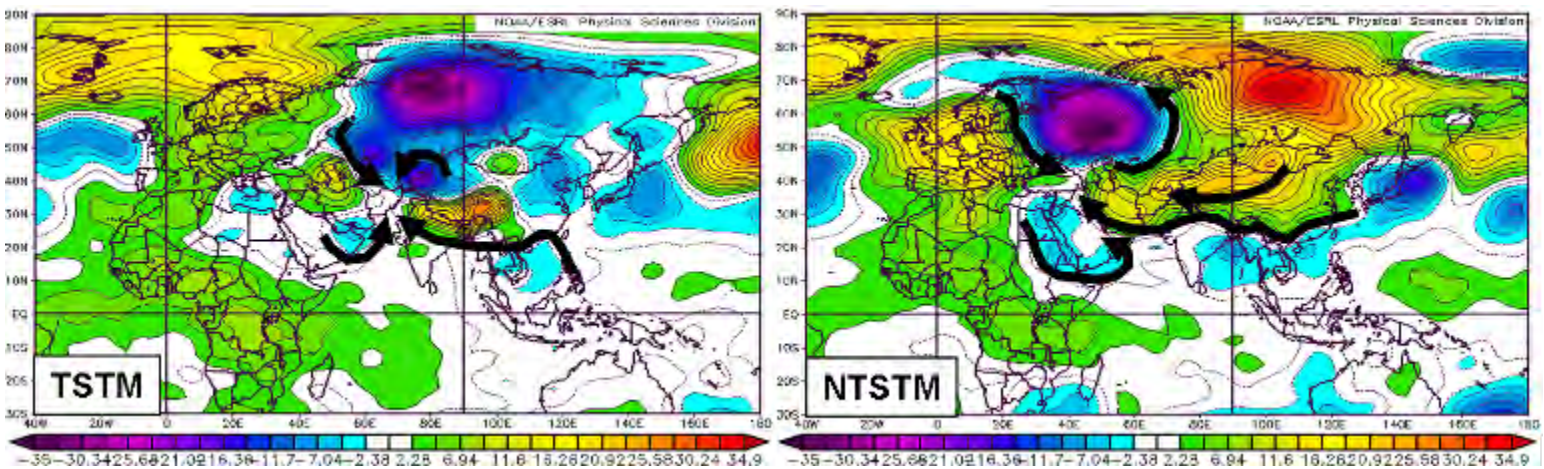

Figure 50. TSTM (left) and NTSTM (right) conditional composite anomalies of 850 hPa geopotential height (Z850; gpm) for MAM. Based on Kabul TSTM and NTSTM observations during 04 Mar 2002–31 Jul 2010. Black arrows represent corresponding Z850 anomalous winds. Note the indications over and near AFG of anomalous: (1) LLCON of CDAA from the north and WMAA from the south over AFG in the TSTM composite (Figures 28–37); (2) CDAA from the NE and a blocking of ETCs and WMAA from the south over AFG in the NTSTM composite (Figures 40-49).

b. PW TSTM and NTSTM Anomalies

Figure 51 shows clear differences in the TSTM and NTSTM anomalies in PW. In particular, there are (1) positive anomalies over, and indications of moist air advection (MAA) into, AFG-PAK in the TSTM composite, and (2) negative anomalies over, and indications of dry air advection (DAA) into, AFG-PAK in the NTSTM composite.

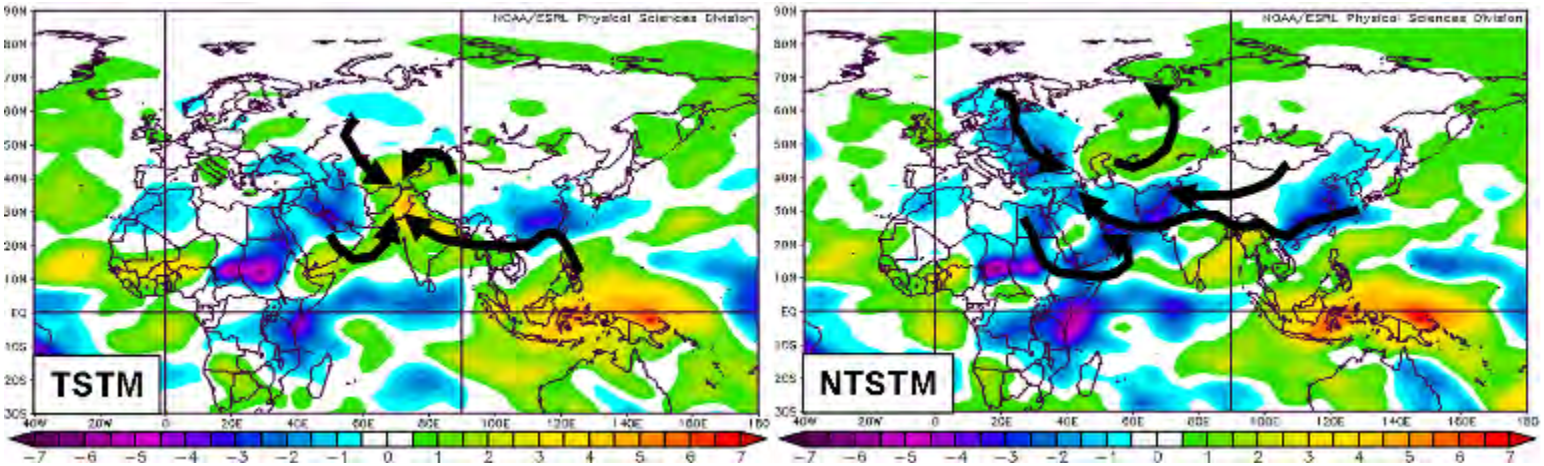

Figure 51. TSTM (left) and NTSTM (right) conditional composite anomalies of precipitable water (PW; kg/m^2) for MAM. Based on Kabul TSTM and NTSTM observations during 04 Mar 2002–31 Jul 2010. Black arrows represent corresponding Z850 anomalous winds. Note the indications over and near AFG of anomalous: (1) MAA from the south and DAA from the north (Figures 28–37) in the TSTM regime; (2) DAA from the northeast and a blocking of MAA from the south into AFG (Figures 40–49) in the NTSTM regime.

c. TSTM and NTSTM Large-Scale Schematics

Figures 52–53 are schematic illustrations of the large-scale, LL anomalous circulation and advection patterns that characterize TSTM and NTSTM periods. These figures highlight the major patterns and processes identified earlier in Chapter II, Section C. Figure 52 shows the anomalous LLCON over AFG of WMA from the NIO, AS, BoB, and SCS with CDA from the north. These anomalies are consistent with the anomalous enhancements of moisture, lift, and instability, which are all favorable for TSTM development over AFG. Figure 53 shows the anomalously high heights over SWA and central Asia that lead to anomalous CDAA into AFG, and blocking over AFG of ETCs and WMA from the south. These anomalies are consistent with unfavorable conditions for TSTM development over AFG.

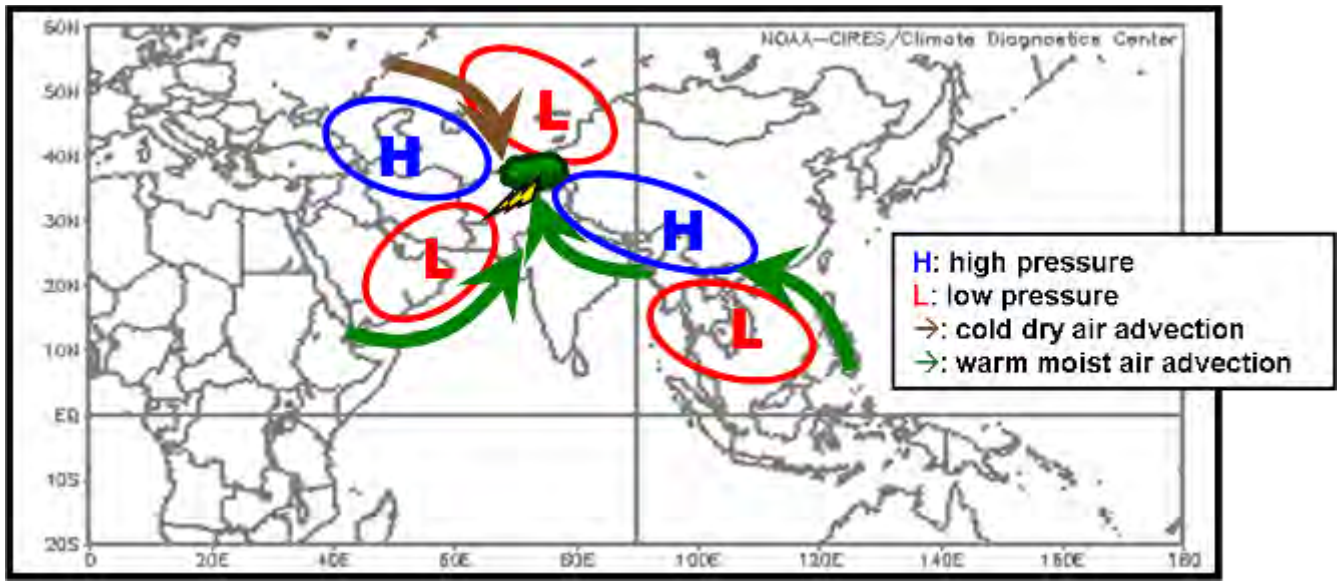

Figure 52. Schematic depiction of the large-scale low level geopotential heights (Z850) and wind anomalies for TSTM periods in Kabul, Afghanistan during spring (March–May). Based on TSTM conditional composite anomalies of Z850 shown in Figure 28. Note the anomalous convergence over AFG of: (1) WMAA from the NIO, AS, BoB, and SCS; and (2) CDA from the north. These circulation anomalies are consistent with: (1) anomalous enhancements of moisture, lift, and instability; and (2) favorable conditions for TSTM development over AFG.

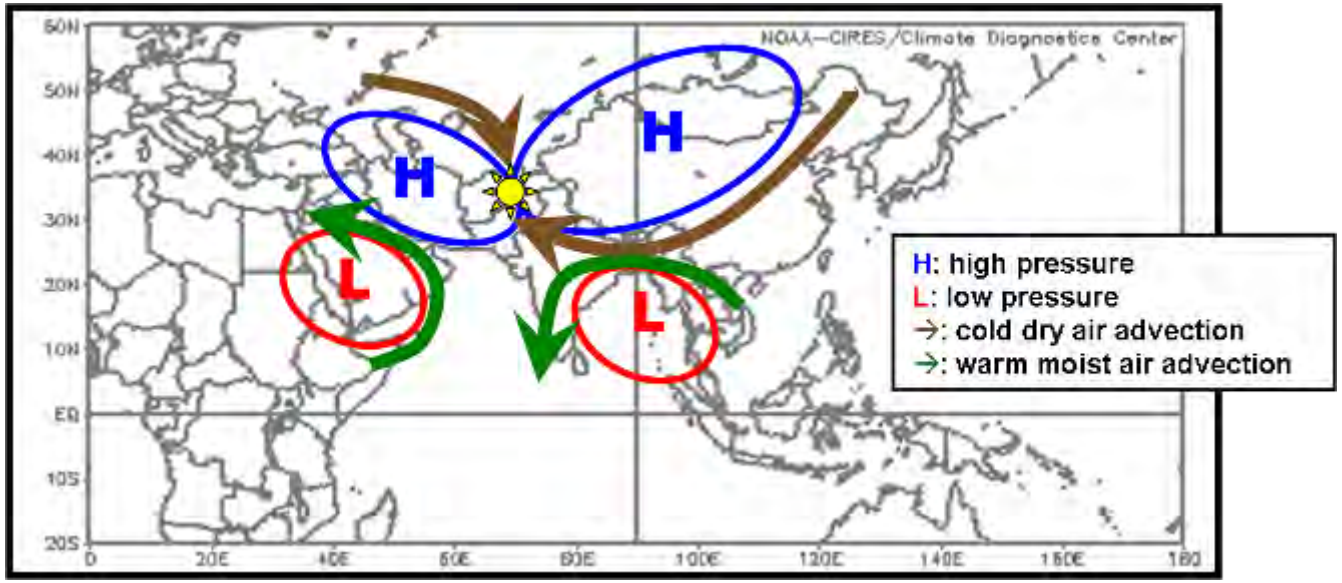

Figure 53. Schematic depiction of the large-scale low level geopotential heights (Z850) and wind anomalies for NTSTM periods in Kabul, Afghanistan during spring (March–May). Based on NTSTM conditional composite anomalies of Z850 shown in Figure 40. Note that the anomalously high heights over SWA and central Asia lead to anomalous CDAA into AFG, and blocking over AFG of ETCs and warm moist air from the south. These circulation anomalies are consistent with unfavorable conditions for TSTM development over AFG.

D. SKEW T – LOG P RESULTS

We used the radiosonde data from the 14 WS and UWY to construct average TSTM and NTSTM soundings by: (1) interpolating the sounding temperature and dew point temperature values to all pressure levels from the surface–100 hPa at 1 hPa intervals for each sounding; and (2) averaging the resulting values at each pressure level over all the TSTM soundings and over all the NTSTM soundings. The sounding winds were vector averaged only for the mandatory levels. These soundings were then analyzed using two different methods as detailed by the USAF Air Weather Service Manual on Skew T – Log P Analysis and Forecasting Methods (AWS/TR-79/006 1979). We calculated the TSTM and NTSTM average values of LI, CCL pressure and temperature, T_c, and the CAPE and CIN areas. Our CAPE and CIN analyses were based on both the heating and lifting of a SFC parcel methods. We did not explicitly calculate the numerical values of CAPE and CIN, due to data processing limitations.

1. TSTM Sounding Analyses

Figures 54 and 55 show the results for the MAM TSTM average sounding for the heated and lifted SFC parcel methods, respectively. Table 5 shows comparison values for the TSTM average values of LI, CAPE, CCL pressure and temperature, and T_c based on 14 WS calculations of these variables (see discussion of the 14 WS Kabul Static Stability Indices and Thermodynamic Levels data set in Chapter II, Section A.3). The individual monthly values shown in Table 5 were obtained by adding all of the values for each sounding during the month, and then dividing that total by the number of soundings used (11 for March, 32 for April, 24 for May). The MAM total weighted average values were calculated by multiplying the March value by a factor of 11, the April value by a factor of 32, and the May value by a factor of 24. Then, the individual weighted monthly values were added together and divided by the total number of observations for March, April, and May (67 total observations) to obtain a total

MAM weighted value. The major results represented in Figures 54–55 and Table 5 are summarized in the following subsections.

a. CAPE, CIN, and LI

Figures 54–55 show that CAPE and CIN determined from the heated SFC parcel method are larger than those determined from the lifted SFC parcel method. For the heated SFC parcel method portrayed, T_c is 20°C (Figure 54), which matches well with the T_c of 20.57°C from the 14 WS (Table 5). These T_c values indicate that daytime heating would need to raise the SFC temperatures to 20°C or greater in order for the air parcel to overcome the CIN and reach the CCL of 640 hPa. The daily mean SFC high temperatures are 13°C for March, 18°C for April, and 24°C for May (28 OWS Kabul FRN 2010). This indicates that from March–May, conditions become more favorable for SFC parcels to reach T_c = 20°C and to have enough energy to overcome the CIN and exploit the relatively large CAPE (Figure 54). However, the March and April daily mean SFC high temperatures are less than 20°C, suggesting that in those months SFC heating will generally be insufficient to overcome the CIN.

The LFC at 580 hPa on the lifted SFC parcel method analysis in Figure 55 is at a higher atmospheric level than the CCL at 640 hPa from the heated SFC parcel method in Figure 54. However, the required lifting mechanism (e.g., lifting associated with a front, orographic forcing, or LLCON) would need to overcome a relatively small amount of CIN.

Table 5 shows that the individual monthly values of CAPE increase from March–May, consistent with the increase in daily mean SFC high temperatures and with the TSTM day, TSTM hour, and precip hour variations shown in Figures 9–10. Table 5 also shows that TSTM activity in Kabul is associated with LI and CAPE values that are much lower than those associated with TSTM activity in CONUS (compare Table 5 to Tables 3–4). This supports

information from the 28 OWS that CONUS based stability/instability threshold values do not accurately represent the potential for TSTM activity in Kabul.

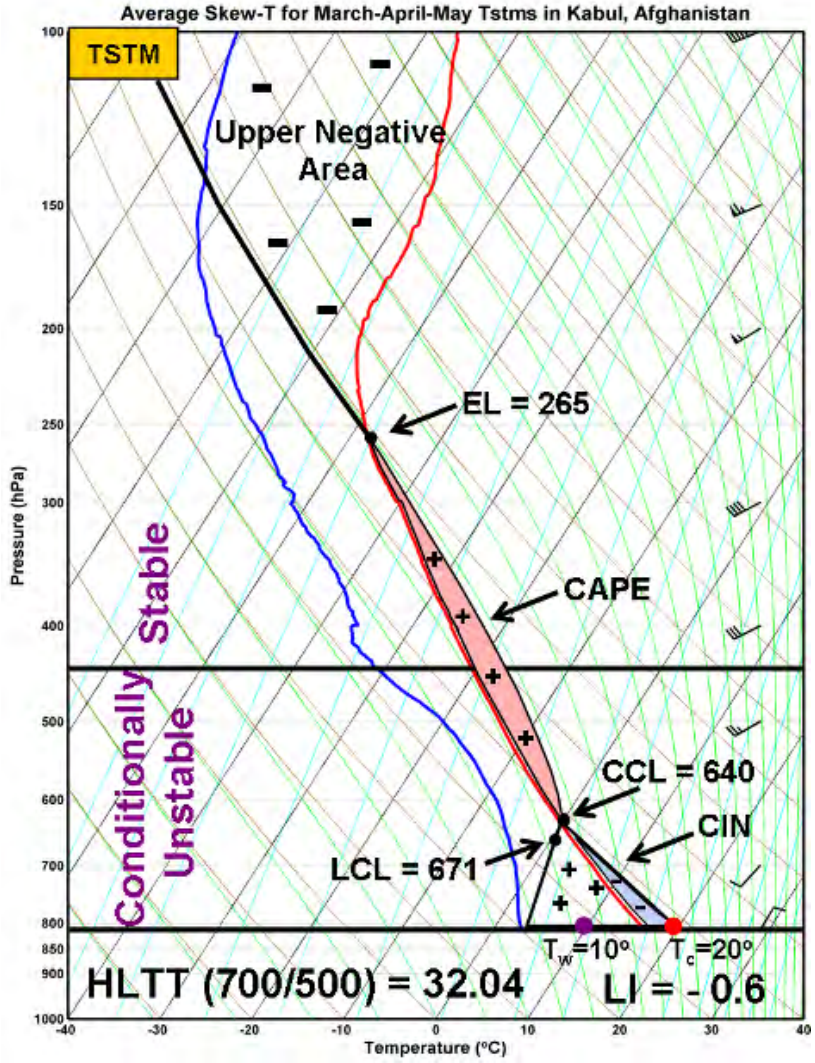

Figure 54. Skew T – log p analysis of average MAM TSTM sounding. Thermodynamic parameters are determined by using the SFC heating of the air parcel method. Based on Kabul TSTM radiosonde observations from the 14 WS during 24 Feb 2003–30 Jun 2010 and the UWY radiosonde observations from 24 Feb 2003–24 Aug 2010. Note the: (1) large CAPE (red + area) and smaller CIN (blue–area); (2) SW-erly wind direction at 700 hPa and higher consistent with WMAA; (3) dew point depression of 5°C or < from 650–500 hPa indicating LL moisture; (4) lower LCL and CCL compared to the NTSTM sounding (Figure 56) indicating more CAPE in TSTM conditions; (5) lower T_c compared to NTSTM T_c (Figure 56); (6) conditionally unstable air associated with LL moisture; (7) HLTT and LI values that are consistent with instability.

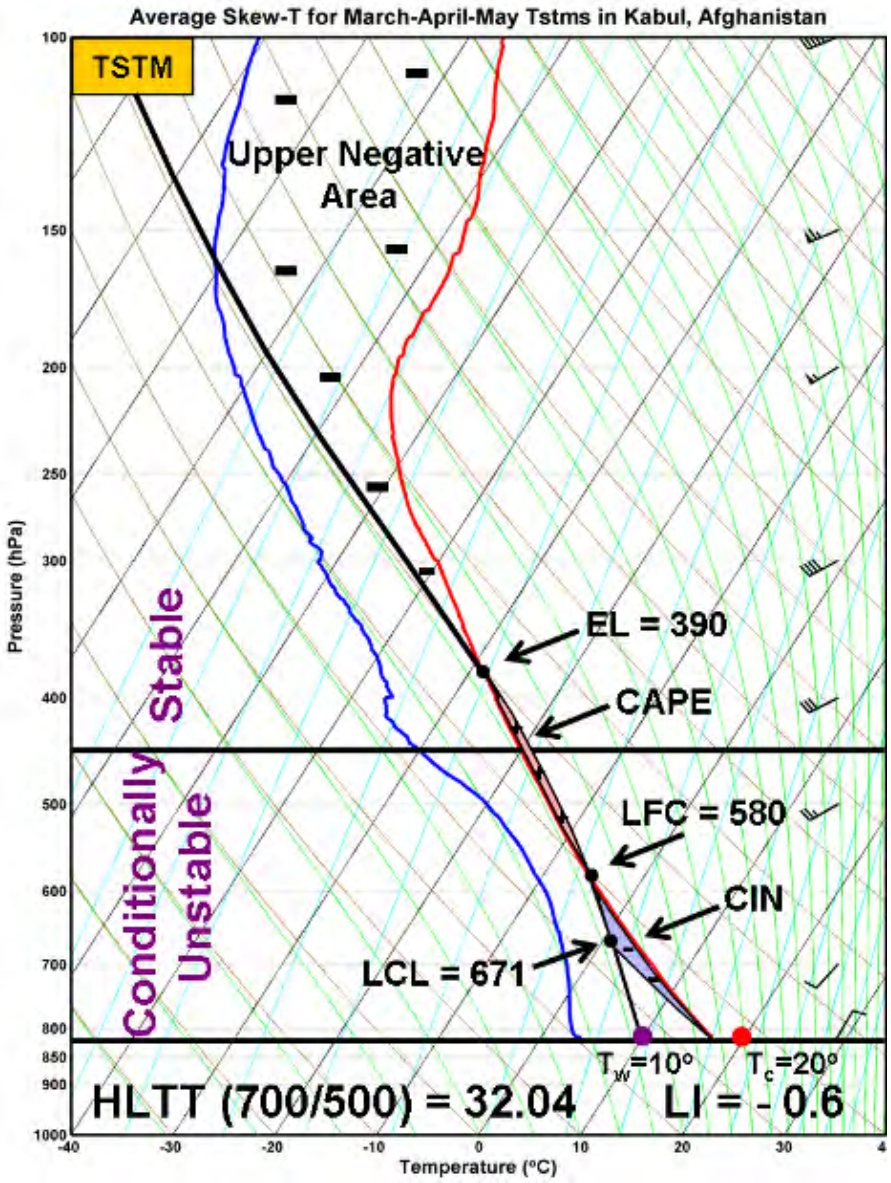

Figure 55. Skew T–log p analysis of average MAM TSTM sounding. Thermodynamic parameters are determined by using the SFC lifting of the air parcel method. Based on Kabul TSTM radiosonde observations from the 14 WS during 24 Feb 2003–30 Jun 2010 and the UWY radiosonde observations from 24 Feb 2003–24 Aug 2010. Note the: (1) small CAPE (red + area) and relatively small CIN (blue - area); (2) SW-erly wind direction from 700 hPa and up consistent with WMAA; (3) dew point depression of 5°C or < from 650–500 hPa indicating LL moisture; (4) lower LCL and a LFC compared to the NTSTM LCL and lack of LFC (Figure 57) indicating more CAPE in TSTM conditions; (5) lower T_c compared to NTSTM T_c (Figure 57); (6) conditionally unstable air made associated with LL moisture; (7) HLTT and LI values that are consistent with instability.

Table 5. MAM weighted average instability index values for TSTM periods. Weighted average index values calculated from individual index values provided by the 14 WS. The process used to identify TSTM periods is described in Chapter II, Section B.3.

# of Obs. Available	Month	LI (^{0}C)	CAPE (J/kg)	CCL pressure (hPa)	CCL temperature (^{0}C)	Tc (^{0}C)
11	March	-0.08	489	676	-0.14	15.29
32	April	-0.56	638	661	0.91	18.82
24	May	-0.22	579	598	-0.71	25.33
Total = 67	**MAM**	**Average = -0.36**	**Average = 592**	**Average = 641**	**Average = 0.16**	**Average = 20.57**

b. Winds

Figures 54–55 show that during TSTM periods, the winds tend to be from the NE at the SFC, where topographic forcing is strong, and from the SW at 700–100 hPa, where large-scale regional factors are more likely to be important. These actual winds are broadly consistent with the TSTM conditional composite anomaly analyses that showed TSTM periods are associated with anomalous winds from the south at LLs and the SW at upper levels (Chapter II, Section C.1).

c. Moisture

Figures 54–55 show a dew point depression of about 5°C in approximately the 650–500 hPa layer, indicating high relative humidity (80% or greater) and the presence of clouds (AWS/TR-79/006 1979). This moist layer is consistent with the TSTM conditional composite anomaly analyses (Section C.1). Increased LL moisture acts to lower the LCL, LFC, and CCL heights, thereby allowing for a larger vertical area of CAPE to develop, which provides more positive buoyant energy to the air parcel for TSTM development (Wallace and Hobbs 2006).

Mid-level dry air entrainment between 400–450 hPa is also suggested by the colder dew point temperatures and increased dew point depression in this layer (Figures 54–55). This entrainment acts to steepen mid-level lapse rates and thereby decrease the stability of the mid-levels and increase convective development (AWS/TR-79/006 1979).

d. High Level Total Totals (HLTT)

The HLTT value for the MAM TSTM average sounding was 32.04°C (see bottom of Figures 54–55). This compares well with the HLTT values that Milne (2004) calculated (Table 1) and thresholded for use in the elevated desert mountain regions of Reno, NV. AN HLTT value of 32.04°C corresponds with isolated to scattered TSTMs in Reno, NV. Unfortunately, our data sets were insufficient to allow us to relate Kabul HLTT values to TSTM severity, as Milne was able to do. These results reinforce the idea that static stability indices need to be developed based on conditions in Kabul (and other parts of AFG), rather than relying on standard CONUS based indices.

2. NTSTM Sounding Analyses

Figures 56 and 57 show the results for the MAM NTSTM average sounding for the heated and lifted SFC parcel methods, respectively. Table 6 shows comparison values for the TSTM average values of LI, CAPE, CCL pressure and temperature, and T_c based on 14 WS calculations of these variables (see discussion of the 14 WS Kabul Static Stability Indices and Thermodynamic Levels data set in Chapter II, Section A.3). The individual monthly and MAM values shown in Table 6 were obtained using the methods described in Chapter III, Section D.1.

a. CAPE, CIN, and LI

Figures 56–57 show results that are consistent with the expectations for NTSTM conditions. Figure 56 shows that the MAM NTSTM

CAPE (CIN) analyzed using the heated SFC air parcel method is smaller (larger) than the corresponding TSTM CAPE (CIN) (Figure 54). Table 6 shows that the 14 WS total weighted average value for MAM CAPE is 220 J/kg, which is much lower than the 14 WS total weighted average MAM TSTM CAPE of 592 J/kg (Table 5). The MAM NTSTM T_c is 25°C, which is 5°C higher than the MAM TSTM T_c. The daily mean SFC high temperatures for Kabul in March, April, and May are all less than 25°C (see Chapter II, Section D.1.a). These results indicate that SFC heating is much less likely to overcome CIN than under NTSTM conditions than under TSTM conditions. The MAM NTSTM LI value of 2.3°C (bottom of Figures 56–57) and the 14 WS MAM total weighted average LI value of 2.28°C (Table 6) are consistent with each other and indicate stable conditions when using CONUS based thresholds (Table 4). These results suggest that CONUS based stability/instability indices may be more appropriate for describing stable conditions in Kabul than unstable conditions.

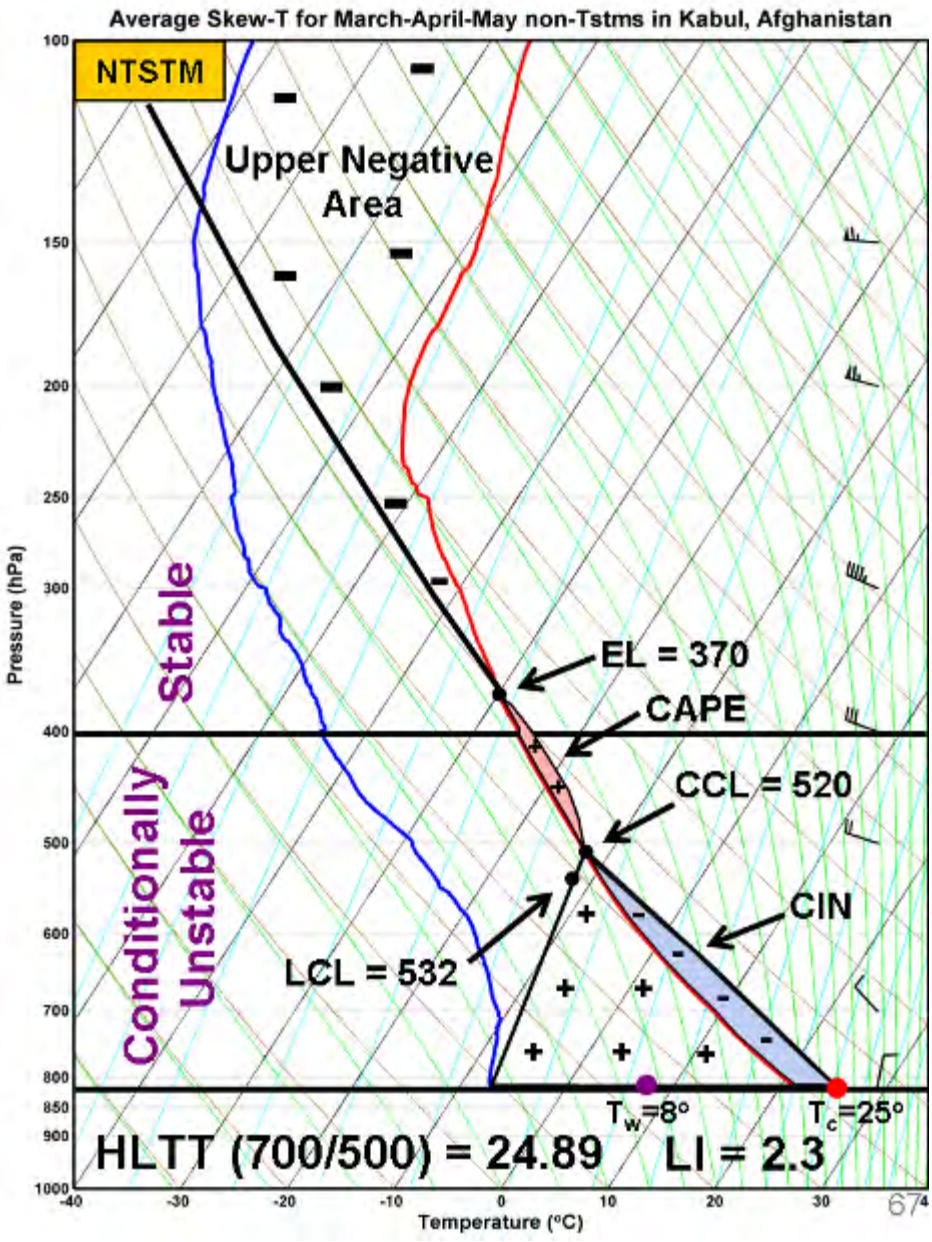

Figure 56. Skew T–log p analysis of average MAM NTSTM sounding. Thermodynamic parameters are determined by using the SFC heating of the air parcel method. Based on Kabul NTSTM radiosonde observations from the 14 WS during 24 Feb 2003–30 Jun 2010 and the UWY radiosonde observations from 24 Feb 2003–24 Aug 2010. Note the: (1) small CAPE and large CIN; (2) NW-erly winds at and above 700 hPa; (3) SFC dew point depression of 29°C; (4) higher LCL and CCL compared to the TSTM LCL and CCL (Figure 54) consistent with small CAPE; (5) higher T_c compared to TSTM T_c (Figure 54); (6) unrealized conditionally unstable air due to lack of LL moisture; (7) HLTT and LI values consistent with stable conditions.

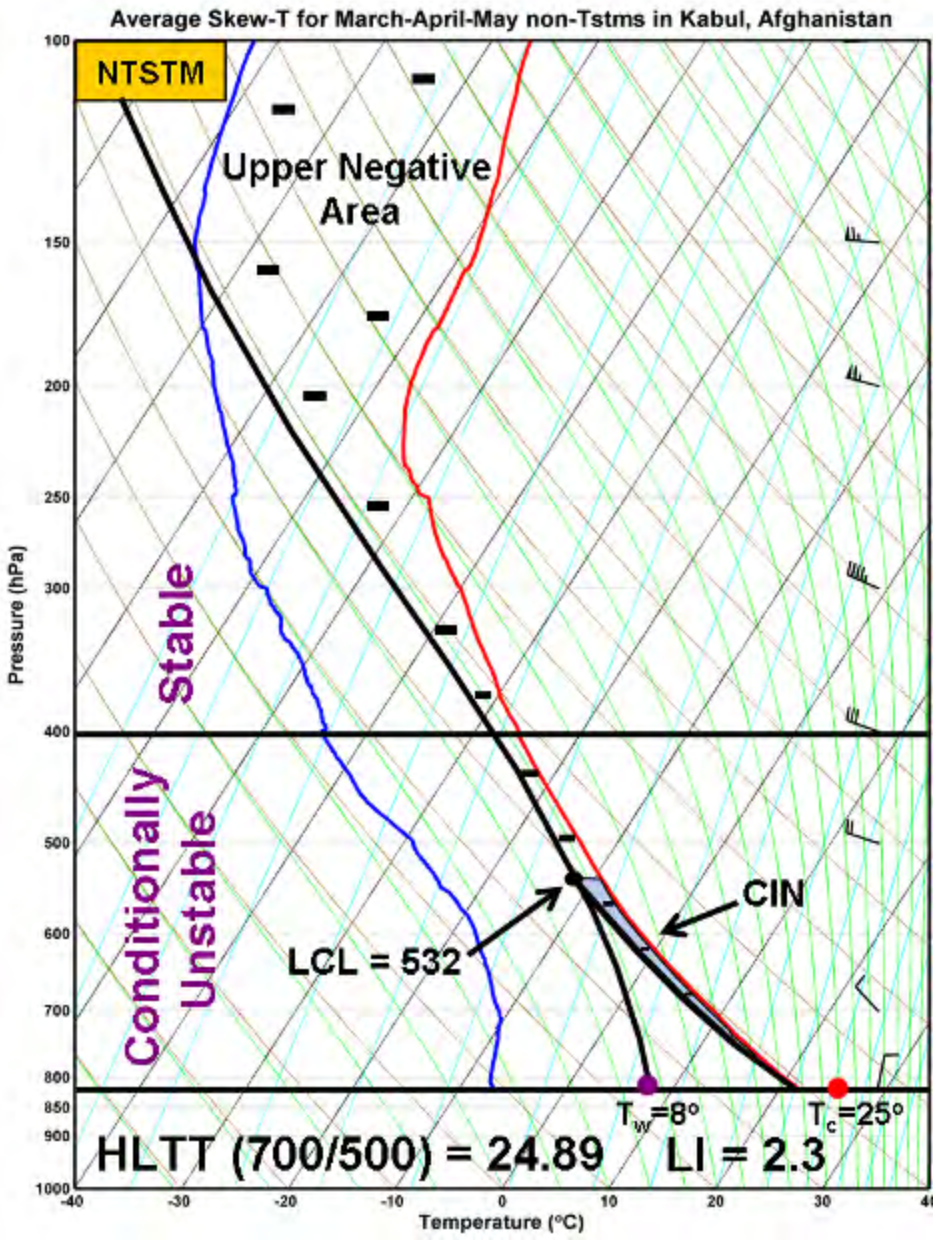

Figure 57. Skew T–log p analysis of average MAM NTSTM sounding. Thermodynamic parameters are determined by using the SFC lifting of the air parcel method. Based on Kabul NTSTM radiosonde observations from the 14 WS during 24 Feb 2003–30 Jun 2010 and the UWY radiosonde observations from 24 Feb 2003–24 Aug 2010. Note the: (1) lack of CAPE and large CIN; (2) NW-erly winds at and above 700 hPa; (3) SFC dew point depression of 29°C; (4) higher LCL compared to the TSTM LCL (Figure 55) consistent with low CAPE; (5) higher T_c compared to TSTM T_c (Figure 55); (6) unrealized conditionally unstable air due to lack of LL moisture; (7) HLTT and LI values consistent with stable conditions.

Table 6. MAM weighted average instability index values for NTSTM periods. Weighted average index values calculated from individual index values provided by the 14 WS. The process used to identify NTSTM periods is described in Chapter II, Section B.3.

# of Obs. Available	Month	LI (°C)	CAPE (J/kg)	CCL pressure (hPa)	CCL temperature (°C)	Tc (°C)
14	March	2.72	160	570	-8.98	20.72
36	April	1.88	283	528	-11.22	24.31
26	May	2.62	166	507	-10.18	29.65
Total = 76	**MAM**	**Average = 2.28**	**Average = 220**	**Average = 529**	**Average = -10.45**	**Average = 25.48**

b. Winds

Figures 56–57 show that during NTSTM periods, the winds tend to be from the North at the SFC, where topographic forcing is strong, and from the NW at 700–100 hPa, where large-scale regional factors are more likely to be important. These winds are broadly consistent with the NTSTM conditional composite anomaly analyses that showed NTSTM periods are associated with anomalous winds from the NE at LLs and from the NW at ULs (Section C.2).

c. Moisture

The MAM NTSTM average dew point depressions (Figures 56–57) are much larger than the corresponding TSTM values (Figures 54–55). One of the largest dew point depressions of 29°C is found at the SFC. This indicates much drier LL air and less favorable conditions for TSTM development. These dry conditions are consistent with the NTSTM composite anomaly results that indicated blocking of ETCs and WMAA from the tropics, and CDAA from the NE (Chapter II, Section C.2).

The decrease in LL moisture acts to raise the LCL, LFC, and CCL heights; for example: (1) the NTSTM LCL is at 532 hPa (Figures 56-57) while the

TSTM LCL pressure is at 671 hPa; and (2) the NTSTM CCL is at 520 hPa while the TSTM CCL is at 640 hPa. The NTSTM LFC does not even exist and therefore CAPE does not exist in the lifted air parcel analysis because the NTSTM LCL is too high to yield CAPE (Figure 57).

d. High Level Total Totals (HLTT)

The HLTT value for the MAM NTSTM average sounding was 24.89°C (see bottom of Figures 56-57). This compares well with the HLTT values that Milne (2004) calculated (Table 1) and thresholded for use in the elevated desert mountain regions of Reno, NV. AN HLTT value of 28–29°C indicates the possibility of isolated TSTMs in Reno, NV, and is the lowest threshold value for the occurrence of TSTMs in that area. Thus, the NTSTM value of 24.89°C suggests little or no chance of TSTM activity (see Figure 8). Unfortunately, our data sets were insufficient to allow us to relate Kabul HLTT values to TSTM severity, as Milne was able to do. These results reinforce the idea that static stability indices need to be developed based on conditions in Kabul (and other parts of AFG), rather than relying on standard CONUS based indices.

E. NEWLY DEVELOPED KABUL STATIC STABILITY AND INSTABILITY INDICES

The results in the prior section indicate that there is a need for static stability/instability indices tailored for use in Kabul, AFG. The HLTT appears to describe Kabul TSTM and NTSTM conditions better than convectional CONUS based indices but there is room for improvement. To develop an improved index for Kabul, we analyzed the distribution of the sounding data according to HLTT value and TSTM and NTSTM conditions based on the 90 TSTM and 90 NTSTM soundings (Chapter II, Section B.2). Figure 58 shows a large overlap in the TSTM and NTSTM distributions in the 26–34°C HLTT range (8°C overlap) and a near overlap in the TSTM and NTSTM peaks. This indicates that the HLTT has

difficulty distinguishing between TSTM and NTSTM conditions and would lead to a large number of false alarms (e.g., indicating TSTM activity during a NTSTM period) and misses if used in Kabul.

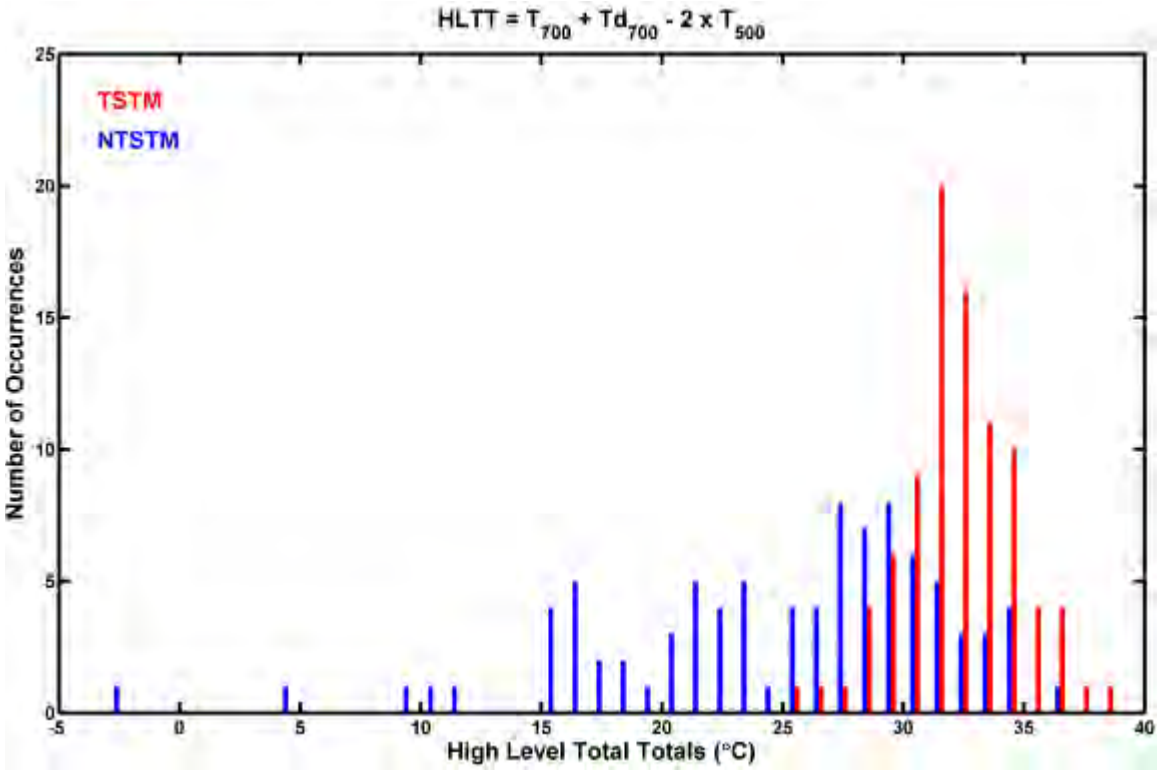

Figure 58. The number of soundings by HLTT value and by TSTM (red) and NTSTM (blue) conditions. Based on Kabul TSTM and NTSTM radiosonde observations from the 14 WS during 24 Feb 2003–30 Jun 2010 and the UWY radiosonde observations from 24 Feb 2003–24 Aug 2010. Notice the large overlap in the distributions in the 26–34°C HLTT range and the similar HLTT values for the TSTM and NTSTM peaks.

1. Kabul High Level Total Totals (KHLTT)

To develop an index that could reliably distinguish between TSTM and NTSTM conditions, we compared the MAM average TSTM and NTSTM soundings. Figure 59 shows that the largest TSTM-NTSTM differences in both temperature and dew point temperature moisture occur in the LLs near 800 hPa.

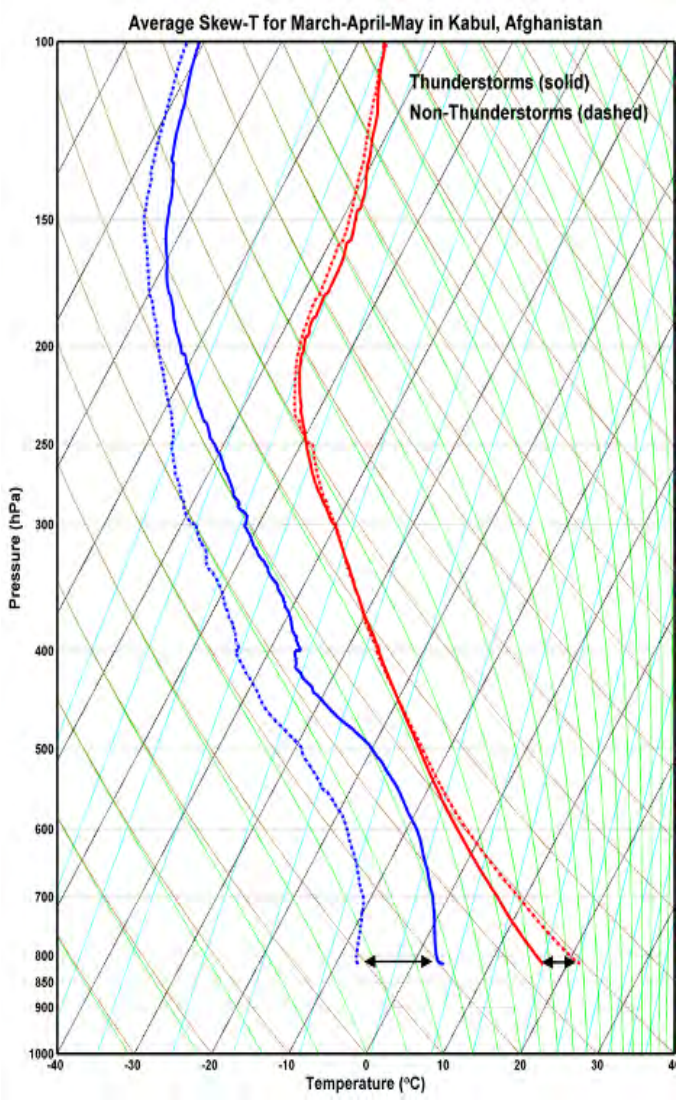

Figure 59. MAM TSTM (solid) and NTSTM (dashed) soundings. Based on Kabul TSTM and NTSTM radiosonde observations from the 14 WS during 24 Feb 2003–30 Jun 2010 and the UWY radiosonde observations from 24 Feb 2003–24 Aug 2010. Note that the largest TSTM-NTSTM differences occur at about 800 hPa for both temperature and dew point.

With this knowledge, we developed a new static stability index for Kabul called the Kabul HLTT (KHLTT). Equation 5 outlines the computation that is involved.

Equation 5. Kabul High Level Total Totals (KHLTT)

$$KHLTT = T_{800} + Td_{800} - 2*T_{700}$$

We emphasized the large temperature and moisture differences near 800 hPa and kept the doubling of the temperature at 700 hPa. Figure 60 shows the distribution of the TSTM and NTSTM KHLTT values that were computed from the 90 TSTM and 90 NTSTM soundings (Chapter II, Section B.2). Notice the overlap of TSTM and NTSTM distributions from approximately -4 to 4°C (still an 8°C overlap) and the greater separation of the TSTM and NTSTM peaks compared to the HLTT results (Figure 58). This means that the KHLTT is less likely than the HLTT to produce false alarms and misses.

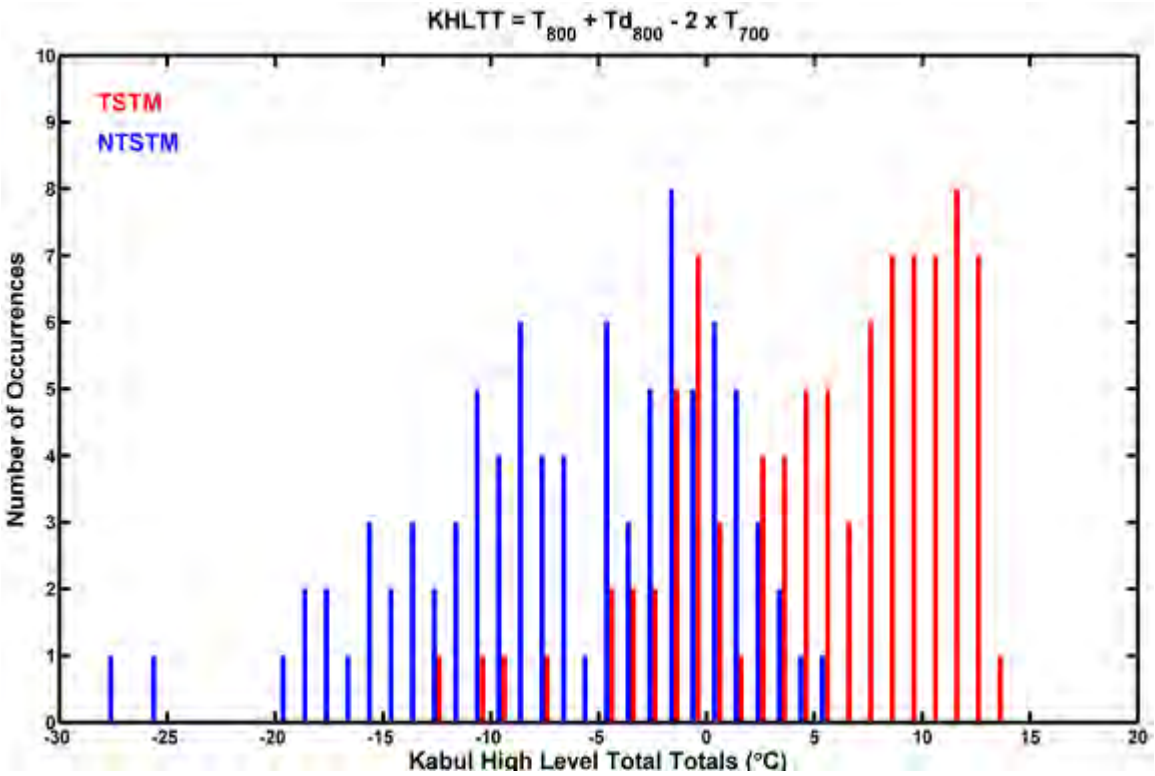

Figure 60. The number of soundings by KHLTT value and by TSTM (red) and NTSTM (blue) conditions. Based on Kabul TSTM and NTSTM radiosonde observations from the 14 WS from 24 Feb 2003 to 30 Jun 2010 and the UWY radiosonde observations from 24 Feb 2003–24 Aug 2010. Notice how the peaks in TSTM and NTSTM occurrence are more widely spaced than those for the HLTT distributions (Figure 58).

2. Kabul Thunderstorm Index (KTI)

Since the largest differences in Kabul TSTM and NTSTM temperatures and dew points are near the 800 hPa level, we developed an additional index based only on values at 800 hPa that we termed the Kabul Thunderstorm Index (KTI). For the KTI, the dew point temperature is doubled to emphasize the large TSTM-NTSTM moisture differences (Figure 59). Equation 6 shows the KTI formula.

Equation 6. Kabul Thunderstorm Index (KTI)

$$KTI = T_{800} - 2 * Td_{800}$$

Figure 61 shows the distribution of the TSTM and NTSTM KTI values that were computed from the 90 TSTM and 90 NTSTM soundings (Chapter II, Section B.2). Notice the overlap of TSTM and NTSTM distributions from approximately 17-25°C (an 8°C overlap) but the much better separation of majority of TSTM and NTSTM events, and of the TSTM and NTSTM peaks, compared to the HLTT and KHLTT results (Figures 58, 60). This indicates that the KTI is less likely than the HLTT or KHLTT to produce TSTM false alarms or misses.

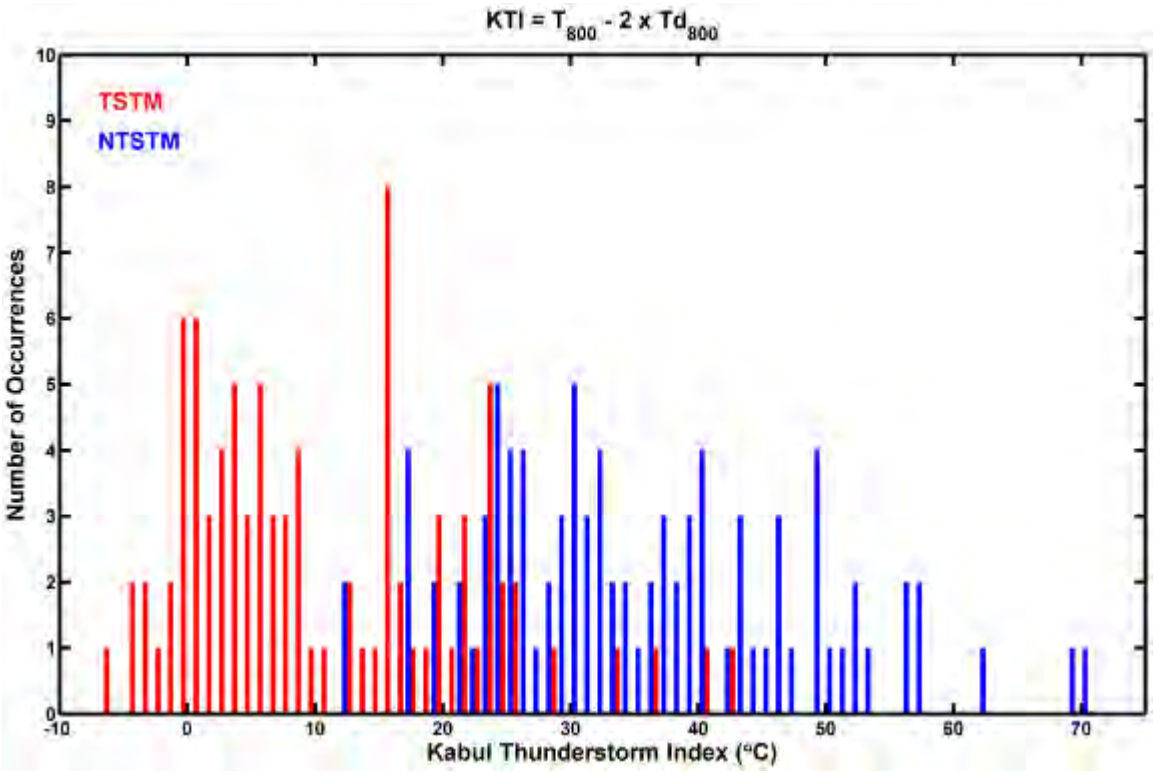

Figure 61. Distributions for TSTM and NTSTM KTI values. Based on Kabul TSTM and NTSTM radiosonde observations from the 14 WS during 24 Feb 2003–30 Jun 2010 and the UWY radiosonde observations from 24 Feb 2003–24 Aug 2010. Notice how the TSTM and NTSTM peak occurrences and overall distributions are farther spread apart than the KHLTT distributions. This indicates that the KTI predicts stability and instability more accurately than the KHLTT.

We used the KTI to hindcast TSTM and NTSTM conditions for the 90 TSTM and 90 NTSTM conditions. We verified the hindcasts using probability of detection (PoD) and false alarm rate (FAR) as our measures of skill (Wilks 2006). The PoD is defined as the percentage of forecasts that correctly predicted the observed events. The best (worst) result is 100 (0). The POD was calculated as:

Equation 7. Probability of Detection (PoD)

$$PoD = (Hits / Hits + Misses) * 100$$

The FAR is the percentage of forecasts that for which TSTM or NTSTM conditions were forecasted but did not happen. The FAR is the ratio of false alarms to the total number of non-occurrences of the forecast event or the conditional relative frequency of a wrong forecast given the event does not occur. The best (worst) result is 0 (100). The FAR was calculated as:

Equation 8. False Alarm Rate (FAR)

$$FAR = (FalseAlarm / FalseAlarm + Correct\,\mathrm{Re}\,jection) * 100$$

Figure 62 shows the POD and FAR results—for example: (1) a KTI value of 10°C has a PoD of 58% for correctly forecasting TSTM events and has a FAR of zero; (2) a KTI value of 20°C has a PoD of 80% for correctly forecasting TSTM events and has a FAR of 10%. The KTI thresholds that have lower FARs are desirable but come at the cost of lower PODs. Figure 62 allows this tradeoff between FAR and POD to be readily optimized. In particular, the figure indicates that KTI threshold values of 20-24°C may be optimal, with a KTI of 24°C yielding a PoD of 90% and a FAR of 16%. Capt. Smith, former Flight Commander for the 28 OWS, said that forecasts based on conventional CONUS based static stability indices had a 50% FAR. Therefore, the KTI results in Figure 62 are encouraging.

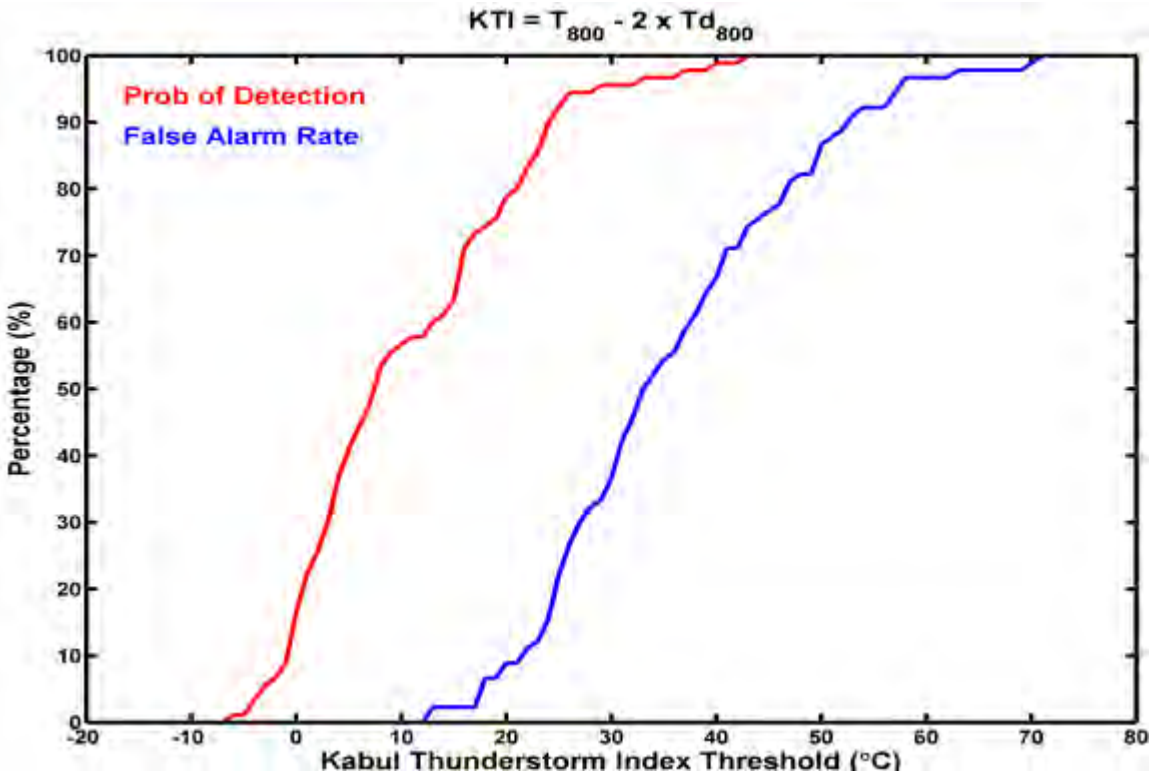

Figure 62. Probability of detection (PoD, red line) and false alarm rate (FAR, blue line) for 90 TSTM and 90 NTSTM KTI values. Based on Kabul TSTM and NTSTM radiosonde observations from the 14 WS during 24 Feb 2003–30 Jun 2010 and the UWY radiosonde observations from 24 Feb 2003–24 Aug 2010. Note that KTI threshold values of 20-24°C provide the best PoD to FAR ratios, with a KTI of 24°C yielding a PoD of 90% and a FAR of 16%.

For the HLTT, KHLTT, and KTI results shown in this section, we used only 90 MAM NTSTM events to match the 90 MAM TSTM events in our data set—the maximum number in the set for which we had sounding data (see Chapter II, Sections B.1-2). The 90 NTSTM events were carefully selected to represent NTSTM conditions (Chapter II, Sections B.1-2), but there are certainly more than 90 NTSTM events within our data set. In future research, additional NTSTM events should be used in testing stability/instability indices.

Future research should also investigate developing a modified KTI based on (1) just the dew point at 800 hPa data for computations, since the largest TSTM-NTSTM differences are in dew point at 800 hPa, and (2) middle and

upper-level winds, as well as temperature and/or dew point at 800 hPa, since there are significant wind differences between TSTM and NTSTM conditions. An index that is based on just 800 hPa dew point and winds would be especially useful to develop and test.

F. TSTM AND NTSTM REGIME INDICES RESULTS

The TSTM and NTSTM conditional composite anomalies and climate variation analysis that was presented in Chapter III, Section C.1-3, revealed that each regime has different large-scale anomalous circulation patterns, which alter the temperature and moisture characteristics, and therefore stability, of the environment over AFG. This information has the potential to be useful in forecasting, and so we developed large-scale indices based on anomalous circulation regimes to analyze and forecast TSTM and NTSTM events.

The TSTM regime index was based on five centers of Z850 circulation anomalies that are favorable for TSTMs in Kabul (Figure 63). The five regions, denoted by the five black boxes, were chosen because they represent the centers of the anomalous circulations that engender TSTMs in Kabul during MAM. The advection of WMA into AFG is represented by the boxes centered over the Strait of Hormuz (SoH) and the Stans region. The advection of CDA into AFG are represented by the boxes centered over the Caspian Sea and south-central China. The south-central China area was spilt into two boxes, a “China-west” box and “China-east” box, to capture the large area of positive height anomalies in the region. Table 7 lists the latitudes and longitudes of the TSTM index boxes.

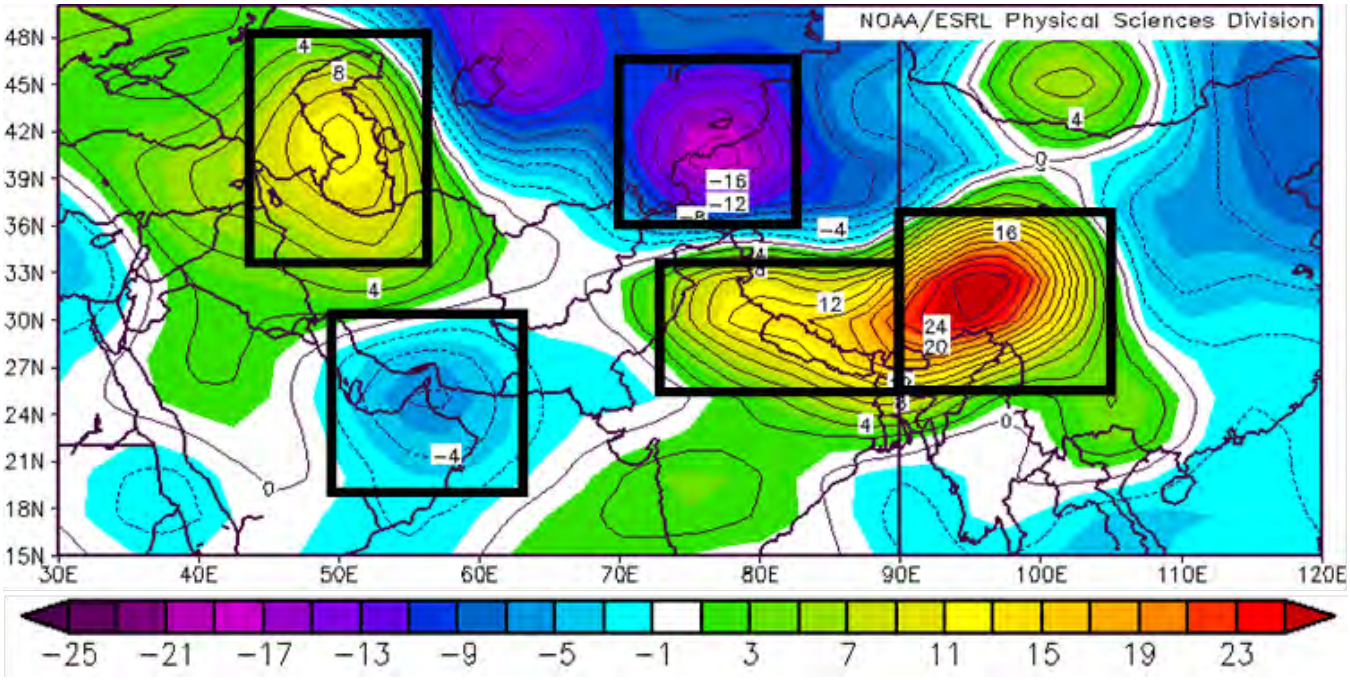

Figure 63. The five regions (outlined by five black boxes) from which the Z850 anomalies were used to calculate the TSTM climate regime index. The color shading and contours show the TSTM conditional composite Z850 anomalies for MAM (Figure 28). The five boxes were selected to represent the centers of the circulation anomalies that are favorable for TSTM activity over AFG.

Table 7. Latitudes and longitudes for the five TSTM index boxes.

Index Box	Latitude (degrees)	Longitude (degrees)
Strait of Hormuz (SoH)	30N – 19N	049E – 063E
Stans	46N – 36N	070E – 083E
Caspian Sea	48N – 34N	043E – 056E
China-west	34N – 26N	073E – 090E
China-east	37N – 26N	090E – 105E

We used the Z850 anomalies in these five boxes to represent the anomalous MAM TSTM circulation regime, and to develop an index of that regime, termed the TSTM Regime Index (TRI). More positive TRI values should in general correspond to higher levels of TSTM activity in Kabul and/or nearby regions. The TRI equation is:

TRI = (Caspian Z'850 + China Z'850) – (Stans Z'850 – SoH Z'850)

We identified within our Kabul TSTM SFC observation data set (Chapter II, Section B.1) the 15 most active TSTM days—that is, the days with the highest number of TSTM hours. For days with equal numbers of TSTM hours, we used the corresponding number of precip hours to determine their relative ranking. We then subjectively analyzed the Z850 anomaly values in each box for these 15 days and entered them into the TRI equation for each day. This led to positive TRI values for 14 of the 15 cases (93.3%). This indicated that the TRI, or a similar large-scale regime based tool, may be a useful indicator of TSTM activity.

We applied the same process for developing a similar index of NTSTM activity. Figure 64 shows the Z850 anomalies and four areas that we used to represent the NTSTM regime. The four regions, denoted by the four black boxes, were chosen because they represent the centers of the anomalous circulations that engender NTSTMs in Kabul during MAM. The two areas from

where WMAA into AFG would originate, if they were not blocked by the strong anomalous higher heights and pressures over western China, are represented by the boxes centered over the Red Sea (RS) and the Bay of Bengal (BoB). The two areas that block AFG, and from where CDAA into AFG originates from the northeast, are represented by the boxes centered over Iran and western China. Table 8 lists the latitudes and longitudes of these NTSTM index boxes.

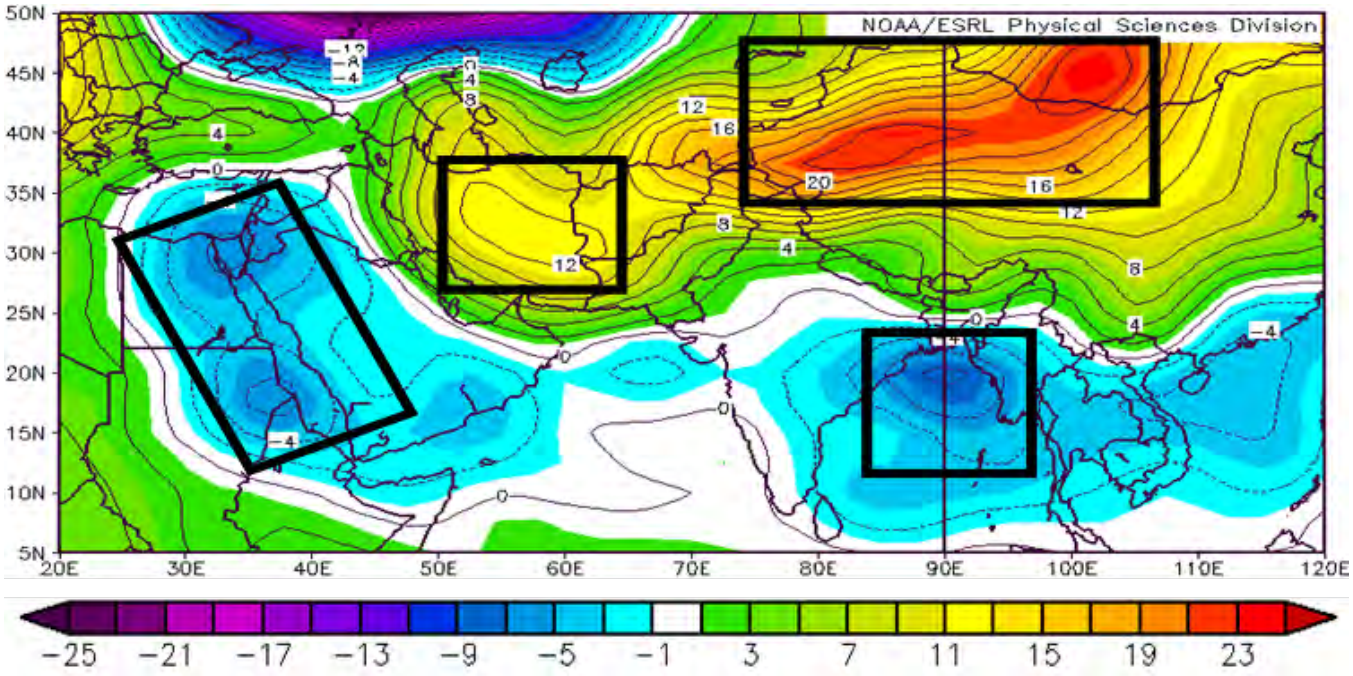

Figure 64. The four regions (outlined by four black boxes) from which the Z850 anomalies were used to calculate the NTSTM climate regime index. The color shading and contours show the NTSTM conditional composite Z850 anomalies for MAM (Figure 40). The four boxes were selected to represent the centers of the circulation anomalies that are favorable for NTSTM activity over AFG.

Table 8. Latitudes and longitudes for the four NTSTM index boxes.

Index Box	Latitude (degrees)	Longitude (degrees)
Red Sea (RS)	35-31N – 16-12N	025-035E – 038-049E
Bay of Bengal (BoB)	23N – 12N	084E – 097E
Iranian	37N – 26N	051E – 065E
Western China	48N – 35N	075E – 107E

We used these boxes to develop an index of NTSTM conditions, the NTSTM Regime Index (NRI). More negative NRI values should in general correspond to higher levels of NTSTM activity in Kabul and/or nearby regions. The NRI equation is:

NRI = (Red Sea Z'850 + Bay of Bengal Z'850) - (Iranian Z'850 + Western China Z'850)

We then calculated the NRI values for the 15 days with strongest NTSTM conditions, using a process similar to that for the TRI. For 13 of the 15 cases (86.7%), the NRI was a negative NRI value for a correct forecast of NTSTMs. This indicated that the NRI, or a similar large-scale regime based tool, may be a useful indicator of NTSTM activity.

The TRI and NRI are highly experimental indices and need further improvement using a more objective process applied to more cases. However, these initial results show promise and suggest that the TRI and NRI could be useful in forecasting.

G. OLRA PRECURSORS AND POTENTIAL PREDICTORS FOR MEDIUM AND LONG RANGE FORECASTING

In Chapter III, Section C.3.b, we discussed the potential correlation between (a) OLRAs over the western tropical Pacific Ocean, SPCZ, BoB, and NIO with (b) TSTM and NTSTM activity over AFG. We explored the potential use

of OLR as a precursor or predictor of TSTM and NTSTM activity by examining tropical OLRAs at 5, 10, and 15 days prior to the beginning of TSTM and NTSTM events.

1. TSTM OLRAs for Minus 15 to 5 Days

Figure 65 shows the OLRAs at leads of 15, 10, and 5 days prior to the 129 MAM TSTM events. Note the indications of decreasing convection over the NIO, BoB, SCS, and SPCZ as the lead-time decreases. OLRAs in these areas have the potential to stimulate anomalous circulation over the NIO and southern Asia that could contribute to the Z850 anomalies associated with TSTM activity (Figure 28; cf. Vorhees 2006; Stepanek 2006; Moss 2007; DeHart 2011).

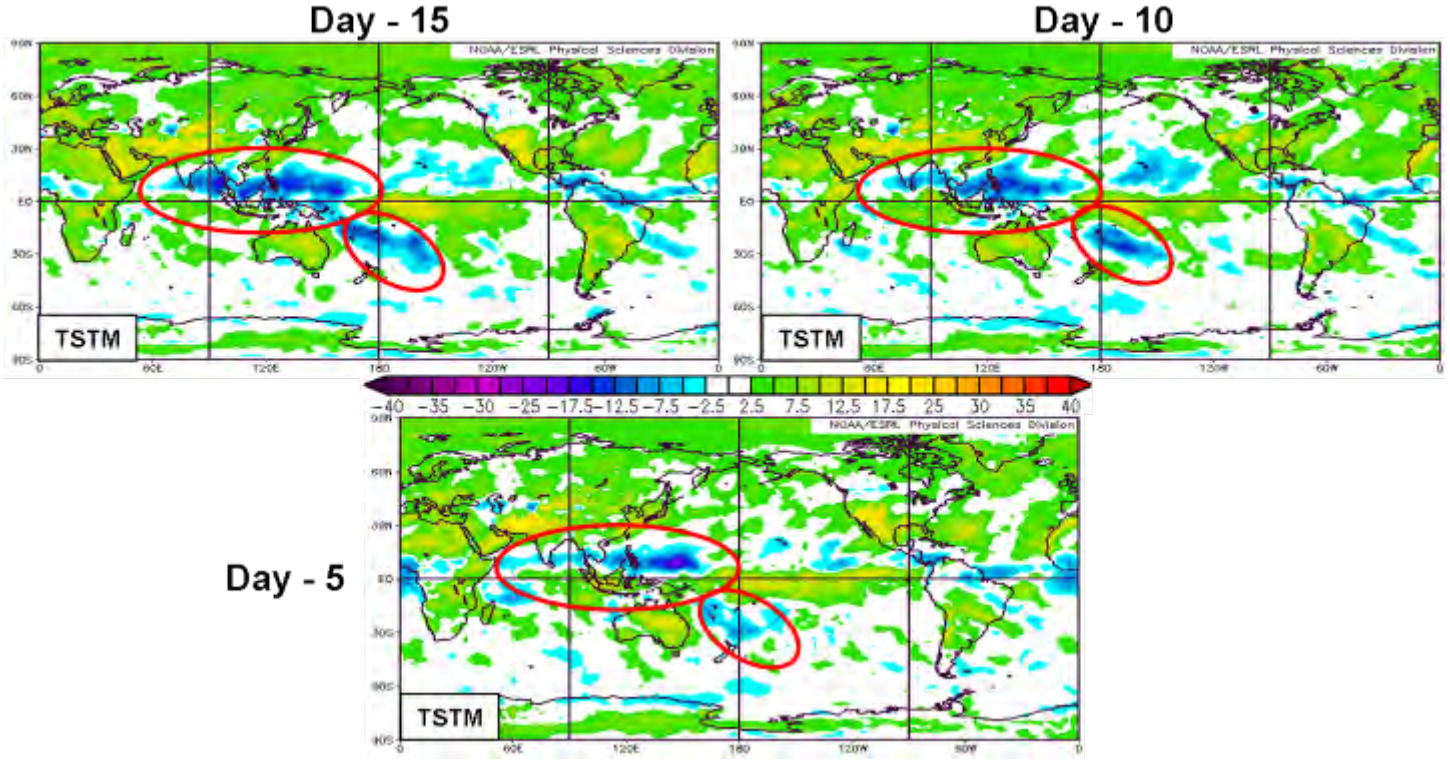

Figure 65. TSTM conditional composite anomalies of outgoing longwave radiation (OLR; W/m^2) during MAM for 15 days before TSTM event (top left), 10 days before TSTM event (top right), and 5 days before TSTM event (bottom). Based on Kabul TSTM observations during 04 Mar 2002–31 Jul 2010. Note the general decrease in implied convection over the NIO, BoB, SCS, and SPCZ as the lead-time decreases.

2. NTSTM OLRAs for Minus 15 to 5 Days

Figure 66 shows the OLRAs at leads of 15, 10, and 5 days prior to the 129 MAM NTSTM events. Note the indications of increasing convection over the NIO, BoB, SCS, western Tropical Pacific, and SPCZ as the lead time decreases. OLRAs in these areas have the potential to stimulate anomalous circulation over the NIO and southern Asia that could contribute to the Z850 anomalies associated with NTSTM activity (Figure 40; cf. Vorhees 2006; Stepanek 2006; Moss 2007; DeHart 2011).

The results shown in Figures 65–66 suggest that there is potential to exploit information about remote tropical forcings of, and teleconnections within, the climate system to develop medium to long lead forecasting systems for TSTM and NTSTM activity in AFG and nearby regions.

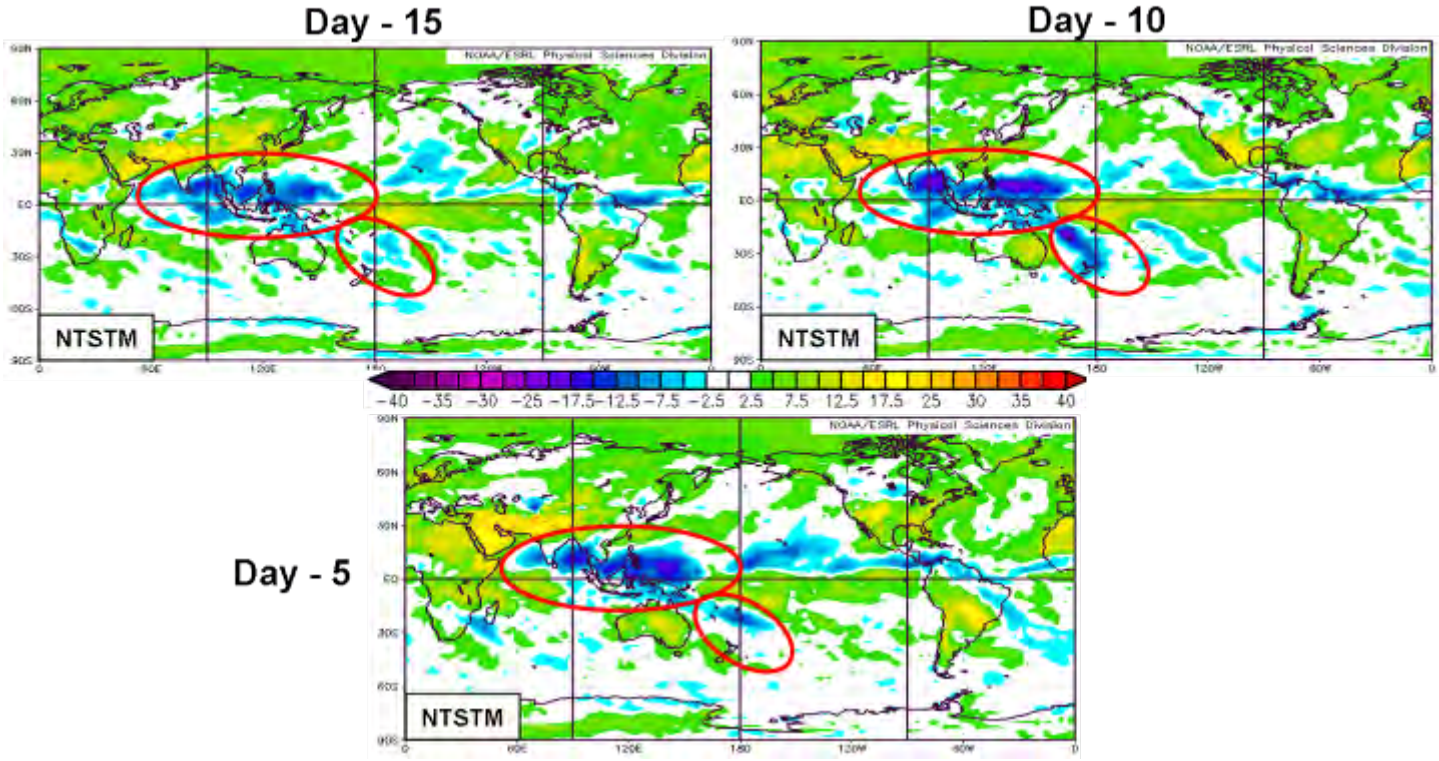

Figure 66. NTSTM conditional composite anomalies of outgoing longwave radiation (OLR; W/m^2) during MAM for 15 days before NTSTM event (top left), 10 days before NTSTM event (top right), and 5 days before NTSTM event (bottom). Based on Kabul NTSTM observations during 04 Mar 2002–31 Jul 2010. Note the general increase in implied convection over the NIO, BoB, SCS, western tropical Pacific, and SPCZ as the lead-time decreases.

IV. SUMMARY, CONCLUSIONS, AND RECOMMENDATIONS

A. KEY RESULTS AND CONCLUSIONS

We investigated the potential for improving TSTM forecasting in Kabul, AFG, by using state-of-the-science observational and reanalysis datasets and methods. Our primary focus was to improve the scientific understanding of the processes that lead to TSTM and NTSTM activity in Kabul and nearby regions. To do so, we analyzed the large-scale conditions that characterize TSTM and NTSTM periods, and their relationship to the local scale conditions in Kabul.

We used in situ SFC and radiosonde data sets from the 14 WS and UWY to identify temporal patterns in TSTM and NTSTM regimes in Kabul. We focused our study on MAM, the period with the most TSTM activity. We then used the RI reanalysis data set to identify the anomalous patterns and processes that contribute to the development of TSTM and NTSTM events. We determined that during a TSTM event, large-scale anomalous circulation patterns develop over Asia and the NIO that lead to anomalous LLCON over AFG of WMA from the south with CDA from the north. The convergence of these air masses led to anomalous instability and favorable conditions for TSTMs over AFG. During NTSTM periods, large-scale anomalous circulation patterns develop that contribute to blocking over, and CDAA from the northeast into, AFG. This led to an anomalously high stability and unfavorable conditions for TSTMs over AFG.

We also analyzed local MAM TSTM and NTSTM conditions using average TSTM and NTSTM soundings for Kabul. From these analyses, we tested an existing stability index (HLTT), then developed and tested two new experimental stability indices (KHLTT, KTI) that are based on sounding data. The new indices appear to be a significant improvement over existing CONUS based indices that are currently being used to forecast TSTMs in AFG and for which forecast skill is low.

We also developed and tested two experimental indices of TSTM and NTSTM events that are based on anomalous large-scale circulation regimes (TRI, NRI). Initial results showed promise for the use of these regime-based indices in analyzing and potentially forecasting TSTM and NTSTM activity in Kabul at the medium-range (MRF) and long-range (LRF) forecast periods.

Finally, we identified several OLRAs over multiple tropical ocean basins, which are likely associated with large-scale climate variations (e.g., MJO, ENLN, IOZM,) and which appear to be precursors and potentials of TSTM and NTSTM events at long, medium, and short lead times.

B. MOTIVATION AND APPLICABILITY TO DOD OPERATIONS

TSTMs provide some of the most dangerous operating environments for U.S. forces in SWA, due to thunder, lighting, hail, flooding, strong winds, and dust storms, which can negatively impact flight and ground operations. In our research for this thesis, we did not come across any empirical studies that focused on TSTMs in AFG or Kabul. Forecasters are using forecast tools that were not developed, or intended, for use in SWA, AFG, or Kabul specifically. The need for such information within the DoD is great, and it is our intention to provide such support through this research.

C. RECOMMENDATIONS FOR FURTHER RESEARCH

Based on the results of this thesis, it is evident that TSTM forecasting in Kabul and nearby regions can be improved upon. Our results contribute to meeting that need, but additional research is still needed. In particular, we recommend the following research efforts.

1. Complete similar research with temporally and spatially more extensive and resolute SFC and radiosonde data sets. Results from this study will prove critical in creating climatologies for TSTM and NTSM regimes and associated phenomena.

2. Apply newer and higher resolution reanalysis datasets to assess regional and global scale processes, such as the Climate Forecast System Reanalysis.

3. Complete research that assesses possible teleconnections to regional and global climate variations (e.g., MJO, ENLN, IOZM).

4. Investigate additional factors that contribute to variations in TSTM and NTSTM activity (e.g., winter snowpack). Experienced AFG forecasters have noted that an above normal winter snowpack tends to lead to above normal TSTM activity in the following spring, and vice versa.

5. Refine and further test TSTM and NTSTM regime indices, and develop automated, objective methods for determining these indices such that they can become operational.

6. Continue research on the HLTT and KHLTT indices to account for thresholding, seasonal, and analysis level modifications. Also, incorporate the use of virtual temperature instead of temperature to refine the results.

7. Refine and further test the KTI (e.g., via a greater weighting of moisture and winds) and develop automated objective methods for determining these indices such that they can become operational.

8. Further investigate the potential for skillful long, medium, and short lead forecasting of TSTM and NTSTM periods in AFG.

THIS PAGE INTENTIONALLY LEFT BLANK

LIST OF REFERENCES

14th Weather Squadron (14 WS), cited 2011: Climate services. [Available online at https://notus2.afccc.af.mil/SCISPublic/.]

14th Weather Squadron Afghanistan Climatology Report (14 WS AFG CR), cited 1991: [Available online at https://notus2.afccc.af.mil/SCISPublic/.] Accessed March 2011.

28th Operational Weather Squadron (28 OWS), cited 2011: Training Portal. [Available online at https://weather.sc.afcent.af.mil/.] Accessed March 2011.

28th Operational Weather Squadron Kabul Forecast Reference Notebook (28 OWS Kabul FRN), cited 2010: Forecast Reference Notebook for Kabul International Airport. [Available online at https://weather.sc.afcent.af.mil/.] Accessed March 2011.

Afghan Facts, cited 2011: Afghana search engine. [Available online at http://www.afghana.com/Directories/Facts.htm.]

Air Weather Service (AWS/TR-79/006), cited 1979: The use of the skew t-log p diagram in analysis and forecasting. [Available online at http://www.dtic.mil/cgibin/GetTRDoc?Location=U2&doc=GetTRDoc.pdf&AD=ADA221842.]

American Meteorological Society, cited 2011: Amer. Meteor. Soc. Glossary of Meteorology (GoM). [Available online at http://amsglossary.allenpress.com/glossary.]

Cantrell, M., MOAA, cited 2004: Weather and War. [Available online at http://www.moaa.org/magazine/March2004/f_weather.asp.] Accessed March 2011.

Cercone, E.J., 2007: Severe weather forecasting for Laughlin AFB, TX. Dept. of Meteorology, Naval Postgraduate School, 99 pp.

CIA, cited 2011: The world factbook. [Available online at https://www.cia.gov/library/publications/the-world-factbook/geos/af.html.]

DeHart, J., 2011: Long-range forecasting in support of operations in Pakistan. M.S. thesis, Dept. of Meteorology, Naval Postgraduate School, 83 pp.

Djuric, D., 1994: *Weather Analysis.* Upper Saddle River, NJ: Prentice-Hall Inc., 304 pp.

Earth Systems Research Laboratory (ESRL), cited 2011: Daily Mean Composites. [Available online at http://www.esrl.noaa.gov/psd/data/composites/day/.]

Hanson, C., 2007: Long-range operational military forecasts for Iraq. M.S. thesis, Dept. of Meteorology, Naval Postgraduate School, 77 pp.

Kalnay, E., and Co-authors, 1996: The NCEP/NCAR 40-year reanalysis project. *Bull. Amer. Meteor. Soc.,* **77,** 431-471.

Lemke, B. D., 2010: Long-range forecasting in support of operations in the horn of Africa. M.S. thesis, Dept. of Meteorology, Naval Postgraduate School, 155 pp.

Liebmann, Brant, and Smith, C.A., 1996: Description of a complete (Interpolated) outgoing longwave radiation dataset. *Bull. Amer. Meteor. Soc.,* **77,** 1275-1277.

Milne, R., cited 2004: A modified total totals index for thunderstorm potential over the intermountain west. [Available online at http://www.wrh.noaa.gov/wrh/04TAs/ta0404.pdf.]

Moss, S.M., 2007: Long-range operational military forecasts for Afghanistan. M.S. thesis, Dept. of Meteorology, Naval Postgraduate School, 99 pp.

Nagorski, T., cited 2010: Editor's notebook: Afghan War now country's longest. [Available online at http://abcnews.go.com/Politics/afghan-war-now-longest-war-us-history/story?id=10849303.] Accessed March 2011.

Stepanek, A., 2006: North Pacific - North American circulation and precipitation anomalies associated with the Madden-Julian oscillation. M.S. thesis, Dept. of Meteorology, Naval Postgraduate School, 119 pp.

Stratton, M. B., 2006: Convective indices for the central and western tropical Pacific. M.S. thesis, Dept. of Meteorology, Naval Postgraduate School, 119 pp.

Secretary of the Air Force (AFMAN 15-129), cited 2010: Air and space weather operations-processes and procedures. [Available online at http://www.af.mil/shared/media/epubs/AFMAN15-129.pdf.]

Secretary of the Air Force (AFI 15-128), cited 2010: Air and space weather operations-roles and responsibilities. [Available online at http://www.af.mil/shared/media/epubs/AFPD15-1.pdf.]

Secretary of the Air Force (AFMAN 15-111), cited 2010: Surface weather observations. [Available online at http://www.af.mil/shared/media/epubs/AFMAN15-111.pdf.]

Vorhees, D., 2006: The impacts of global scale climate variations on Southwest Asia. M.S. thesis, Dept. of Meteorology, Naval Postgraduate School, 175 pp.

Wallace, J.M., and Hobbs, P.V., 2006: *Atmospheric Science an Introductory Survey.* 2nd ed. Elsevier Academic Press, 483 pp.

Wilks, D., 2006: Statistical Methods in the Atmospheric Sciences, Academic Press, 627 pp.

THIS PAGE INTENTIONALLY LEFT BLANK

INITIAL DISTRIBUTION LIST

1. Defense Technical Information Center
   Ft. Belvoir, Virginia

2. Dudley Knox Library
   Naval Postgraduate School
   Monterey, California

3. Prof. Tom Murphree
   Naval Postgraduate School
   Monterey, California

4. Mr. Paul Frederickson
   Naval Postgraduate School
   Monterey, California

5. Mr. Neal Triplett
   28th Operational Weather Squadron
   Shaw Air Force Base, South Carolina

6. Maj Darren Murphy or librarian
   Air Force Combat Climatology Center (14 Weather Squadron)
   Asheville, North Carolina

7. Ms. Cathy Smith
   Earth Systems Research Laboratory
   Boulder, Colorado